Hydrodeoxygenation of bio-oil model compounds using alumina, zirconia and carbon supported metal catalysts

Master Thesis

Moldir Alda-Onggar

Supervisors:

Professor Dmitry Yu. Murzin & Docent Päivi Mäki-Arvela

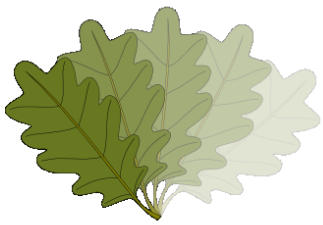

Johan Gadolin
Process Chemistry Centre

Laboratory of Industrial Chemistry and Reaction Engineering

Faculty of Science and Engineering

Åbo Akademi University

Finland, 2018

Abstract

Moldir Alda-Onggar

Hydrodeoxygenation of bio-oil model compounds using alumina, zirconia and carbon supported metal catalysts

The work was carried under the supervision of Prof. Dmitry Murzin and Docent Päivi Maki-Arvela in the Laboratory of Industrial Chemistry and Reaction Engineering at Åbo Akademi University, Finland

Keywords HDO, isoeugenol, guaiacol, vanillin, alumina, zirconia, carbon, iridium-rhenium catalysts, platinum-rhenium catalysts.

Bio-oil is an attractive alternative to petroleum oil and important renewable source of energy and chemicals. Through hydrodeoxygenation (HDO) it can be transformed into transportation fuel by removal of oxygen. Because of bio-oil complex composition, HDO of its model compounds is of high interest. In the current work, mainly HDO of isoeugenol (not previously studied) as a model compound was investigated over a range of metals on mildly acidic (Al_2O_3 and ZrO_2) and a neutral support (carbon), with dodecane as a solvent. The fresh and spent catalysts were characterized using different physico-chemical methods. Several catalysts allowed higher selectivity towards propylcyclohexane and complete conversion of dihydroeugenol. Gas samples taken after isoeugenol and guaiacol HDO were investigated using GC and GC-MS techniques, demonstrating high abundance of ethane and methane. First influence of reaction temperatures (150, 200 and 250℃) was investigated with the most suitable one being 250℃. Bimetallic catalysts containing iridium-rhenium and platinum-rhenium over alumina and carbon supports resulted in higher molar concentration of propylcyclohexane in comparison with monometallic ones. Low gas chromatography based sum of the reactants and products in the liquid phase analysis (GCLPA) was obtained in isoeugenol HDO at 250℃ and 30 bar. The effect of pressure was

investigated in isoeugenol HDO over two alumina supported catalysts, showing that high pressure of hydrogen favored high selectivity towards propylcyclohexane. Optimization tests were done with different substrate to catalyst ratio illustrating that HDO was not effective in terms of propylcyclohexane selectivity in the presence of too high isoeugenol concentration. Solventless isoeugenol HDO was performed over Ir-C catalyst at 150℃ (a semi-batch mode) and 200℃ (a batch mode) and the total pressure of 11 bar giving a complete conversion of isoeugenol to dihydroeugenol.

Iridium and nickel catalysts over zirconia support applied in HDO of isoeugenol and guaiacol at 250℃ and 30 bar and vanillin HDO at 100℃ and 30 bar demonstrated different distribution of products, the two latter ones giving mainly different alcohols, while isoeugenol HDO resulted in propylcyclohexane as the main product. However, low GCLPA was observed indicating high formation of gaseous products and adsorption of compounds.

Acknowledgements

A very special gratitude goes to my supervisors Professor Dmitry Yu. Murzin and Docent Päivi Maki-Arvela. Professor Dmitry Murzin - for trusting and giving me this opportunity to grow and expand my knowledge and abilities. Docent Päivi Maki-Arvela – for providing me with the best guidance, support and engagement in the different projects. Furthermore, thank you both for the inspiration and encouragement.

I would like to thank Docent Narendra Kumar for helping and teaching me synthesis and characterization techniques of the catalysts. I am grateful to Dr Atte Aho for helping with FTIR and XPS methods and Dr. Käri Eranen for supporting me with important technical advices.

I am very thankful to my family, especially Mom and Dad being in my life, providing me with a window of opportunities and moral and emotional support throughout this special journey. I am very grateful to my close friends for encouraging me and being around.

I am also grateful to all colleagues that I met at the Laboratory of Industrial Chemistry and Reaction Engineering.

It has been an incredible experience being a research assistant in the Laboratory of Industrial Chemistry and Reaction Engineering, Faculty of Science and Technology, at Åbo Akademi University, Finland.

Thank you!

List of Figures

List of Tables

Contents

1 Introduction

1.1 Bio-oil and model compounds

1.1.1 Bio-Oil (its properties)

In the 1970s the energy crisis allowed to focus on an alternative source of energy such as bio-oil [1], which can be obtained from biomass. It is the energy/heat source substitute as well as a source of chemicals with a strong potential to replace finite petroleum supplies [1]. Residual biomass can originate from wood, woody crops, agricultural wastes and others [2]. From wood, paper and other biological masses ca. 60 to 95 wt.% of bio-oil can be obtained, while focusing only on wood – ca. 72-85 wt.% can be produced [3]. In contrast to fossil fuels such as crude oil, gas or coal, biomass is renewable not affecting the carbon cycle [1]. Therefore, bio-oils are a clean power source [1].

Bio-oils are dark hazel colored liquids of a complex structure with a strong smoke filled scent [4]. It is the multicomponent organic mix, achieved by depolymerization and fragmentation of lignocellulosic biomass such as cellulose (27-55 %), hemicellulose (17-35 %) and lignin (17-35 %) [4-5]. There are several ways to produce bio-oils for further upgrading to transportation fuels. Fast pyrolysis or hydrothermal liquefaction of biomass is considered as the simplest and most inexpensive method to produce bio-oils [5]. As bio-oil differs by its composition depending on the feedstock and the method of processing, the common benefits as well as drawbacks are presented in Table 1.

Table 1 Properties of bio-oil

Benefits	Drawbacks
grey listed substance to carbon dioxide and greenhouse gas (GHG) [1]	high water proportion (15-30 %) [4] causing phase separation [3]
	highly viscous (0.035-1 Pa*s at 40°C) [4]
negligible quantity of sulfur, therefore no SO_x taxes [1]	significant amount of oxygen (around 40 %) [4], leading to low heating value (50 % of the energy from crude oil [6])
twofold smaller production of NO_x than the diesel oil [1]	increased ash content causing erosion and device obstruction
	poor volatility [4]

	acidic (pH of 2-3) due presence of organic acids such as acetic and formic acids [4]

Therefore, as can be seen from Table 1, there are several factors restraining use of bio-oils as transportation fuels, i.e. further upgrading is required [5].

1.1.2 Model compounds of bio-oil

Due the complexity of bio-oils and instability during upgrading process, the model compounds of bio-oils are often utilized in the literature. The constituents of bio-oils vary and based on the wood oil pyrolysis the generalized version of the major constituents is presented in Table 2 [5].

Table 2 General composition of bio-oil obtained from wood pyrolysis

Constituent of bio-oil	Division (compounds)
water	-(water)
simple oxygenates	• acids (formic acid, etc.); • esters (methyl acetate, etc.); • alcohols (methanol, etc.); • ketones (acetone, etc.); • aldehydes (formaldehyde, etc.)
mixed oxygenates	-(glycolaldehyde, 1-hydroxyl-2-propanone, etc.)
sugars	-(levoglucasan, glucose, fructose, etc.)
furans	-(furan, furfural, furfuryl alcohol, etc.)
hydrocarbons	• alkene (methyl-propene, etc.); • aromatics (toluene, xylene, etc.)
phenolics	• phenols (phenol, alkylphenols, etc.); • anisoles (anisole, alkyl-anisoles, etc.); • cathecols (cathecol, alkyl-cathecols, etc.), • guaiacols (guaiacol, alkyl-guaiacols, eugenol, etc.); • syringols (syringol, alkyl-syringols, etc.); • others (vanillin, vanillin acid, etc.)
heavy weight	-(dimer, trimer, oligomers of lignocellulosic biomass)

Bio-oil components such as mixed oxygenates, sugars and furans are originating from cellulose and hemicellulose of biomass, while phenolics are obtained from the lignin fractions (Table 2) [5]. The simple oxygenates are derived from the fragmentation of

miscellaneous oxygenates, sugars and furans [5]. The heavy molecules such as dimers, trimers and oligomers possess molecular weight in the range from 200 to more than 5000 and they are initially the oligomers of phenolics [5].

1.2 Upgrading of bio-oils

1.2.1 Upgrading methods (focus on hydrotreating)

In order to make bio-oil comparable to the crude oil possessing similar properties, a high oxygen content in bio-oil is diminished using various upgrading methods such as utilization of zeolites, aqueous phase treating and hydrotreating [5]. In addition, using these processes, the carbon number is maintained [7]. Fractionating and condensing technologies are utilized prior to the mentioned above to enhance upgrading [5]. The resulting products can be utilized as feedstock to petrochemical units as gasoline [7]. For instance, compounds with six to eight carbon numbers are utilized as solvents in polymer manufacturing, while compounds with nine to twelve carbon numbers are arenes for gasoline production [7].

1.2.1.1 Zeolite upgrading

Zeolite upgrading is comparable to catalytic cracking in oil refining where breaking of the long chain hydrocarbons using acidic zeolites occurs at the ambient pressure and in the temperature range of 400℃ to 500℃ [1, 5]. Oxygen is removed forming carbon monoxide, carbon dioxide and water, in addition to arenes and aliphatics [5]. Nevertheless, this method results in insufficient selectivity to hydrocarbons, coking, removal of aluminum from the zeolites caused by presence of water [5], blockage of reactors and an expensive process [1].

1.2.1.2 Aqueous phase processing

For the aqueous phase processing some part of bio-oil is transformed to produce alkanes and hydrogen in the presence of water [5]. Specifically, the aqueous fraction is sent either to aqueous-phase reforming resulting in hydrogen or to aqueous phase dehydrogenation/ hydrogenation where alkanes are produced [5].

1.2.1.3 Hydrotreating

The conventional way to treat bio-oil is hydrotreating, where by hydrodeoxygenation the oxygen content is diminished and hydrocarbons and water are produced [5]. Hydrotreating of bio-oil occurs at high hydrogen pressure and temperature in the range of 125℃ and 500℃ using supported catalysts [5]. The hydrogen pressure varies depending on the reactor type being in the case of batch reactors between 40 and 200 bar, and in the case of continuous fixed bed reactors 10 to 40 bar [7]. High pressure of hydrogen is needed to enhance deoxygenation, resulting in saturation of the aromatic ring producing low octane number hydrocarbons prior to removal of oxygenates [7]. In addition, hydrogen is expensive [7]. Therefore, deoxygenation is needed to reduce hydrogen utilization and preserve aromatics [5]. As a result, the energy density enhances and the viscosity of fuel decreases [5]. Drawbacks include a high probability of coke formation, reactor blockage and catalyst deactivation [5].

1.3 Catalysis in hydrodeoxygenation of model compounds

Different model compounds are utilized to study hydrodeoxygenation. According to Shafaghat et al. [8], who studied phenolic compounds transformation using different catalysts, hydrogenation and hydrogenolysis happen on the active metal sites, whereas dehydration, isomerization, alkylation and condensation proceed over the acid sites [8]. Although the acidic conditions accelerate the hydrodeoxygenation of model compounds, the use of acids also leads to coke formation and further catalyst deactivation [9]. Due to neutrality of carbon supports, acidity and coking can be avoided influencing positively deoxygenation, based on Lyu et al. [10]. During the experimental work in this study, metallic and bimetallic catalysts (Ir, Re, Pt, Ir-Re, Pt-Re) supported by alumina, zirconia and carbon were utilized to investigate hydrodeoxygenation of isoeugenol and diminish the drawbacks of acidic supports at the same time enhancing deoxygenation. Zirconia supported catalysts were also tested in the current work in hydrodeoxygenation of guaiacol and vanillin.

1.3.1 HDO of isoeugenol

Isoeugenol is an aromatic monomer, 4-propenyl-2-methoxyphenol, which includes functional groups close to lignin and coniferyl alcohol [9]. Initially, it was separated

from the ylang-ylang tree (Cananga odorota) [11], produced from the clove oils and cinnamon [12]. Commercially, a more common way of isoeugenol production is to isomerize eugenol at high temperatures using potassium hydroxide in high molecular weight alcohols [13] leading to formation of cis and trans isomeric types of isoeugenol. The schematic version of eugenol isomerization can be seen in Figure 1.

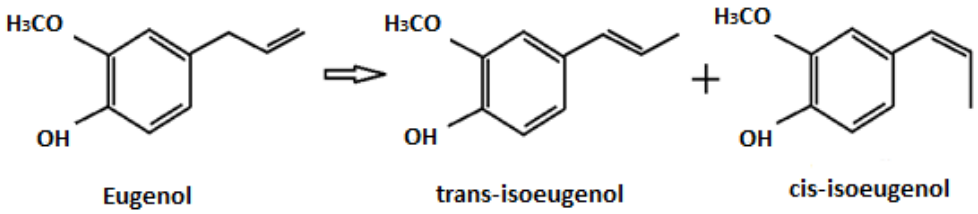

Figure 1 Eugenol reaction pathway into isoeugenol [13].

Isoeugenol as a model compound for hydrodeoxygenation started to gain its momentum recently as in the case of Bomont et al. [14] using Pt-H-Beta-300 catalyst which resulted in 89 % selectivity of propylcyclohexane at 200℃ and 30 bar, therefore HDO of eugenol is summarized below.

Reaction pathways of eugenol hydrodeoxygenation vary depending on the catalyst type (metal and supports). The reaction routes are demonstrated in Figure 2, accounting for both non-catalytic and catalytic routes (with acidic or neutral supports) [9]. As can be seen, eugenol (1) undergoes **hydrogenation** producing dihydroeugenol (2) and **isomerization** giving isoeugenol (8), the products of which pass through **hydrogenolysis** resulting in the cleaved methoxy (-OCH_3), allyl (e.g. -C_2H_5) and hydroxyl (-OH) groups.

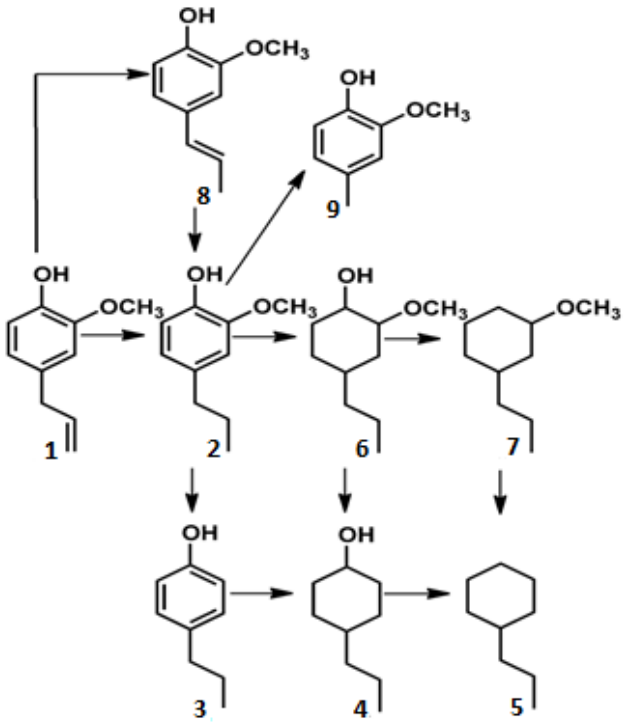

Figure 2 Proposed reaction pathways of eugenol HDO [9].

(1 – eugenol, 2 – dihydroeugenol, 3 - 1-hydroxyl-4-propylbenzene, 4 – propylcyclohexanol, 5 – propylcyclohexane, 6 - 1-hydroxy-2-methoxy-propylcyclohexane, 7 - 1-methoxy-3-propylcyclohexane, 8 – isoeugenol, 9 - 1-hydroxy-2-methoxy-4-methylbenzene).

For non-catalytic hydrodeoxygenation of eugenol different results were reported (Table 3). According to Deepa and Dhepe [9], no products were formed during one hour of eugenol HDO at 250℃ and 30 bar, while according to Bjelic et al. [15], dihydroeugenol and isoeugenol were formed during 3 hours at 225℃ and 275℃ and 50 bar. In addition, isoeugenol was further transformed into dihydroeugenol to a certain extent throughout the course of eugenol HDO at 225℃ and 275℃ [15]. In the absence of any catalyst, eugenol HDO proceeds with hydrogenation and isomerization [15], shown as routes 1→2 and 1→8 in Figure 2. The reasons for such discrepancy in products are unclear, therefore, blank experiments were conducted to confirm production of dihydroeugenol via hydrogenation of isoeugenol, as discussed in Section 4.2.1.

Table 3 Results of non-catalytic eugenol HDO at different operational conditions

Entry	Catalyst	Solvent	Con-version of eugenol, %	Operational conditions (duration, temperature, pressure)	Main products	Refe-rence
1	-	hexa-decane	-	1 hour, 250℃ and 30 bar	-	[9]
2	-	hexa-decane	-	3 hours, 225℃ and 50 bar	dihydroeugenol, isoeugenol	[15]
3				3 hours, 275℃ and 50 bar		

1.3.1.1 Isoeugenol HDO over alumina supported catalysts

In isoeugenol HDO γ-Al_2O_3 was used, which is typically considered as a Lewis acid [16]. In order to investigate eugenol HDO, Deepa and Dhepe [9] performed experiments with palladium, platinum and ruthenium supported on alumina resulting in complete conversion of eugenol (Table 4). As can be seen from these results, hydrodeoxygenation activity was more prominent over Pd/Al_2O_3, producing 10 % of propylcyclohexane. Zhang et al. [17] demonstrated 99 % conversion of eugenol using 10 wt.% Ni/γ-Al_2O_3 resulting in 77 % of hydrocarbons production (not specified). Therefore, the support and metal type as well as operational conditions are the main parameters determining the product distribution in eugenol HDO.

Table 4 Various conditions and results of eugenol HDO using alumina supported catalysts

En-try	Cata-lyst	Sol-vent	Con-version of euge-nol, %	Operational conditions (reaction duration, temperature, pressure)	Main products (selectivity %)	Re-ference
1	Pd/Al_2O_3[a]	hexa-decane	100	1 hour, 250℃ and 30 bar	dihydroeugenol (46 %), 1-hydroxyl-4-propylbenzene	[9]

					(20 %), propylcyclohexane (20 %)	
2	Ru/ Al_2O_3[a]	hexa-decane	100	1 hour, 250℃ and 30 bar	dihydroeugenol (59 %), 1-hydroxy-2-methoxy-4-methylbenzene (13 %)	
3	Pt/ Al_2O_3[a]	hexa-decane	100	1 hour, 250℃ and 30 bar	dihydroeugenol (92 %), 1-hydroxyl-4-propylbenzene (2 %),	
4	10 wt.% Ni/γ-Al_2O_3	octane	99	16 h, 300℃ and 50 bar	hydrocarbons (77 %)	[17]

[a] metal loading varies between 2 to 3.5 wt.% for alumina supported metal catalysts.

1.3.1.2 Isoeugenol HDO over carbon supported catalysts

Carbon supports attracted a lot of attention, due to the mentioned above ability to operate under acidic conditions. In addition, it can withstand high temperature in presence of oxygen and hydrogen (below 223℃ and 427℃ respectively) and behaves as an amphoteric compound with addition of oxygenated functional groups. Furthermore, metals can be recycled by burning carbon [18]. It is also economically advantageous in comparison with alumina [18]. Throughout experimental work in this thesis carbon supported catalysts were used to investigate HDO of isoeugenol. Information about this reaction using metals supported on carbon is summarized in Table 5.

Table 5 Various conditions and results of eugenol HDO using carbon supported catalysts

Entry	Catalyst	Solvent	Conversion of eugenol, %	Operational conditions (reaction duration, temperature, pressure)	Main products (yield %)	Reference
1	Pd/C	hexadecane	100	1 hour, 250℃ and 30 bar	1-hydroxy-2-methoxy-propylcyclohexane (89 %)	[9]
2	Ru/C	hexadecane	100	1 hour, 250℃ and 30 bar	dihydroeugenol (77 %), 1-hydroxyl-4-propylbenzene (6 %)	
3	Pt/C	hexadecane	100	1 hour, 250℃ and 30 bar	1-hydroxy-2-methoxy-propylcyclohexane (95 %)	
4	4 wt. % Ru/C	hexadecane	100 ($C_{0,r}$=232.6 mol/m^3)	3 hours, 275℃ and 40 bar	Dihydroeugenol (34 %), 4-propylcyclohexanol (30 %), propylcyclohexane (17 %)	[15]
5			100 ($C_{0,r}$=238.4 mol/m^3)	3 hours, 275℃ and 50 bar	Dihydroeugenol (39 %), 4-propylcyclohexanol (32 %), propylcyclohexane (22 %)	
6			100 ($C_{0,r}$=244.2 mol/m^3)	3 hours, 275℃ and 60 bar	Dihydroeugenol (43 %), 4-propylcyclohexanol (31 %), propylcyclohexane (24 %)	

Entry	Catalyst	Solvent	Conversion of eugenol, %	Operational conditions (reaction duration, temperature, pressure)	Main products (yield %)	Reference
7	4 wt. % Ru/C	hexadecane	100 ($C_{0,r}$=241.3 mol/m^3)	3 hours, 275℃ and 70 bar	Dihydroeugenol (47 %), 4-propylcyclohexanol (29 %), propylcyclohexane (14 %)	[15]
8	5 wt. % Pd/C	water	-	4 hours, 240℃ and 20 bar	2-methoxy-4-propyl-cyclohexanol, 2-methoxy-4-propyl-cyclohexanol, 4-propyl-cyclohexanol	[19]

As can be seen from Table 5, hydrogenated and partially deoxygenated products were obtained with full conversion of eugenol. In the first three entries, 1-hydroxy-2-methoxy-propylcyclohexane (89 % and 95 % respectively) was formed using Pd/C and Pt/C catalysts along the same reaction pathway during one hour of the reaction. On the other hand, Ru/C catalyst favoured dihydroeugenol (77 %) at the same reaction conditions using Pd/C and Pt/C catalysts. Considering entries 4-7, partial oxidation was observed over 4 wt.% Ru/C, giving similar products and the hydrodeoxygenated product such as propylcyclohexane after 3 hours of the reaction. With an increase of hydrogen pressure, the initial hydrogenation reaction becomes faster, and at the same time deoxygenation is less prominent [15]. Higher hydrogenation and deoxygenation rates can be seen in entry 4 than in entry 2 over Ru/C catalyst. Consequently, there are limitations at low and high hydrogen pressure, in the case of entries 2 and 7 respectively. In the case of 5 wt.% Pd/C, only hydrogenation occurred due to a low hydrogen pressure and the metal type.

Summarizing eugenol HDO, complete deoxygenation of eugenol is not easy even using Pd, Ru, Pt noble metal catalysts supported on alumina or carbon supports. While

a combination Ir and Re has not been applied in eugenol HDO yet, they have been demonstrated to be active in hydrodeoxygenation of high carbon furylmethane giving aviation fuel [20]. According to Chen et al. [21] and Amada et al. [22], Ir/ReO_x-SiO_2 catalyst resulted in hydrogenolysis of the C-O bond. Therefore, in this work, differently prepared rhenium modified iridium catalysts, supported on alumina, were utilized and tested in isoeugenol HDO. In addition, a combination of Pt and Re metals supported on alumina, carbon and zirconia were tested in isoeugenol HDO. Zirconia supported catalysts have not been applied in eugenol HDO previously, being previously utilized in guaiacol HDO.

1.3.2 HDO of guaiacol

Guaiacol, a phenolic compound with methoxy (-OCH_3) group, is obtained via isolation of Guaiac resin and from oxidation of lignin [23]. It is another attractive model compound for hydrodeoxygenation, which can be completely deoxygenated at high temperature or low temperature and a relative high pressure depending on the catalyst type [24]. Furthermore, blank test of guaiacol HDO at 250 ℃ and 100 bar demonstrated only 2 % of guaiacol conversion [25], therefore, the reaction is catalytically driven. It is known that guaiacol is strongly adsorbed on the catalyst surface [26]. Figure 3 demonstrates possible reaction pathways of guaiacol HDO where hydrogenation, demethoxylation and dehydration are taking place to produce cyclohexane.

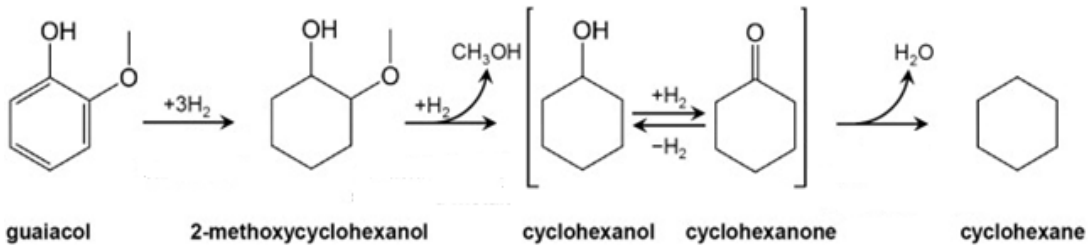

Figure 3 Hydrodeoxygenation reaction pathways of guaiacol adapted from [27].

During the experimental work in this thesis, two zirconia supported catalysts were utilized in guaiacol HDO to investigate their activity (Ir/ZrO_2 and 10 wt. % Ni/ZrO_2). Zirconium oxide exhibits both acidic and basic properties combined with high thermal and chemical stability [28]. However, it is still weaker in comparison with alumina [29]. Table 6 presents results from guaiacol HDO with ZrO_2 supported catalysts.

Table 6 Results of guaiacol HDO at different operational conditions using zirconia supported catalysts

En-try	**Cata-lyst**	**Sol-vent**	**Conver-sion of guaia-col, %**	**Operational conditions (reaction duration, temperature, pressure)**	**Main products (yield %)**	**Re-fe-renc e**
1	5 wt.% Ni/ZrO_2 -DR[a]	1-octanol	100	250℃ and 100 bar	Cyclohexanol (30 %), cyclohexane (1 %), 2-methoxycyclohexanol	
2	5 wt.% Ni/ZrO_2 -CR[b]		100	250℃ and 100 bar	Cyclohexanol (50 %), cyclohexane (30 %), 2-methoxycyclohexanol	
3	10 wt.% Ni/ZrO_2	dode-cane	44	8 h, 300℃ and 50 bar	Cyclohexane (75 %), phenol (10 %)	[30]
4	3 wt.% Rh/ZrO_2	n-de-cane	99	1 h, 250℃ and 40 bar	2-methoxycyclohexanol (89 %), cyclohexanol (5 %), cyclohexane (1 %)	[27]
5	5 wt.% Ru/ZrO_2	water	99	4 h, 170℃ and 40 bar	Cyclohexanol (58 %), 2-methoxycyclohexanol (36 %)	[31]
6	RhPt/ ZrO_2	n-hexa-decane	≈100	100℃, 80 bar	1-methyl-1,2-cyclohexanediol, cyclohexanol	[32]

[a]DR-directly reduced, [b]CR-calcined and reduced

As can be seen from Table 6, the reaction proceeds only in the presence of a catalyst converting guaiacol (conversion≥44 %) to such products as alcohol and cycloalkanes (entry 3). Calcined and reduced 5 wt.% Ni/ZrO_2 gave 30 % cyclohexane selectivity,

while without calcination only 1 % cyclohexane was formed, i.e. calcination is very important to activate the catalyst and enhance hydrodeoxygenation (entries 1 and 2). 10 wt.% Ni/ZrO_2 catalyst showed only 44 % of guaiacol conversion because high metal loading with selectivity of 75 % to cyclohexane. Application of 3 wt.% Rh/ZrO_2 and 5 wt.% Ru/ZrO_2 catalysts produced mainly hydrogenated products such as 2-methoxycyclohexanol (89 % and 36 % respectively) and cyclohexanol (5 % and 36 %). Bimetallic catalysts supported on zirconia produced high yields of alcohols while no deoxygenated compounds were formed (entry 6). Concluding available data on guaiacol HDO it can be stated that in order to achieve high selectivity to hydrodeoxygenated compounds, acidic catalysts, metal type and operational conditions are important, i.e. temperature should be more than 250℃.

1.3.3 HDO of vanillin

The main important constituent of vanilla, which is widely known as a food flavor, is vanillin, also called 4-hydroxy-3methoxybenzaldehyde, the compound containing three oxygen atoms in its structure [33]. It can be received from beans of the tropical Vanilla orchid [33]. Vanillin obtained synthetically is utilized in different fields not only in food industry but also for production of pharmaceuticals and chemicals [33]. Around 50 percent of vanillin production is used for latter ones [33]. Previously, commercially available synthetic vanillin was prepared from eugenol, while nowadays it can be produced from guaiacol or lignin [34]. A substantial part (85 %) of synthetic vanillin is produced from guaiacol via the Riedel process [35]. The rest of vanillin is generated from lignin (15 %) using the sulfite pulping process [35]. By hydrogenation and hydrogenolysis vanillyl alcohol and creosol can be obtained from vanillin [36-37]. The reaction pathways are shown in Figure 4. Hydrogenated and deoxygenated compounds can also be produced from vanillin such as methylcyclohexane and cyclohexane, as in the case when Ni/SiO_2-ZrO_2 catalyst yielded 65 % of methylcyclohexane and 31 % of cyclohexane at 300℃ and 30 bar [24]. Vanillin was not converted completely (conversion 83 %) over Ni/SiO_2-ZrO_2 at 300℃ and 50 bar [24].

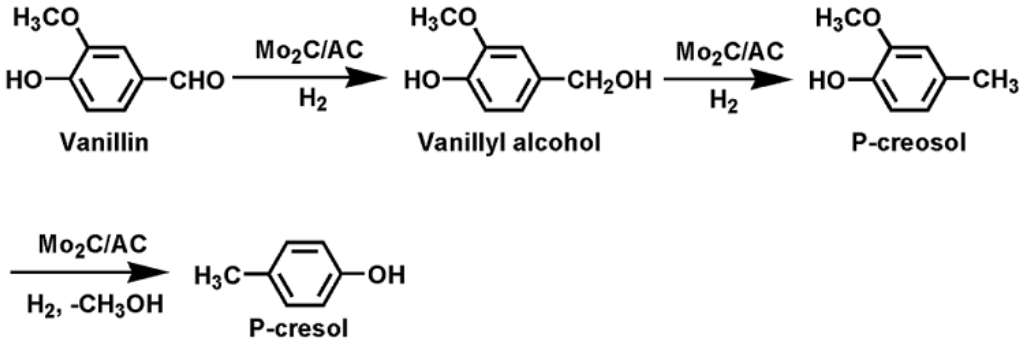

Figure 4 Hydrodeoxygenation reaction pathways of vanillin [38].

1.4 Objectives and scope

Transformations of bio-oil using hydrodeoxygenation brought a lot of attention as a way of valorization of bio-fuel to transportation fuels. In this work, mainly hydrodeoxygenation of isoeugenol process was investigated using Al_2O_3, ZrO_2 and C supported catalysts loaded with metals (IrRe, Ir, Re, Pt-Re, Pt). Guaiacol and vanillin HDO were also included to study the influence of ZrO_2.

Therefore, the following objectives were set to investigate isoeugenol HDO:

1. Characterize catalysts which were used in isoeugenol HDO such as specific surface area, acidity, etc.
2. Perform a thermal experiment to investigate non catalytic production of dihydroeugenol from isoeugenol.
3. Determine the optimum operational conditions for catalytic HDO of isoeugenol by varying reaction temperature at a constant total pressure of 30 bar.
4. Compare the performance of different metal containing catalysts supported on alumina, zirconia and carbon supports.
5. Investigate the pressure effect for the best catalysts at the optimum reaction temperature.
6. Perform repeatability and recyclability tests of the best catalysts at optimum operational conditions.
7. Determine the gas phase products using gas chromatography.

8. Compare HDO activity of zirconia supported catalysts using three different reactants (isoeugenol, guaiacol and vanillin).

2 Methods of catalyst characterization and reaction mixture analysis

2.1 Catalyst characterization methods

Studying the physical and chemical properties of the catalysts allows to understand and explain their behavior during the reaction. Therefore, the following characterization techniques were used, which will be described further:

1. Liquid nitrogen physisorption;
2. FTIR spectroscopy with pyridine adsorption/desorption for determination of acidity;
3. Scanning electron microscopy and X-Ray microanalysis (SEM-EDX);
4. Transmission electron microscopy (TEM);
5. Thermogravimetric analysis (TGA);
6. Size exclusion chromatography (SEC);
7. X-ray photoelectron spectroscopy (XPS).

2.1.1 Liquid nitrogen physisorption

Most heterogeneous catalysts are porous solids [39]. Pores are classified according to their size or diameter into the following three types [40]:

1. microporous (diameter less than 2 nm);
2. mesoporous (2-50 nm);
3. macroporous (more than 50 nm).

A well-established method used to measure the specific surface area and porosity of the catalysts is nitrogen physisorption [40]. This method is carried out at constant temperature of -196℃ enabling determination of the adsorption isotherm, thus providing information of the investigated porous solids [40]. High specific surface area of a support facilitates high dispersion of the active metals. Hence supports of high specific surface area are desirable. Pores are usually formed during drying or calcination of hydroxide precipitates or gels. The size and number of pores determine the internal surface area. Pore size also determines accessibility of the reactants to the active sites and ability of the product to diffuse back to the bulk fluid. Therefore, the

pore structure and surface area must be optimized to provide maximum utilization of active sites for a given feedstock.

Nitrogen physisorption was developed in the 1930s by Brunauer, Emmett and Teller, thus the method is called as the BET method [40]. The measurements include adsorption, followed by desorption at liquid nitrogen temperature [41].

Nowadays, this method is utilized extensively despite considerable drawbacks in the mathematical treatment, giving large differences between experimental data and the model predictions at higher relative pressures [40]. In order to avoid disadvantages of BET theory, the BET model is adequately used in the range of relative pressures 0.05±0.35 allowing calculation on the specific surface area [39]. For mesoporous solids the following method is utilized giving the monolayer volume of the adsorbate and specific surface area using the following formula [39]:

$$A_s = (V_m/22414) * A_m * N_a$$

where:

A_s - specific surface area, m^2/g;

V_m - monolayer volume, cm^3/g;

A_m - area occupied by one molecule, m^2/molecule;

N_a - Avogadro's number, $6.023*10^{23}$ molecules/mol.

For microporous materials, the Dubinin-Radushkevich isotherm model was applied. It relates the adsorbate volume and the monolayer volume as follows [40]:

$$V = V_m \, exp[-B \frac{RT^2}{\beta^2} * ln^2(\frac{p_0}{p})]$$

2.1.2 Fourier-transform infrared spectroscopy (FTIR) spectroscopy with pyridine adsorption/desorption for determination of acidity

Activity of solid catalysts during the reaction is influenced by the surface acid sites [42]. The Fourier-transform infrared spectroscopy (FTIR) of the adsorbed probe molecules is a widely used technique for distinguishing the Lewis and Brønsted acid sites on the surface of catalysts [43].

The modified Michelson interferometer is utilized for the spectrometer, which was developed by and named after Michelson [44]. It operates in such way that the transmitted infrared energy is divided into two in the beam splitter and the beams are sent to the fixed-position mirror and the moving mirror [44]. As the beams return back to the beam splitter, they are coalesced and one-half is addressed to the sample compartment, while the other comes back to the source [44]. The remaining light from the sample directed to the detector is measured and an interferogram is developed [44]. A fast Fourier transform is a mathematical calculation, developed by Fourier [44], which changes the interferogram (an encoded interference pattern) to an infrared spectrum of a single beam.

The probe molecules used for FTIR vary from strong to weak bases [43]. The strong bases are amines, ammonia and pyridine, while the weak bases are carbon oxide, carbon dioxide and hydrogen [43]. Since pyridine is a weaker base than ammonia, it associates with the sites comprehensively differing in acidity. According to [43], the benefit of the pyridine adsorption desorption method is that it can distinguish Lewis and Brønsted acid sites giving adsorption bands at 1455 cm^{-1} and 1545 cm^{-1} respectively.

2.1.3 Scanning electron microscopy and X-Ray microanalysis (SEM-EDX)

The scanning electron microscope (SEM) is one of the instruments to investigate and analyze the microstructure of solids on a nanometer (nm) to micrometer (μm) scale [45]. In addition, topographic photos can be acquired in the enlargement scale from 10 to 10,000x [45]. In order to make images and acquire analysis at a specific location, the part of interest is exposed to radiation with a highly focused electron beam [45]. SEM utilizes a beam of high energy electrons causing a variation of signals at the solid specimens surface [46]. The signals provide information about the morphology, chemical composition, crystalline structure and position of the sample constituents [46]. Electron microscopy combined with energy-dispersive spectrometer (EDX) provide qualitative and quantitative data of the components in a heterogeneous sample in the width of 1 μm and in depth of 1 μm [45]. In addition, EDS can recognize the characteristic X-rays of components above atomic number 4 and with heavy weight percentage of more than 10 wt.% [45].

2.1.4 Transmission Electron Microscopy (TEM)

Transmission Electron Microscopy (TEM) is comparable to SEM, having, however, much better ability of the specimen penetration [47]. The enlargement scale varies from 10^2 to 10^7 [40]. A specimen is placed on a copper grid, layered with a thin graphite, and then in a vacuum chamber. An electron beam of high voltage in the range of 100 keV to 300 keV is transmitted through the specimen using an electron gun [40]. A beam of electrons is speeded up by an anode, which is concentrated by the electrostatic and electromagnetic lenses, and passes through the sample which is to a certain extent transparent to electrons and to a certain extent scatters them out of the beam [40].

The constituents of the catalyst such as the precursor, support and supported phase are differentiated, if there is a clear difference in d-spacing of the specimen [40]. For instance, composites consisting of oxides are more difficult to discriminate than the composites containing metals [40]. In addition, the obtained images demonstrate the heavy weight compounds darker due to the sideways adsorption of the electron beam [40].

2.1.5 Organic Elemental Analysis (CHNS)

Elemental analysis is performed in order to identify carbon, hydrogen, nitrogen and sulfur content of different types of materials in solids, liquids and vapors [48].

In order to perform CHNS analysis a high burning temperature is needed which is obtained with a large amount of oxygen in the system [48]. The burning process can be conducted under steady or dynamic conditions, meaning that either a fixed amount of oxygen is introduced or oxygen is added continuously for a certain period of time [48]. The furnace operates at 1000℃, where carbon is oxidized to CO_2, hydrogen to H_2O, nitrogen to N_2 or nitrogen oxides, sulfur to SO_2. Afterwards, these burned products are removed with an inert gas (helium) and proceeded to the heated copper of high purity (of 600℃) which is used to withdraw unreacted oxygen and change nitrogen oxides into N_2 [48]. Later, the gases are routed to the adsorbent traps [48].

The essentials of CHNS analyzer are two gas stocks which are an inert carrier gas (e.g. helium) and super clean oxygen [48]. A need of pure oxygen is related to the requirement to decrease the nitrogen 'blank' input to an insignificant degree [48].

2.1.6 Thermogravimetric analysis

Thermal analysis is a method in which the influence of heating or cooling is investigated on the specimen indicating the physical changes against temperature variations [49].

Three approaches exist in the thermal analysis such as taking measurement of the specimen masses, so-called thermogravimetry; the speed of mass losses, so-called derivative thermogravimetry; and comparing and recording differences in the temperature between the specimen and a standard sample, so-called differential thermal analysis [49]. Basically, during heating of a compound at a constant speed the temperature is recorded versus one of the physical characteristics [49]. In addition, throughout the experiment, the atmosphere around the sample has to be maintained and be without any fluctuations using an inert gas (nitrogen), a reactive gas (air, oxygen) or vacuum [49]. Various materials can be analyzed such as inorganics, metals, organics, complex materials, etc. [50]. The temperature varies from 25 to 900℃ and 1000℃ or even 1600℃ depending on the requirements [50].

2.1.7 Coke extraction and size exclusion chromatography (SEC)

Coke formation is one of the main reasons for catalyst deactivation during hydrotreatment. In order to investigate the origin of coke, it is extracted from the spent catalysts [51]. This process can be carried out in the accelerated solvent extraction (ASE), Soxhlet extraction or by solvent evaporation [51]. ASE is considered as the leading efficient apparatus for coke removal [51]. Various solvents can be to acquire more information, such as heptane, toluene, tetrahydrofuran, pyridine, methanol or dichloromethane [51].

The size exclusion chromatography (SEC) can be applied, which is used to ascertain the morphology of the porous sample in the mixture using high performance liquid chromatography (HPLC) [52]. The solvent utilized for this procedure typically has

polarity varying from water to tetrahydrofuran (THF) [52]. The specimen is filled with dry or slurry techniques in the stainless steel tubes of chromatography.

The pores of the specimen strains the standardized probe molecules dissolved in the nonstationary phase [52]. Because there are no interactions between the solution and the sample, retention times of various molecules are associated with their movement through the pores [52]. Smaller molecules can go through the pores, while the larger molecules cannot [52], i.e. for the smaller molecules the retention time is longer [52].

2.1.8 X-ray photoelectron spectroscopy (XPS)

X-ray photoelectron spectroscopy is a multipurpose tool which can be used to investigate the surface of different types of materials such as metals, oxides, etc. [53]. The technique comprises a comprehensive energy analysis of electrons emitted from the specimen surface under high vacuum [53]. Such analysis allows to examine the composition and oxidation state of components [53]. The method utilizes 200-2000 eV X-rays to study the inner shell electrons at the core [53]**.** The origin of X-rays are Mg K_α with light radiation of 1253.6 eV and Al K_α with light radiation of 1486.6 eV [53].

There is a corresponding binding energy for each element connected with atomic orbitals at the core which results in the peaks formation in the spectrum at the corresponding energies, demonstrating existence of a particular element in the specimen [53]. The peak intensity is directly proportional to the concentration of an element in the sample [53]. The XPS measures all compounds exhibiting atomic percentage more than 0.5, excluding hydrogen and helium [53]**.** Therefore, it is also known as Electron Spectroscopy for Chemical Analysis (ESCA) [53].

2.2 Analysis of the reaction mixtures

In order analyze the composition of the reaction mixtures, the following characterization techniques are usually used:

1. Gas chromatography for liquid and gas phases;
2. Gas chromatography/mass spectrometry;
3. High performance liquid chromatography (HPLC).

2.2.1 Gas chromatography for liquid and gas phases

Gas chromatography (GC) is a tool in which gases per se or evaporated liquids are transported by the carrier gas (e.g. hydrogen or helium) through a column. In order to differentiate the constituents of sample a stationary phase is utilized along a mobile phase [54]. Capillary columns are favored for efficient separation of different species [55].

2.2.2 Gas chromatography/mass spectrometry

Gas chromatography combined with a mass spectrometer detector is a very powerful tool [55], allowing identification of compounds in various mixtures [56].

In GC-MS the electron ionization ion source is utilized to create ions [55]. Tungsten wire heated for the analysis emits the electrons, which are speeded up into the ion source chamber by exerting the difference of potentials (from 50 to 70 eV) between the fiber and the chamber producing kinetic energy [55]. Neutral molecules in the sample interact with negatively charged particles (electrons) to take away electron and generating positively charged molecular ions [55]. Since the first ionization energy is ca. 10 eV, molecules with a net electric charge created in the electron ionization ion source possess surplus internal energy, and therefore, disintegration is followed to scatter that energy [55]. This results in a mass spectrum considered as a fingerprint of a molecule, allowing its identification.

2.2.3 High performance liquid chromatography (HPLC)

High performance liquid chromatography, also known as high pressure or high speed liquid chromatography, enhances efficiency of the column due to the pressure introduced at the liquid feed line to the column [57]. Pressure applied in HPLC varies in the range of 0.1-345 bar [57]. Influence of temperature in the liquid chromatography is minor [57]. Stationary phases of the packing are designed to resist high pressures [57]. This phase could be an adsorbent, a substance infused with a high boiling fluid, an ion exchange substance or an extremely permeable nonionic gel [57]. The moving phase could be H_2O, salty mixtures, different types of organic solvents, etc. [57].

3 Experimental

3.1 Chemicals and catalysts

3.1.1 Chemicals

Chemicals which were acquired from the commercial sources and used without any further purification in this work are listed in Table 7.

Table 7 Chemicals utilized in this work

Entry	Chemical	Purity, %	Supplier
1	isoeugenol (cis+trans)	≥98	Fluka
2	isoeugenol (cis+trans)	98	Aldrich
3	guaiacol	≥98	Fluka
4	vanillin	≥98	Fluka
5	dodecane	≥99	Alfa Aesar
6	dihydroeugenol	≥99	Sigma-Aldrich
7	2-propanol	≥99.8	Sigma-Aldrich
8	diisopropyl ether	≥99.7	Sigma-Aldrich
9	benzene	≥99	Sigma-Aldrich
10	cyclohexane	99	Lab Scan
11	heptane	≥99	Sigma-Aldrich
12	2,5-dimethylhexane	99	Sigma-Aldrich
13	2-hexanol	99	Aldrich
14	octane	≥99	Fluka
15	propylcyclohexane	99	Aldrich
16	mesitylene	98	Sigma-Aldrich
17	diethylbenzene	≥95	Fluka
18	vanillin alcohol	≥98	Sigma-Aldrich
19	tetrahydrofuran	≥99.9	Sigma-Aldrich

Calibration gases from AGA were utilized to identify gaseous products obtained in isoeugenol and guaiacol HDO at 250℃ and 30 bar. Two different mixtures of gases with their composition are given in Table 8.

Table 8 Gas mixtures applied for identification of gas phase reaction products

Entry	Gas Mixture	Content, vol.%	Manufacturer
1	Carbon dioxide Ethylene Ethane Methane Helium	1.00 0.099 0.972 1.02 basic gas	AGA

Entry	Gas Mixture	Content, vol.%	Manufacturer
2	Methane	1.00	AGA
	Ethane	1.03	
	Propane	0.981	
	Iso-butane	0.983	
	N-butane	0.960	

3.1.2 Synthesis of catalysts

Most of the provided catalysts were synthesized by Dr. Irina Simakova at Boreskov Institute of Catalysis (Novosibirsk, Russia) such as Ir/Al_2O_3, Re/Al_2O_3, $IrRe/Al_2O_3$-DP, $IrRe/Al_2O_3$-Impr2, $IrRe/Al_2O_3$-Impr1, Pt/Al_2O_3, Ir/C (rbb), 3 wt.% Pt-3 wt.% Re/Al_2O_3, PtRe/C-31, PtRe/C-13, Ir/ZrO_2 and 10 wt.% Ni/ZrO_2.

3.1.2.1 Synthesis of metal catalysts supported on alumina

Pt/Al_2O_3, Ir/Al_2O_3, Re/Al_2O_3 catalysts were synthesized applying precursors such as H_2PtCl_6 (0.1 M), H_2IrCl_6 (0.5 M), $HReO_4$ (1 M) respectively to γ-Al_2O_3 aqueous suspension, followed with drying overnight for 17 hours at 110°C. Reduction was performed at 400°C (Pt/Al_2O_3 and Re/Al_2O_3) and 420°C (Ir/Al_2O_3) for 3 hours with the temperature ramp of 2 °C/min.

$IrRe/Al_2O_3$ catalyst was prepared in three different ways. $IrRe/Al_2O_3$-DP (IRA-DP) catalyst was synthesized using the deposition-precipitation method, while the synthesis of $IrRe/Al_2O_3$-Impr2 and $IrRe/Al_2O_3$-Impr1 was performed using incipient wetness impregnation. For synthesis of IRA-DP, H_2IrCl_6 (0.5 M) was deposited-precipitated with Na_2CO_3 (1 M) and further reduced with formic acid at 80°C. Thereafter, the catalyst was washed, dried at 110°C through the night and reduced in hydrogen flow for three hours at 400°C (temperature ramp of 2°C/min). In the next stage it was impregnated with $HReO_4$, dried and reduced at 420°C for three hours (temperature ramp 2°C/min).

For synthesis of $IrRe/Al_2O_3$-Impr2 and $IrRe/Al_2O_3$-Impr1 catalysts initially alumina (Al_2O_3, S_{BET}=146 m^2/g) was impregnated with H_2IrCl_6 and dried overnight in an oven at 110°C. Thereafter, the catalyst was calcined at 500°C for four hours. This sample was divided into two parts to prepare $IrRe/Al_2O_3$-Impr2 and $IrRe/Al_2O_3$-Impr1. The

first part of the catalyst was reduced at 450℃ for three hours with the temperature ramp of 2 ℃/min and afterwards, it was impregnated with $HReO_4$. Denoted as $IrRe/Al_2O_3$-Impr2 (IRA-Impr2), this sample was dried at 110℃ and reduced at 417℃ for three hours. Denoted $IrRe/Al_2O_3$-Impr1 (IRA-Impr1) was directly impregnated with $HReO_4$, afterwards dried at 110℃ and reduced for three hours at 417℃.

3 wt.% Pt-3 wt.% Re/Al_2O_3 was prepared by consecutive impregnation of γ-Al_2O_3 with $HReO_4$ and H_2PtCl_6. After impregnating γ-Al_2O_3 with $HReO_4$, the sample was first dried at 110℃ for 17 hours, thereafter impregnated with H_2PtCl_6 followed by drying at 110℃ for 17 hours. The dried mixture containing rhenium and platinum was reduced at 400℃ for 3 hours (temperature ramp 2℃/min).

3.1.2.2 Synthesis of metal catalysts supported on zirconia

For zirconia supported catalysts, $Ni(NO_3)_2$ $6H_2O$ (≥98.0%, GOST 405570, Souzchimprom, Novosibirsk), $IrCl_3$ hydrate (TU 2625-067-00196533-2002 OAO "V.N. Gulidov Krasnoyarsk factory of nonferrous metals, Krasnoyarsk), zirconia (Acros Organics, S_{BET}= 106 m^2/g) were utilized.

Zirconia was pre-calcined in air at 500℃ for 2 hours prior to the catalysts preparation.

Ir/ZrO_2 catalyst was synthesized using the incipient wetness impregnation method with an aqueous solution of iridium (III) chloride hydrate, followed by drying at 110℃ for 17 hours and reduction with hydrogen at 400℃ (temperature ramp rate 2℃/min) for three hours.

10 wt.% Ni/ZrO_2 catalyst was prepared using the incipient wetness impregnation procedure with an aqueous solution of $Ni(NO_3)_2$. Afterwards, it was dried at 110℃ and calcined in air at 540℃ for two hours. The catalyst was then reduced under molecular hydrogen at 450℃ (temperature ramp rate 2℃/min) for 3 hours.

3.1.2.3 Synthesis of metal catalysts supported on carbon

PtRe/C-13, 3 wt.% Pt-1 wt.% Re/C (S_{BET}=317.5 m^2/g and pore volume=0.38 cm^3/g) were synthesized using an impregnation method applying various mesoporous Sibunit carbon supports (with variation in specific surface area and pore volume). The carbon

mix is washed with HCl and afterwards with distilled water to contamination, followed with impregnation. For 3 wt.% Pt-1 wt.% Ir/C the size range of carbon support was from 100 to 200 μm.

5 wt.% Ir/C catalyst was synthesized via impregnation where the solution of $IrCl_4$ precursor is added to the carbon support (10 g) with water (15-20 cm^3) [58]. When the catalyst slurry became acidic, sodium carbonate was added to create hydroxyl groups on the support and make their reduction easier [58]. In order to stop the metal coagulation sodium acetate was added. The catalyst was chemically reduced by adding drop-wise formic acid under agitation at 90℃ for 1 hour [58]. When the mixture was cooled to room temperature, it was taken for the qualitative investigation to confirm absence of chloride ions [58].

3.1.3 Catalyst reduction

Prior to HDO of isoeugenol, guaiacol and vanillin, the fresh catalysts were reduced with hydrogen (AGA, 99.999 %) one day before. First, 50 mg of catalyst was flushed with argon flow for 10 minutes and then with hydrogen for 10 minutes. The program was set to heat up from room temperature to 350℃ in 33 minutes (with temperature ramp of 10℃/min) and keep at 350℃ for 3 hours under hydrogen flow. Afterwards, as the program was completed and temperature cooled to 100℃, the catalyst was flushed with argon (AGA, 99.999 %) for 10 minutes and 10 ml of solvent (dodecane) was added onto the catalyst and kept overnight.

3.1.4 Regeneration of the catalyst for reproducibility tests

Reproducibility tests were performed for two catalysts such as $IrRe/Al_2O_3$-DP and $IrRe/Al_2O_3$-Impr1. After isoeugenol HDO at 250℃ and 30 bar the spent catalyst was washed with acetone and dried in air. Thereafter, it was calcined. The temperature programme utilized for the spent catalyst is given in Table 9.

Table 9 Calcination temperature program used for regeneration of IRA-DP and IRA-Impr1 catalysts

Duration, min	**Temperature,** ℃
65	150
40	150

75	400
180	400
100	25
0	0

3.1.5 Reactor setup

Hydrodeoxygenation of isoeugenol, guaiacol and vanillin was performed using 300 ml cylindrical stainless steel batch reactor (PARR Instruments) equipped with an axial mechanical stirrer. Sampling occurred through a sampling line, first by purging to clean the line, and then by taking ca. 0.8 ml into 4 ml vial. Afterwards, the liquid sample was filtered and placed in the GC vial. Argon (AGA, 99.999%) and hydrogen (AGA, 99.999%), as used in Section 4.1.2, were connected to the reactor for flushing and hydrogenation respectively. Heating of the reactor occurred using a heating mantle. The temperature was efficiently kept within ±1℃, since the reactor was equipped with an automatic temperature control system in which a cooling coil connected to tap water was located inside the reactor. The stirring speed was 900 rpm to suppress mass transfer limitations.

Typically, for HDO of isoeugenol and guaiacol, 50 mg of catalyst, 100 mg of the reactant (isoeugenol or guaiacol) and 50 ml of dodecane were used. Liquid and gas samples were taken (7x) during experiments and analyzed by GC and GC/MS.

For HDO of vanillin 50 mg of a catalyst, 100 ml of water and 50 mg of vanillin were utilized. The liquid samples (7x) were analyzed by HPLC.

3.2 Methods of catalyst characterization and analysis of the reaction mixture

3.2.1 Catalyst characterization methods

3.2.1.1 Liquid nitrogen adsorption

Liquid nitrogen physisorption was performed using Carlo Erba Sorptomatic 1900 device in order to measure the specific surface area and pore volume of the catalysts. Based on the catalyst structure, two programs were applied for the analysis, BET for mesoporous and Dubinin-Radushkevich for microporous catalysts. For the catalysts

containing alumina and zirconia supports the mesoporous program was used, while for carbon both programs were utilized depending on the type of support.

Ca. 0.2 gram of the catalyst was heated at 150℃ and a pressure below 8 mbar for three hours in an earlier outgassed burette. This procedure is done to remove moisture and organic compounds. Afterwards, the burette with the catalyst was cooled down and placed in liquid nitrogen for the physisorption analysis.

3.2.1.2 FTIR spectroscopy with pyridine adsorption/desorption for determination of acidity

Using FTIR spectroscopy the Brønsted and Lewis acid sites in the catalysts were determined. The device for identification of acidity was ATI Mattson FTIR with pyridine as a probe molecule (Sigma-Aldrich, ≥99.5%, a.r.). A catalyst sample was pressed into a thin pellet with the weight in the range between 10 and 20 mg. The prepared pellet was located in the spectrometer cell for one hour outgassing in vacuum at 450℃. Thereafter, the sample was cooled down to the set temperature of 100℃, followed by adsorption of pyridine on the pellet surface for 30 min and then recording the scanned spectra. Subsequently, to obtain the acid strength distribution such as weak, medium and strong Brønsted and Lewis acid sites, thermal desorption of pyridine was performed at 250℃, 350℃ and 450℃. The spectral bands integrated at 1455 cm^{-1} and 1545 cm^{-1} provided data on the Brønsted and Lewis acid sites concentrations using the extrusion coefficients of Emeis [59].

Acidity of some other catalysts was determined in a different way due to inability to press a thin pellet of 10-20 mg. Namely 50 mg of catalyst was placed in 50 ml of distilled water under agitation with a magnetic stirrer. After mixing for ca. one or two minutes the pH of catalyst slurry was measured using pH electrode Mettler Toledo.

3.2.1.3 Scanning electron microscopy and X-Ray microanalysis (SEM-EDX)

The scanning electron microscopy coupled with energy dispersive X-ray analyzer was utilized to obtain information on the morphology and elemental analysis of the fresh and spent catalysts. Zeiss Leo Gemini 1530 microscope was combined with secondary electron and backscattered electron detectors. Acceleration voltage of 15 kV was used for the X-ray analyzer. In order to perform analysis, the catalyst was placed as a thin

layer on top of the carbon coating to enhance conductivity allowing high quality of magnified images.

3.2.1.4 Transmission Electron Microscopy (TEM)

Transmission electron microscopy was utilized to study the metal particle size. JEM-1400Plus (by JEOL ltd. Japan) with 120 kV maximal acceleration voltage was applied. Interpretation of TEM images and determination of particle sizes of the fresh and spent catalysts were done using ImageJ software.

3.2.1.5 Organic elemental analysis (CHNS)

ThermoFisher Scientific Flash 2000 – Combustion CHNS/O analyzer was used to quantify such elements as carbon, hydrogen, nitrogen and sulfur in the fresh and spent catalysts.

3.2.1.6 Thermogravimetric analysis (TGA)

Thermogravimetric characterization of the fresh and spent catalysts was carried out using SDT Q600 (V20.9 Build 20) instrument. Depending on the support the gas atmosphere was chosen, e.g. air and nitrogen were utilized alumina, while only nitrogen was used for zirconia and carbon supports. Ca. 7 mg of the catalyst was placed on an aluminum oxide pan as well as on an empty pan as a reference and heated from room temperature to 1000℃ (temperature ramp - 10℃/min). The volumetric gas flowrate was 100 ml/min.

3.2.1.7 Coke extraction and size exclusion chromatography (SEC)

In order to perform size exclusion chromatography identifying the existence of oligomers and polymers on the catalyst surface, coke extraction from the spent catalysts was performed using heptane as a solvent [51]. The spent catalyst of 10-20 mg was placed in the round bottom boiling flask of 25 ml with a magnetic stirrer and a reflux cooler. Thereafter, 20 ml of heptane (Sigma-Aldrich, ≥99%) was added to the flask. Extraction of the spent catalyst was performed for 4 hours at 125℃, which is higher than the boiling point of heptane (98.4℃). The stirring speed was 375 rpm.

The mixture was poured into 50 ml beaker (placed in a bigger beaker of water) heated below with 40℃. The procedure was run under the nitrogen flow until the extractive

agent (heptane) was completely evaporated. Thereafter, the organic residue was dissolved in 10 ml tetrahydrofuran to obtain organic material of ca. 2 mg/ml. The sample was then placed into the GC vial for SEC analysis. The sample from the vial was filtered with 0.2 mm membrane filter PTFE and analyzed by SEC-HPLC supplied with two columns, i.e. Jordi Gel DVB 500A (300×7.8 mm) and Guard column (50×7.8 mm). The flowrate and temperature were 0.8 ml/min and 40℃ respectively. The air pressure was 3.5 bar. Some monomers can be evaporated and thus the analysis is not fully quantitative.

3.2.1.8 X-ray photoelectron spectroscopy (XPS)

Perkin-Elmer PHI 5400 spectrometer was used for the fresh and spent catalysts. The source of X-ray was operated at 14 kV and 200 W. The pass energy of the analyzer was 35.45 eV and the energy step was 0.1 eV. The fitting of the peak was performed using XPS Peak 4.1 program and the correction of the background was done applying the Shirley function. The sensitivity factors applied in the quantitative analysis of Al2p, O1s, Re4f and Ir4f were 0.234, 0.711, 3.961 and 5.021 respectively. Al2p (74.4 eV) was utilized as the reference to account for possible charging (Appendix VI).

3.2.2 Reaction mixture analysis

3.2.2.1 Gas chromatography for liquid phase samples

For each experiment on HDO of isoeugenol and guaiacol seven liquid samples were taken for the gas chromatography analysis. DB-1 capillary column (Agilent 122-103e) of 30 m length, 250 μm internal diameter and 0.5 μm film thickness was utilized for GC analysis. Helium (AGA, 99.996 %) was applied as a carrier gas with the flowrate of 1.7 ml/min. The injector temperature was at 60℃ and this temperature was kept for five minutes. Thereafter, the temperature ramping of 3℃/min was used to reach 135℃ and the temperature ramping of 15℃/min to 300℃.

External calibration standards (in Table 7) were utilized for calibration of the compounds obtained from GC. A list of these compounds with corresponding retention times is shown in Table 10.

Table 10 GC retention times of compounds present in the reaction mixtures in isoeugenol and guaiacol HDO

Entry	Compound	Retention time, min
1	2-propanol	1.6
2	diisopropyl ether	2.1
3	benzene	2.5
4	cyclohexane	2.6
5	heptane	3.1
6	2,5-dimethylhexane	3.6
7	2-hexanol	4.8
8	octane	5.3
9	propylcyclohexane	10.5
10	mesitylene*	11.8-11.9
11	diethylbenzene	15.94, 16.25, 16.51
12	guaiacol	17.3
13	dihydroeugenol	31.1
14	isoeugenol (cis+trans)	33.1

mesitelyne*- used calibration as a proxy for 1,2,4-trimethylbenzene appearing at the same retention time.

3.2.2.2 Gas chromatography of gas phase samples

For HDO isoeugenol and guaiacol the gas samples of 1 ml were taken at 0, 1, 30, 60, 120, 180 and 240 minutes of experiment. Agilent 6890N-GC equipped with HP-PLOTQ capillary column (30 m ×530 μm ×40 μm). The temperature program used to identify the composition of gas samples was as follows: holding time 8 min at 350℃, followed by ramping 20℃/min up to 150℃ and holding for 30 min. The pressure and temperature were respectively 1.03 bar and 250℃ and the total gas flow was 55.2 ml/min (with the split ratio of 5:1). Detection was done by FID (300℃) and TCD (250℃).

Identified compounds are presented in Figure 5 with the corresponding retention times.

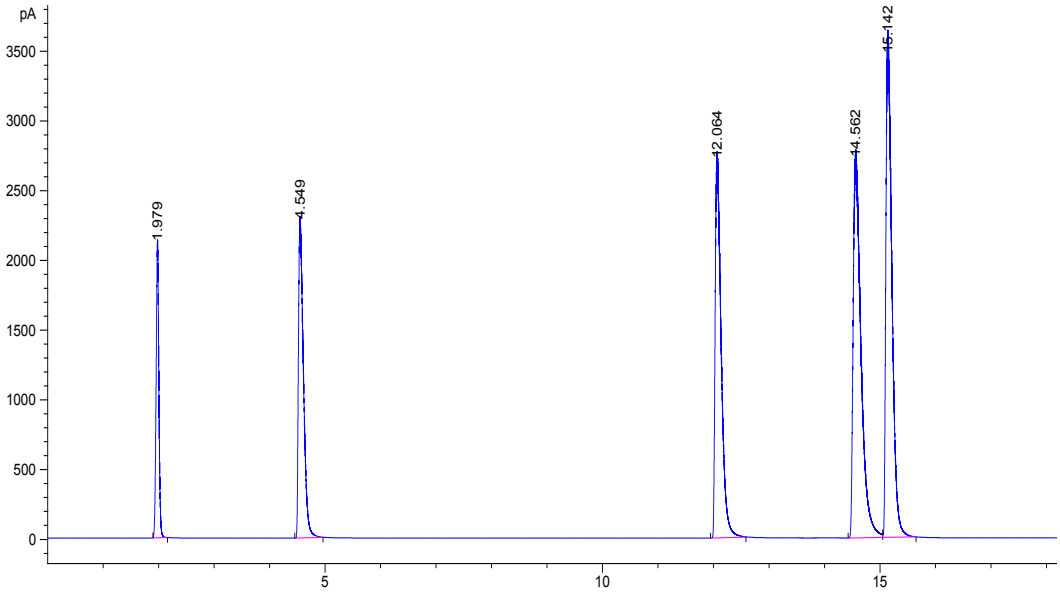

Figure 5 GC retention times for gas compounds present in the gas sample obtained after HDO of model compounds such as isoeugenol and guaiacol (abundance vs time (min)). Notation: Retention times for different gases 1.98-methane (FID), 4.55-ethane (FID), 12.06-propane (FID), 14.56-iso-butane (FID), 15.14-n-butane (FID) and 2.51-carbon dioxide (TC).

3.2.2.3 Gas chromatography/mass spectrometry

Gas chromatography/mass spectrometry was used to identify the compounds at retention times appeared in GC analysis (qualitatively and quantitatively). The same capillary columns were utilized for GC/MS and GC analysis with helium as a carrier gas. The pressure and temperature were 0.8 bar and 250℃ and the total gas flow was 19.3 ml/min (the split ratio of 15:1).

At the beginning, holding of 5 min at the inlet temperature of 60℃ for the liquid and gas samples was applied, however, later temperature was changed to 40℃ for gas to have a better separation of methane, ethane and propane. Thereafter, temperature ramping of 3℃/min up to 135℃ and ramping of 15℃/min up to 300℃ (holding of 30 min) were applied to analyze the sample.

3.2.2.4 High performance liquid chromatography

High performance liquid chromatography was applied for analysis of the samples obtained in HDO of vanillin. HPLC from Agilent Technologies 1100 Series was supplied with a UV-Vis photo diode array detector (273 nm) and a quaternary pump [60]. The column was Ultra Techsphere ODS-5u (C18) (250 mm × 4.6 mm). The non-

stationary phase was a mix of methanol and 0.5 % phosphoric with the flowrate of 0.400 ml/min. The program set for the flow of the mixture (methanol + 0.5 % phosphoric acid) at a certain time is given in Table 11.

Table 11 HPLC program for samples obtained in vanillin HDO

Time, min	Methanol, %	0.5 % Phosphoric acid, %
10	15	85
18	25	75
25	70	30
30	100	0
35	0	100

External calibration standards such as vanillin and vanillyl alcohol have retention times of 30.4 min and 23.8 min respectively [60].

3.3 Definitions

Gas chromatography based sum of the reactants and products in the liquid phase analysis (GCLPA) was calculated as follows:

$$GCLPA = \frac{GCLPA_t}{GCLPA_0} * 100\%$$

where, $GCLPA_0$ – initial gas chromatography based sum of the reactants and products in the liquid phase analysis;
$GCLPA_t$ - gas chromatography based sum of the reactants and products in the liquid phase analysis at time t.
The rest of compounds which could not be detected in the liquid phase are either non-volatile liquid products not eluting from GC, gas phase products and heavy compounds adsorbed on the catalyst.

Conversion of the reactant was calculated using the following equation:

$$X_{a,t} = \frac{C_0 - C_i}{C_0} * 100\%$$

where, $X_{a,t}$ – conversion of reactant at time t, %;

$C_{a,0}$ - initial molar concentration of the reactant, mol/l;

$C_{a,t}$ - molar concentration of the reactant at time t, mol/l.

Selectivity was calculated according to:

$$S_{i,t} = \frac{C_{i,t}}{\sum C_{i+J+f+\cdots,t}} * 100\%$$

where, $S_{i,t}$ – selectivity to product I at certain conversion, %;

$C_{i,t}$ – molar concentration of the product I at a particular conversion, mol/l;

$C_{i+j+f+\ldots,\,t}$ – molar concentration sum of all products at the same conversion, mol/l.

Hydrodeoxygenation degree (%) was evaluated to observe the performance of each catalyst in isoeugenol HDO:

$$HDO = \frac{n_a^0 - n_a^t - \sum n_i * m_o}{n_a^0 - n_a^t} * 100\%$$

where, n_a^0 - initial amount of the reactant, mol;

n_a^t - amount of the reactant at contact time t, mol;

n_i - amount of i−product in the liquid phase, mol;

m_o – the number of oxygen atoms in a molecule of i−product.

4 Results and Discussion

4.1 Catalysts characterization results

Various characterization techniques were utilized for prior reduced catalysts (so called fresh) to isoeugenol HDO and spent catalysts. Reduced catalysts were analyzed using nitrogen physisorption, FTIR spectroscopy, SEM-EDX, TEM, CHNS (specifically IRA series and Ir/C (rbb)), TGA (IRA-Impr1, Ir/C (rbb), Ir/ZrO_2 and 10 wt.% Ni/ZrO_2) and XPS (IRA series). The spent catalysts of interest were characterized using nitrogen physisorption, SEM-EDX, TEM, CHNS (specifically IRA series and Ir/C (rbb)), coke extraction (IRA-Impr1), TGA (IRA-Impr1, Ir/C (rbb), Ir/ZrO_2 and 10 wt.% Ni/ZrO_2) and XPS (IRA series).

4.1.1 Liquid nitrogen physisorption

Nitrogen physisorption results are presented in Table 12.

Table 12 Specific surface area and pore volume of catalysts by N_2 physisorption

Catalyst	**Specific surface area, m^2/g**	**Pore volume, cm^3/g**
Catalysts with alumina support (mesoporous)		
IrRe/Al_2O_3-DP (fresh) (IRA-DP)	101	0.20
IrRe/Al_2O_3-DP (spent)	101	0.19
IrRe/Al_2O_3-Impr2 (IRA-Impr2)	216	0.76
IrRe/Al_2O_3-Impr1 (fresh) (IRA-Impr1)	215	0.70
IrRe/Al_2O_3-Impr1 (spent)	203	0.72
Ir/Al_2O_3 (IA)	101	0.21
Re/Al_2O_3 (RA)	150	0.53
3 wt.% Pt-3 wt.% Re/Al_2O_3 (PRA-33)	243	0.74
Catalysts with zirconia support (mesoporous)		
Ir/ZrO_2	91	0.24
10 wt.% Ni/ZrO_2	108	0.04
Catalysts with carbon support		
Ir/C (rbb) (mesoporous)	158	0.06

PtRe/C-31 (PRC-31) (microporous)	332	0.12
PtRe/C-13 (PRC-13) (microporous)	279	0.10

Specific surface area of 3 wt.% Pt-3 wt.% Re/Al_2O_3 was the highest (243 m^2/g) (Table 12), while the lowest ones were displayed by Ir/Al_2O_3 and $IrRe/Al_2O_3$-DP. According to Samain et al. [61], the commercial mesoporous alumina has a specific surface area of 250 m^2/g, which is the closest to PRA-33. Therefore, influence of the preparation method as well as the metal loadings can be observed in lower specific surface areas of IRA-DP, IRA-Impr2 and IRA-Impr1. The specific surface areas of the impregnated catalysts are almost the same and twofold higher than the deposited-precipitated one (101 m^2/g). The same tendency can be seen in the pore volume of the catalysts, e.g. being more than three times higher for IRA-Impr2 and IRA-Impr1 than for IRA-DP.

For 10 wt.% Ni/ZrO_2 via the impregnation method the specific surface area was 108 m^2/g while its pore volume was very low (0.04 cm^3/g). On the other hand, Ir/ZrO_2 catalyst contained a higher pore volume (0.24 cm^3/g). According to Zhang et al. [30], deposited-precipitated 10 wt.% Ni/ZrO_2 had a specific surface area of only 6.2 m^2/g. According to Mortensen et al. [62], 5 wt.% Ni/ZrO_2 prepared by incipient wetness impregnation had 130 m^2/g of the specific surface area. Therefore, catalysts made via the impregnation method have larger specific surface areas (>100 m^2/g), while, deposition precipitation method gave very low values.

The highest specific surface area (332 m^2/g) and the pore volume (0.12 cm^3/g) among carbon supported catalysts can be observed for PRC-31, i.e. allowing good accessibility to the active sites in pores of this catalyst. PRC-13 catalyst showed a bit lower specific surface area (279 m^2/g) and almost the same specific pore diameter 0.10 cm^3/g. The carbon support of these catalysts is Sibunit, which specific surface varies between 450 and 500 m^2/g, according to ECN [63]. In above cases of bimetallic catalysts the surface areas were diminished with introduction of the metals.

According to the EDX results, Ir/C (rbb) has mesoporous analysis, thus a nitrogen physisorption data were treated with the BET equation giving 158 m^2/g for specific surface area and 0.06 cm^3/g for the pore volume. Based on Puskás et al. [64], commercial activated carbon (CAC) carbonized at 900℃ possesses a specific surface

area of 625 m^2/g using BET analysis. Therefore, surface areas of carbon materials can be significantly affected by the preparation method and the metal type.

4.1.2 FTIR spectroscopy with pyridine adsorption/desorption for determination of acidity

Pyridine adsorption desorption results showed that majority of the catalysts exhibited weak acid sites (Table 13), except IRA-Impr1 and PRA-33 which also contain medium and strong acid sites and IRA-Impr2 and 10 wt.% Ni/ZrO_2 containing medium acid sites.

The highest acidity among the weak Brønsted and Lewis acid sites was exhibited by 10 wt.% Ni/ZrO_2 (70 and 398 $\mu mol/g_{cat}$ correspondingly). This is in line with the work of Moreterra et al. [65], who observed a prominent presence of Lewis acid sites in zirconia.

Table 13 Brønsted and Lewis acid sites determined by FTIR

Catalyst	**Brønsted acid sites ($\mu mol/g_{cat}$)**			**Lewis acid sites ($\mu mol/g_{cat}$)**		
	250°C	350°C	450°C	250°C	350°C	450°C
Catalysts with alumina support						
IRA-DP	19	0	0	0	0	0
IRA-Impr2	10	1	0	109	9	0
IRA-Impr1	1	1	1	106	1	0
PRA-33	16	0	0	88	4	1
Catalysts with zirconia support						
Ir/ZrO_2	1	0	0	157	0	0
10 wt.% Ni/ZrO_2	70	0	0	398	1	0

The results of catalyst acidities obtained by measuring pH of the catalyst slurries (Table 14). The highest acidity was displayed by Ir-C (rbb) with a high metal loading of 4.8 pH. PtRe-C-31 and PtRe-C-13 exhibited neutrality with pH of ca. 6.

Table 14 The pH of catalysts via slurry method

Catalyst	**pH**
Ir/C (rbb)	4.8
PtRe/C-31	6.1

PtRe/C-13	6.0

4.1.3 Scanning electron microscopy and X-Ray microanalysis (SEM-EDX) and Transmission Electron Microscopy (TEM)

4.1.3.1 TEM images, histograms and particle sizes

Transmission electron microscopy allows to analyze the morphology and variation of the active metal cluster sizes of the fresh and spent catalysts used in isoeugenol HDO. The results of this analysis are presented in Table 15.

Table 15 Metal particle sizes of catalysts determined from TEM images

Catalyst	Particle size of fresh, nm	Particle size of spent, nm
Catalysts with alumina support		
IrRe/Al_2O_3-DP	0.9 (HR-TEM)	1.9
IrRe/Al_2O_3-Impr2	0.9 (HR-TEM)	1.4
IrRe/Al_2O_3-Impr1	0.7 (HR-TEM)	0.7
Re/Al_2O_3	3.6	5.3
PtRe/Al_2O_3	3.4	2.8
Catalysts with zirconia support		
Ir/ZrO_2	1.3	2.2

As can be seen from Table 15, despite different synthesis methods IRA-DP and IRA-Impr2 exhibited the same particle size, i.e. 0.9 nm analyzed by high resolution transmission electron microscopy (HR-TEM). On the other hand, slightly smaller metal particles (0.8 nm) were found in IRA-Impr1, prepared via consecutive impregnation of Ir and Re precursors, while slightly larger metal particles (1.0 nm) were present in IRA-Impr2, in which the Ir-supported precursor was reduced prior to impregnation of $HReO_4$. TEM for the spent catalysts used in isoeugenol HDO showed that iridium metal particle sizes varied in the range of 0.7 – 1.9 nm in IRA series catalysts (Table 15). The size range of metal particles in IRA-DP increased slightly due to appearance of agglomerates in the spent catalyst. It should, however, be noted that it is difficult to directly compare the metal particle sizes for the fresh and spent catalysts since different TEM equipment was used. TEM images with particle size distribution histograms are presented in Figures 6-8 for IRA series catalysts (more in Appendix III). The shape of iridium and rhenium of IrRe/Al_2O_3-DP varies being

circular to oval in Figure 6. Extensive sintering of the metal particles, especially in IRA-Impr2 is, however, not probable due to a rather low HDO temperature. TEM images of IRA-Impr1 (Figure 8) revealed presence of some needle shaped large agglomerates with the size varying from ca. 150 nm to 1100 nm in the fresh and spent catalysts. This type of agglomeration was not detected for IRA-1 and IRA-2 catalysts.

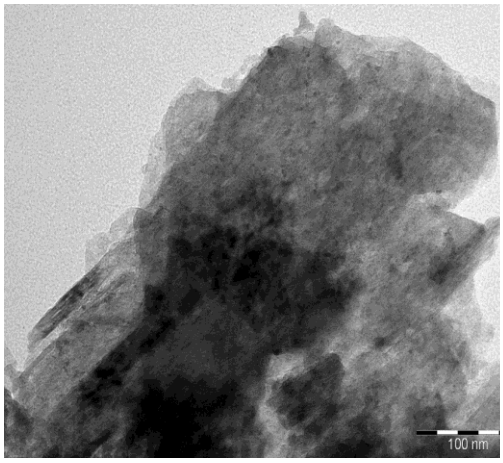

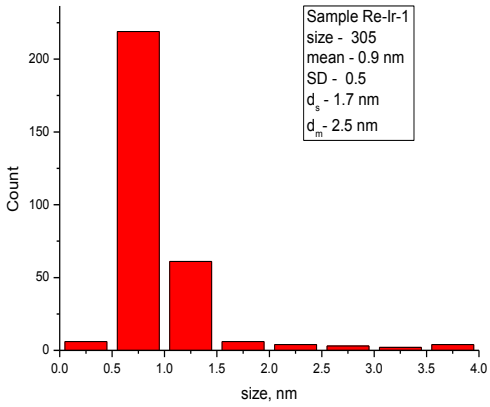

fresh

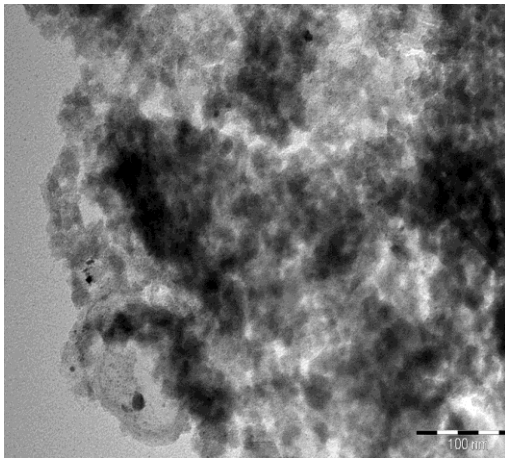

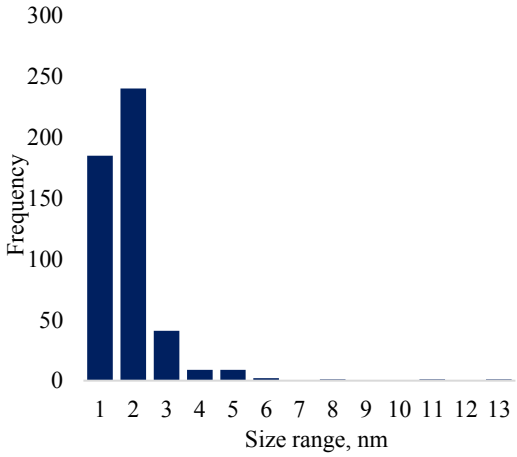

spent

Figure 6 TEM images and histograms of the fresh and spent $IrRe/Al_2O_3$-DP catalyst in isoeugenol HDO at 250℃ and 30 bar total pressure.

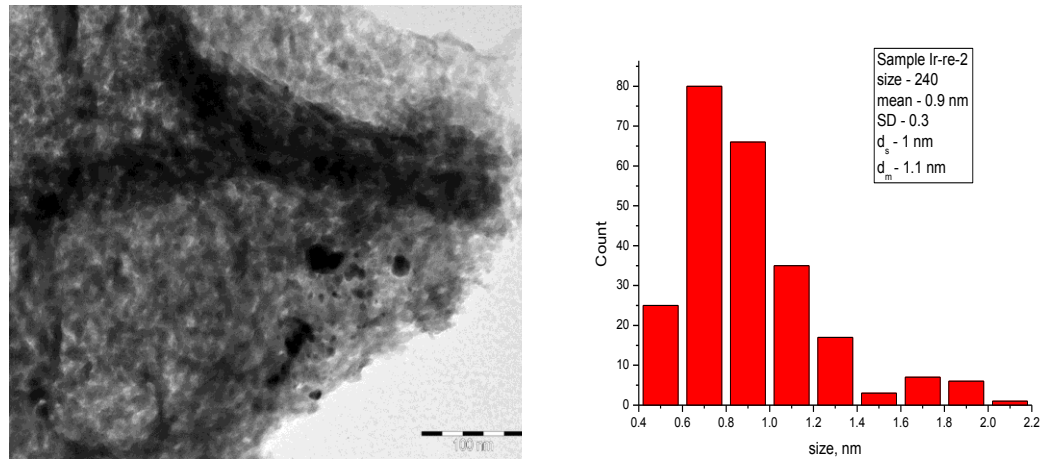

fresh

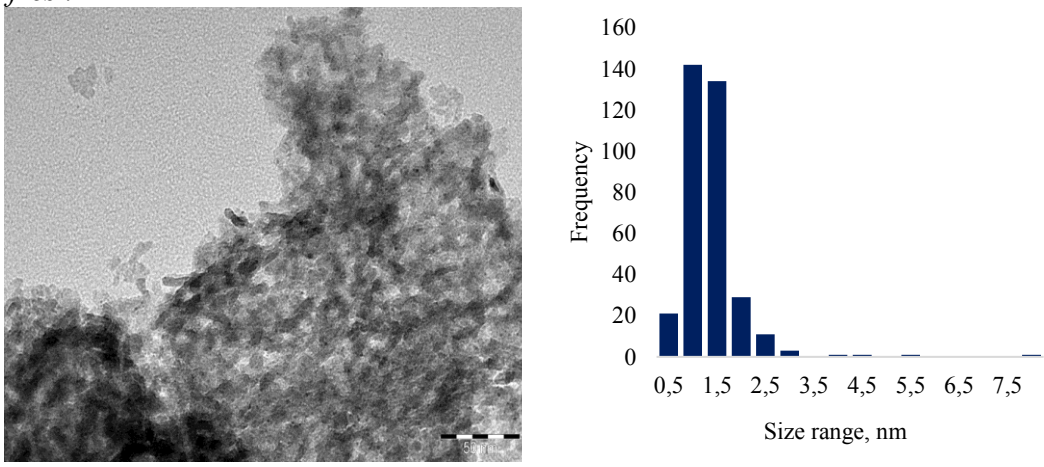

spent

Figure 7 TEM images and histograms of the fresh and spent IrRe/Al_2O_3-Impr2 catalyst in isoeugenol HDO at 250℃ and 30 bar total pressure.

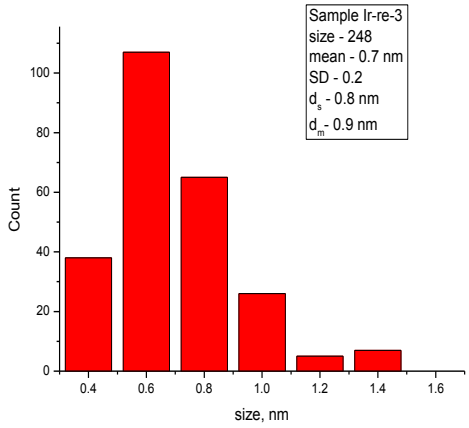

fresh

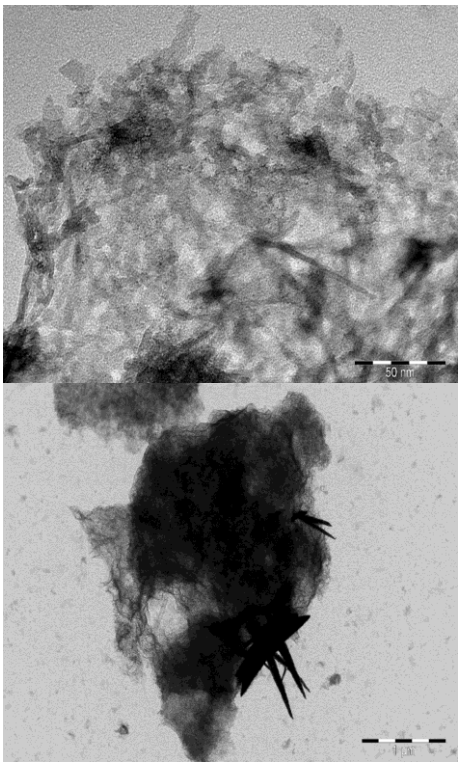

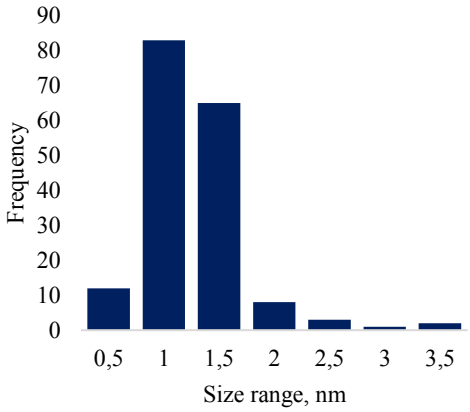

spent

Figure 8 TEM images and histograms of the fresh and spent IrRe/Al_2O_3-Impr1 catalyst in isoeugenol HDO at 250℃ and 30 bar total pressure.

Comparing Re/Al_2O_3 and $PtRe/Al_2O_3$ catalysts in the fresh and spent states, the former exhibited sintering, while the later had almost the same size range of 3 nm (Table 15). It can be noted the monometallic catalyst has a higher size of metal particle in comparison with the bimetallic one.

For Ir/ZrO_2 the particle size in the fresh and spent catalysts is 1.3 nm and 2.2 nm respectively (Table 15). In the case of 10 wt.% Ni/ZrO_2 it was not possible to differentiate between nickel and zirconia (Appendix III), as nickel (59 g/mol) is lighter than zirconia (91 g/mol).

High iridium dispersion can be seen in the TEM image in Figure 9, for the fresh Ir/ZrO_2 catalyst. Although the spent one exhibited high metal dispersion also some agglomerates varying from 4 nm to 14 nm are visible.

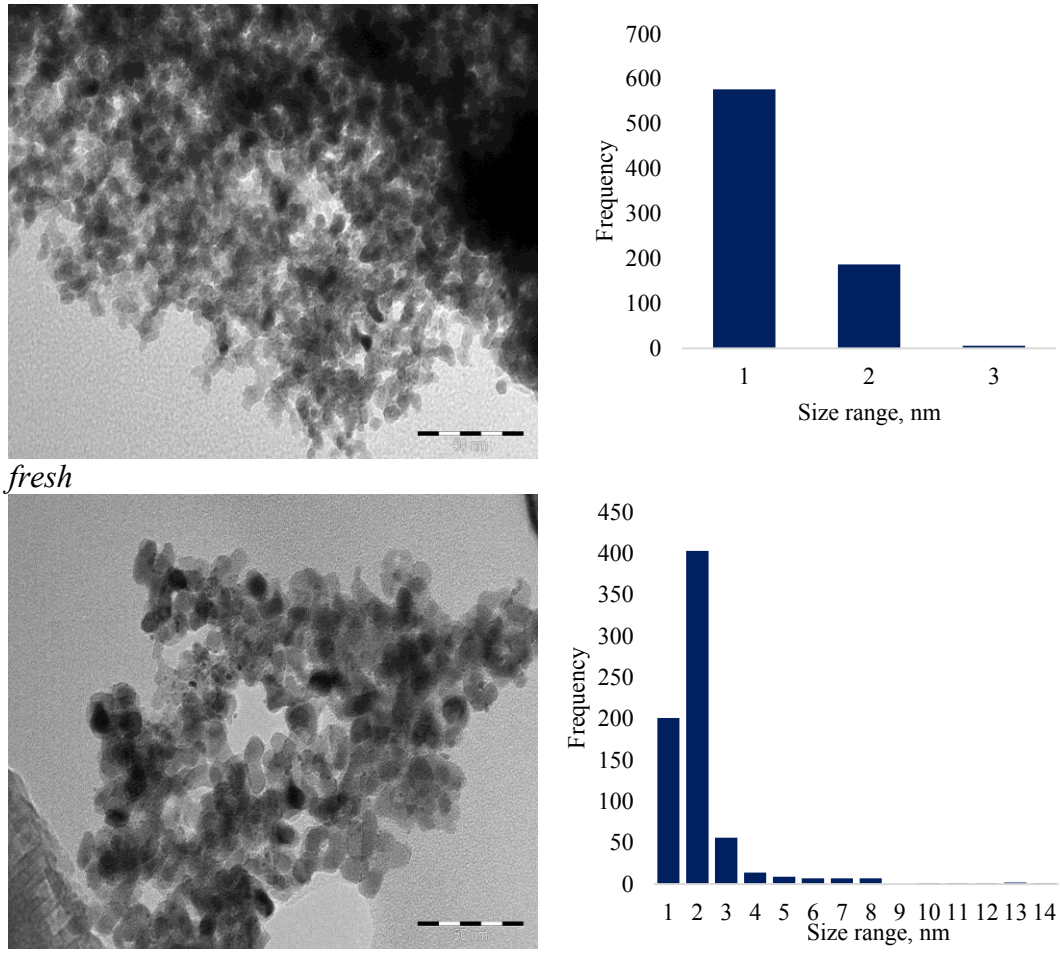

Figure 9 TEM images and histograms of the fresh and spent Ir/ZrO_2 catalyst in isoeugenol HDO at 250℃ and 30 bar total pressure.

4.1.3.2 SEM-EDX results

The most important and relevant SEM images will be presented in this Section (in Figures 10-12), while all other images are given in Appendix IV.

SEM images of Pt/Al_2O_3, Re/Al_2O_3 and $PtRe/Al_2O_3$ can be found in Appendix IV (Figures IVA-IVC). In Pt/Al_2O_3 the size of platinum varied from 25 μm to 180 μm with no big differences seen in the fresh and spent catalysts (Figure IIIB). Fresh Re/Al_2O_3 displayed a smoother surface with small particles of Re, which are less visible in the spent one (Figure IIIC). Bimetallic PRA demonstrated good distribution of metal particles with oval and spherical shapes (Figure IIID), resembling each other and exhibiting irregular particles in the size range between 1 μm to 5 μm.

As can be seen from Figure 10, the morphology of IRA-Impr1 and IRA-Impr2 (impregnated catalysts) is different from IRA-DP catalyst (deposition-precipitation). The shape of IRA-DP particles was poorly defined, while IRA-Impr2 and IRA-Impr1 exhibited mainly spherical and some oval shapes (34-210 μm). In SEM images of IRA-Impr1 and IRA-Impr2 the presence of needle shaped agglomerates (stars) can be observed belonging to iridium metal particles, which was confirmed by SEM-EDX analysis (images B and C in Figure 10).

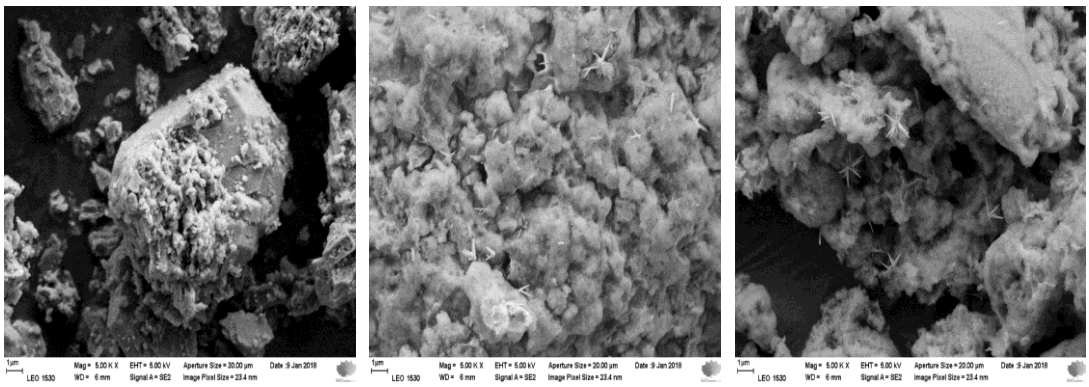

A *B* *C*

Figure 10 SEM images for the fresh catalysts. A – $IrRe/Al_2O_3$-DP, B – $IrRe/Al_2O_3$-Impr2, C – $IrRe/Al_2O_3$-Impr1.

As seen in Figure 11, there are not so big differences in shapes between fresh Ir/ZrO_2 and 10 wt.% Ni/ZrO_2, except the size range. For Ir/ZrO_2 the size is almost in the same range starting from 24 μm and possessing a maximum at 122 μm based on SEM images. For 10 wt.% Ni/ZrO_2 smaller and larger size particles were present (10-160 μm) determined from SEM images. The same trend can be observed for both catalysts in the spent state (Appendix IX, Figures IVE).

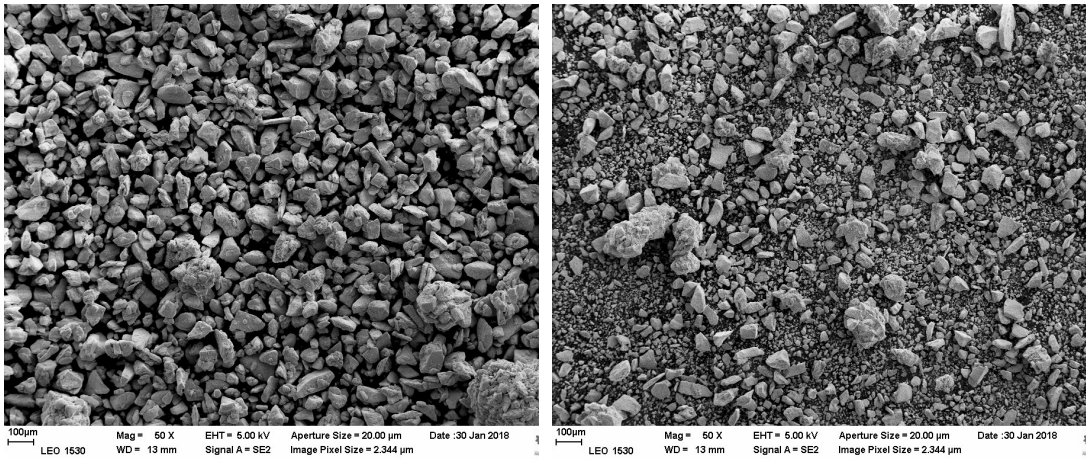

A *B*

Figure 11 SEM images for the fresh catalysts. A – Ir/ZrO_2, B –10 wt.% Ni/ZrO_2.

Figure 12 presents Ir/C (rbb) in the fresh (A) and spent catalysts (B & C) in solventless isoeugenol HDO at 11 bar and 150-200℃ (Entry mao36 in Appendix XI) and solventless isoeugenol HDO at 11 bar and 200℃ (Entry mao43 in Appendix XI) respectively. It can be observed that the carbon support originates from wood as visible especially in image B (Figure 12). A similar structure was also noted in the carbon support made of Algarroba wood [66].

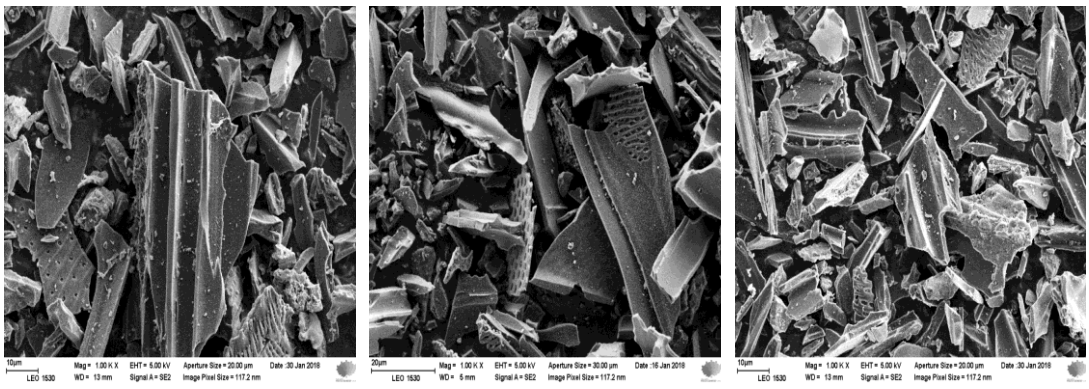

A *B* *C*

Figure 12 SEM images of Ir-C (rbb). A *– fresh Ir/C,* B *– spent Ir/C in solventless isoeugenol HDO at 11 bar and 150-200℃ (mao 36 in Appendix XI),* C *– spent Ir/C in solventless isoeugenol HDO at 11 bar and 200℃ (mao43 in Appendix XI).*

In SEM images of the fresh and spent PtRe/C-31 and PtRe/C-13 catalysts different shapes of particles can be observed as well as no changes in the size and shape (Appendix IV Figure IVF-IVG).

Based on the SEM-EDX analysis (Appendix IV), the metal to metal ratio in bimetallic catalysts and the ratio of corresponding metals to carbon were determined (Table 16). It should be noted that carbon coating placed below the catalyst layer has a minor contribution in the variation of carbon weight percentage.

Table 16 Weight ratio between metal:metal and carbon:metal in Al_2O_3 and ZrO_2 supported catalysts from SEM-EDX

Ratio	Fresh	Spent
IrRe/Al_2O_3-DP		
Re/Ir	4.4	5.6
C/Ir	21	21
IrRe/Al_2O_3-Impr2		
Re/Ir	1.4	1.8
C/Ir	3	10.8
IrRe/Al_2O_3-Impr1		
Re/Ir	2.7	1.8
C/Ir	8.2	8.4
3 wt.% Pt-3 wt.% Re/Al_2O_3		
Re/Pt	1.3	1.1
C/Pt	5.1	4.6
Ir/ZrO_2		
Ir/Zr	0.1	0.1
10 wt.% Ni/ZrO_2		
Ni/Zr	0.2	0.2

Based on SEM-EDX analysis the Re/Ir weight ratio decreased as follows for the fresh IRA catalysts: IRA-DP > IRA-Impr1 > IRA-Impr2 being respectively 4.4, 2.7 and 1.4 (Table 16). In the spent catalysts of IRA series, the weight ratios of metals have increased for IRA-DP and IRA-Impr2. On the other hand, Re/Ir ratio was dropped by one-third of the initial value for IRA-Impr1 (1.8), i.e. more Ir was present in the spent catalyst. Furthermore, for the spent catalysts carbon to metal weight ratio was determined showing that especially IRA-2 exhibited extensive coking, as its C/Ir ratio increased.

3 wt.% Pt-3 wt.% Re/Al_2O_3 exhibited a minor decrease the spent catalyst due to a minor leaching of Re (Table 16). For Ir/ZrO_2 and 10 wt.% Ni/ZrO_2 no changes were observed in terms of the metal content.

In Table 17 for Ir/C (rbb) catalyst utilized in solventless isoeugenol HDO at 150℃ and 200℃ at ca. 11 bar, the ratio of C/Ir is presented. Only for the reaction at 150℃ the C/Ir ratio has increased from 73 to 97 indicating accumulation of carbon on the catalyst surface. While for 200℃ just a minor drop of the weight ratio was observed.

For PtRe/C-31 no influence of the isoeugenol HDO at 250℃ at 30 bar could be seen in Table 17. PRC-13 has a more than twofold higher ratio of metals than PRC-31 in the fresh and spent states (due to high loadings of Pt and Re).

Table 17 Weight ratio between metal:metal and carbon:metal in carbon supported catalysts from SEM-EDX

Ratio	Fresh	Spent
Ir/C (rbb)		
C/Ir	73	97 (at 150℃ isoeugenol HDO)
		69 (at 200℃ isoeugenol HDO)
PtRe/C-31		
Re/Pt	0.6	0.7
C/Pt	15.3	16.3
PtRe/C-13		
Re/Pt	1.1	1.7
C/Pt	13.6	24.5

4.1.4 Organic elemental analysis (CHNS)

Organic elemental analysis showed that the carbon content increased after isoeugenol HDO at 250℃ and 30 bar in the spent IRA catalysts series indicating coke formation (Table 18). Spent IRA-DP and IRA-Impr1 exhibited only minor coking, while in the spent IRA-Impr2 there was a significant increase of the carbon content by ca. 26%, which could explain its low catalytic activity compared to IRA-DP and IRA-Impr1 as discussed below.

Table 18 CHNS results for alumina and carbon supported catalysts

Catalyst	Type	Carbon, % w/w	Hydrogen, % w/w	Nitrogen, % w/w	Sulfur, % w/w
IrRe/Al_2O_3-DP	*fresh*	0.20	0.49	0.00	0.03
	spent (mao38)	1.60	0.60	0.02	0.00
IrRe/Al_2O_3-Impr2	*fresh*	0.13	0.79	0.00	0.00
	spent (mao41)	26.50	4.79	0.03	0.00
IrRe/Al_2O_3-Impr1	*fresh*	0.99	0.78	0.00	0.00
	spent (mao13)	2.80	0.90	0.02	0.00
Ir/C (rbb)	*fresh*	86.50	0.60	0.11	0.00
	spent (mao36)	85.23	1.40	0.13	0.00
	spent (mao43)	85.77	2.13	0.19	0.09

Comparing hydrogen content it can be stated that the fresh as well as spent catalysts contained hydrogen. Due to hydrogen reduction process, fresh catalysts may include hydrogen. In addition, according to the Peintinger et al. [67], hydrogen is accounted as a part of γ-Al_2O_3 surface structure. An increase of hydrogen content in the spent catalysts is apparently related to coking and formation of hydrogen containing carbonaceous deposits. There was also a clear influence of the reaction temperature, as an experiment at 50℃ higher temperature (mao43 vs mao36) resulted in twofold higher hydrogen content.

Nitrogen content varied in the studies catalysts namely fresh IRA series catalysts did not contain any nitrogen, while negligible quantities have appeared in the spent catalysts. The fresh and the spent Ir/C (rbb) catalysts contained nitrogen, which increased slightly after isoeugenol HDO at 150℃ and 200℃ and 11 bar.

Sulfur was not present in the majority of the fresh and spent catalysts, except the fresh IrRe/Al_2O_3-DP. The spent Ir/C catalyst (mao43) showed some sulfur contamination after the solventless isoeugenol HDO at 200℃ and 11 bar, which can point out on a minor presence of sulfur in isoeugenol.

4.1.5 Thermogravimetric analysis (TGA)

TGA was performed for the fresh catalyst as well as for the spent ones after isoeugenol HDO at 250℃ and 30 bar in order to elucidate the mass balance closure by taking into account coke. IRA-Impr1 contained 4.1 wt.% coke in TGA performed in nitrogen, while in air the amount of coke was 1.7 wt.% (Table 19). In air a notable endothermic peak can be observed around 400℃ due to oxidation of a part of coke.

Coking is the highest in nitrogen for Ir/C (rbb) (7.6%). Considering zirconia supported catalysts which were used in HDO of isoeugenol and guaiacol, carbon content is higher for Ir containing catalyst than for Ni.

Spent zirconia supported catalysts after guaiacol HDO at 250℃ and 30 bar total pressure were taken for analysis. The amount of organic coke is shown in Table 19 excluding water content in calculations.

Table 19 Coke content based on TGA data

Catalyst	**Organic coke in nitrogen, %**
IrRe/Al_2O_3-Impr1	4.1 (1.7)[a]
Ir/ZrO_2	3.5[b]
10 wt.% Ni/ZrO_2	2.9[b]
Ir/C (rbb)	7.6[c]
Ir/ZrO_2	5.1[d]
10 wt.% Ni/ZrO_2	3.2[d]

a* – organic coke in air environment, b* – obtained using corresponding spent catalysts from isoeugenol HDO at 250℃ and 30 bar, c* – obtained using spent catalyst from isoeugenol HDO at 200℃ and 30 bar, d* – obtained using corresponding spent catalysts from guaiacol HDO at 250℃ and 30 bar.

Derivative temperature differences (DTD) are also shown in Figures 13-19, including fresh and spent catalysts, where the first downward peak in DTD line means the moisture removal.

While the weight loss difference of 3.3 % can be seen for IRA-Impr1 catalyst in nitrogen environment (Figure 13), no weight loss was observed in air (Figure 14). In nitrogen, there were no significant changes for the fresh and spent catalyst based on the derivative temperature difference (Figure 13). On the other hand, in air a notable

endothermic peak can be observed around 400℃ due to oxidation of a part of organic coke (Figure 14).

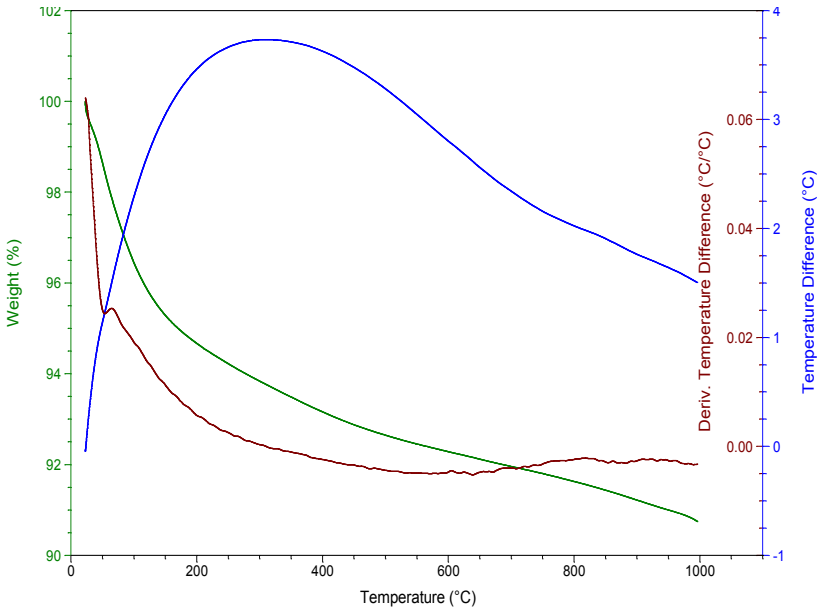

fresh

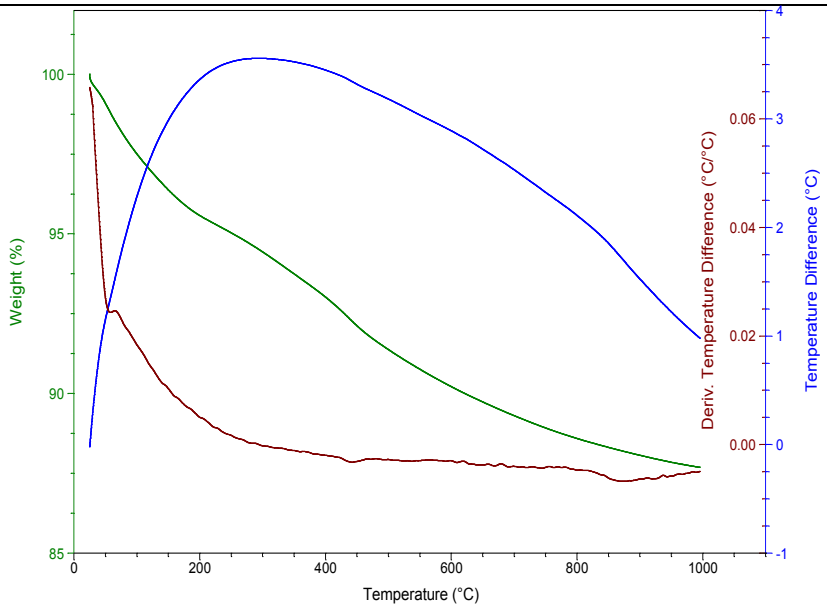

spent

Figure 13 TGA results in nitrogen environment for the fresh and spent IRA-Impr1 in isoeugenol HDO at 250℃ and total pressure of 30 bar.

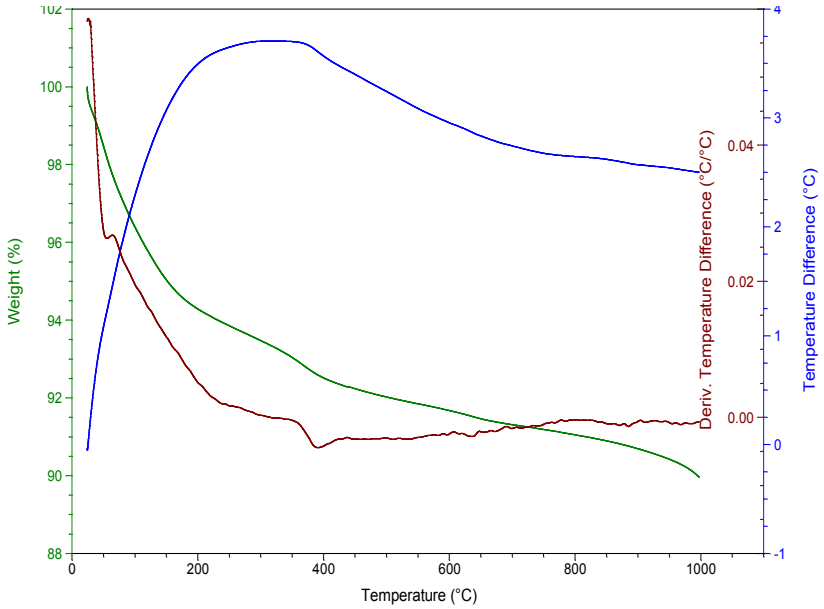

fresh

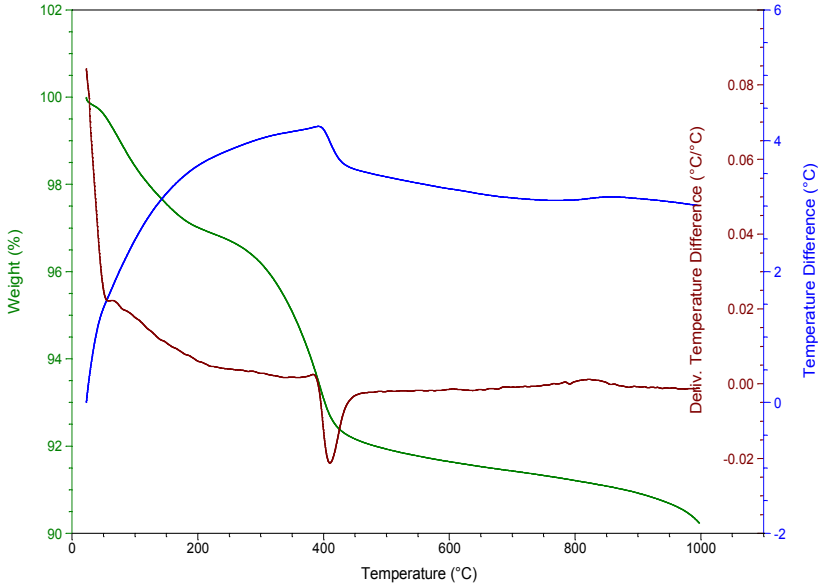

spent

Figure 14 TGA results in air environment for the fresh and spent IRA-Impr1 in isoeugenol HDO at 250℃ and total pressure of 30 bar.

Differences in the weight loss of 2.5% from the fresh to spent catalyst excluding water was observed for Ir/ZrO_2 catalyst (Figure 15). Insignificant endothermic and exothermic peaks were present in both types of samples.

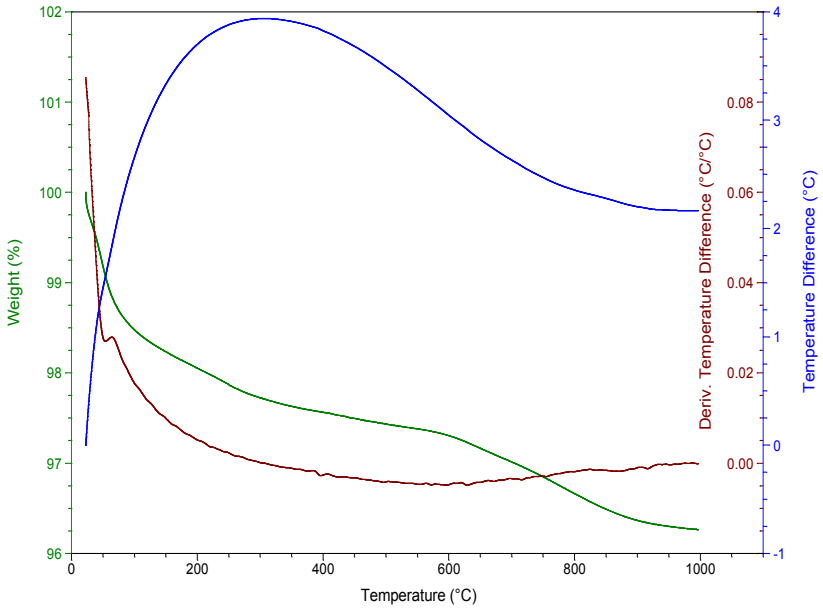

fresh

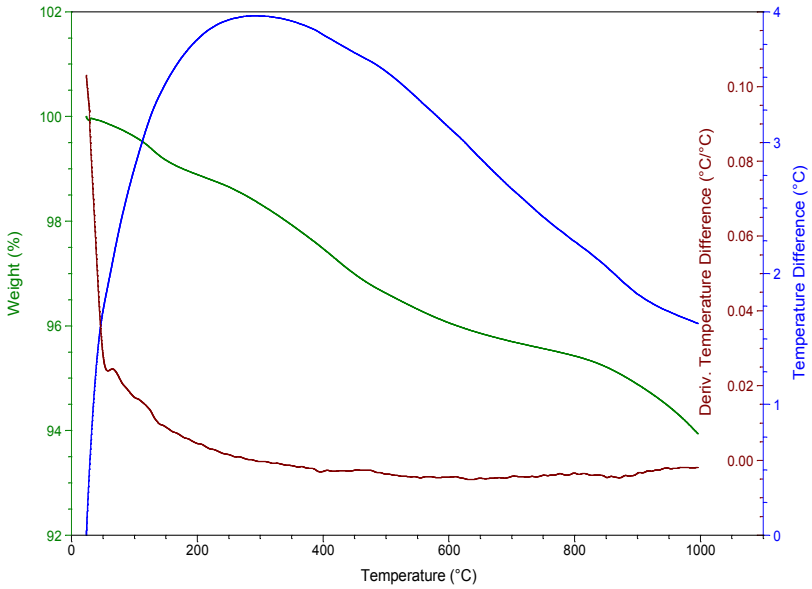

spent

Figure 15 TGA results in nitrogen environment for the fresh and spent Ir/ZrO_2 in isoeugenol HDO at 250℃ and total pressure of 30 bar.

The nickel on zirconia catalyst demonstrated the weight loss difference of 2.5% during TGA in nitrogen (Figure 16). Significant endothermic peak can be seen in the spent 10 wt.% Ni/ZrO_2 at around 275℃.

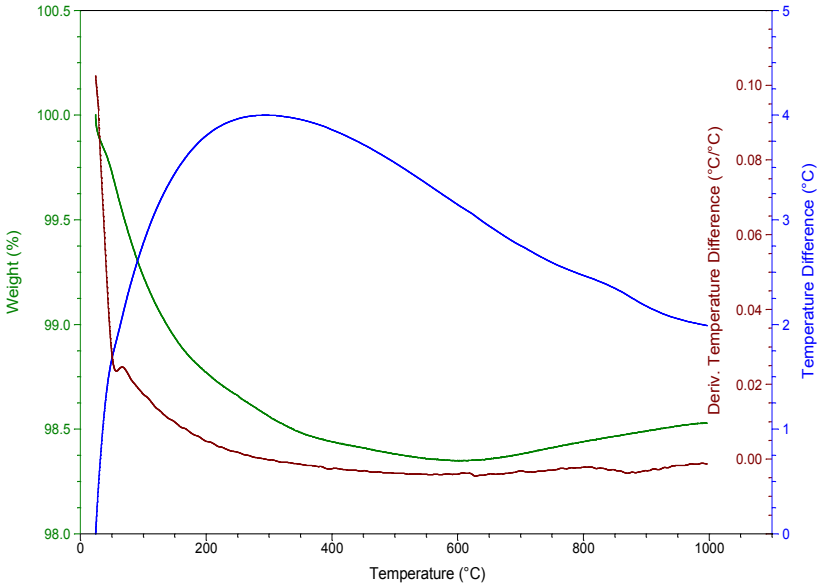

fresh

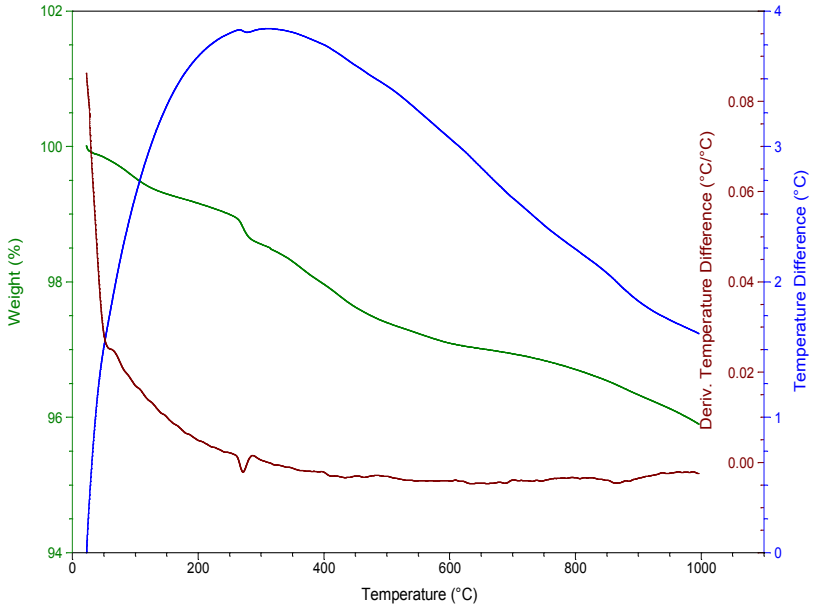

spent

Figure 16 TGA results in nitrogen environment for the fresh and spent 10 wt.% Ni/ZrO_2 in isoeugenol HDO at 250℃ and total pressure of 30 bar.

Ir/C catalyst demonstrated 8.3% difference in the weight loss from the fresh to spent (HDO of isoeugenol at 200℃ and 30 bar) catalysts (Figure 17). Minor endothermic and exothermic (370℃) peaks can be observed from the derivative temperature difference for the fresh and spent catalysts.

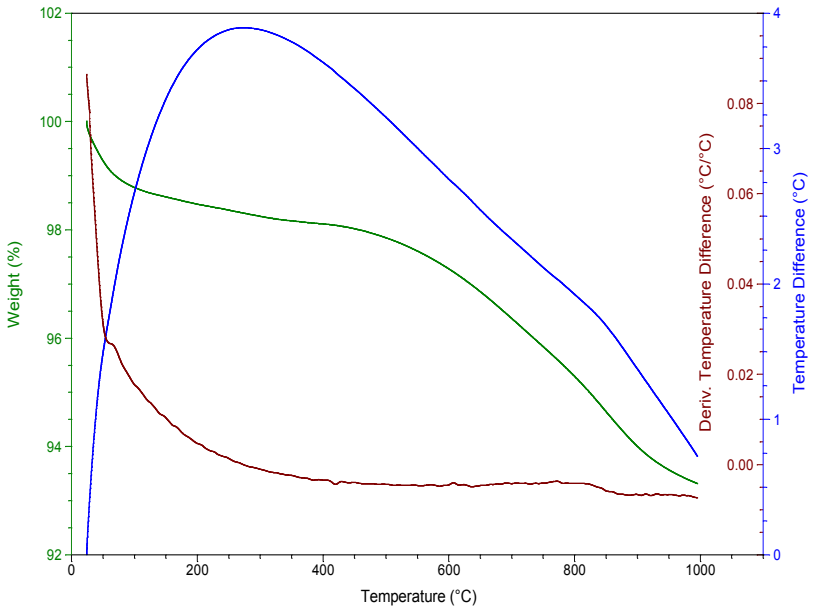

fresh

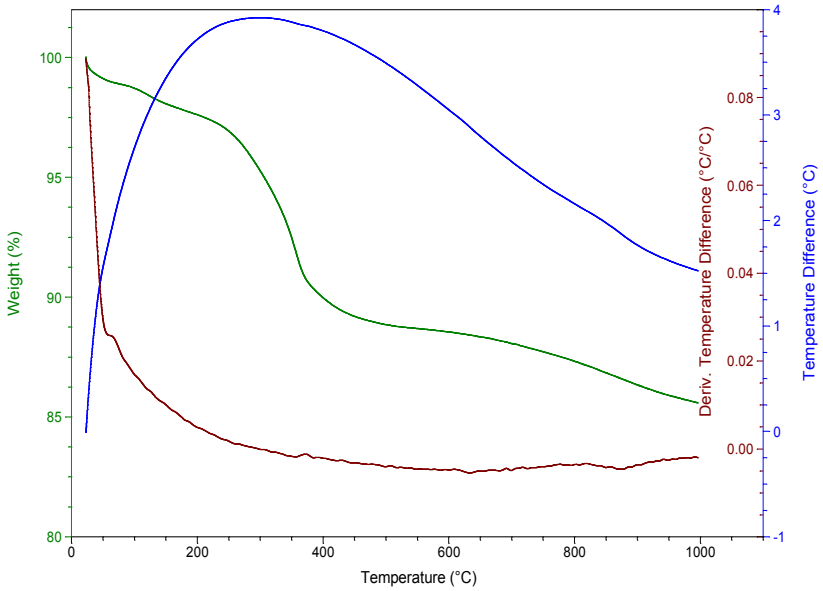

spent

Figure 17 TGA results in nitrogen environment for the fresh and spent Ir/C (rbb) in isoeugenol HDO at 200℃ and total pressure of 30 bar.

For Ir/ZrO_2 catalyst there was a difference in the weight loss of 1.8 % from the fresh to spent state (Figure 18). A minor exothermic peaks at 85 and 110℃ can be seen in the fresh and spent TGA results due to the gradual water removal.

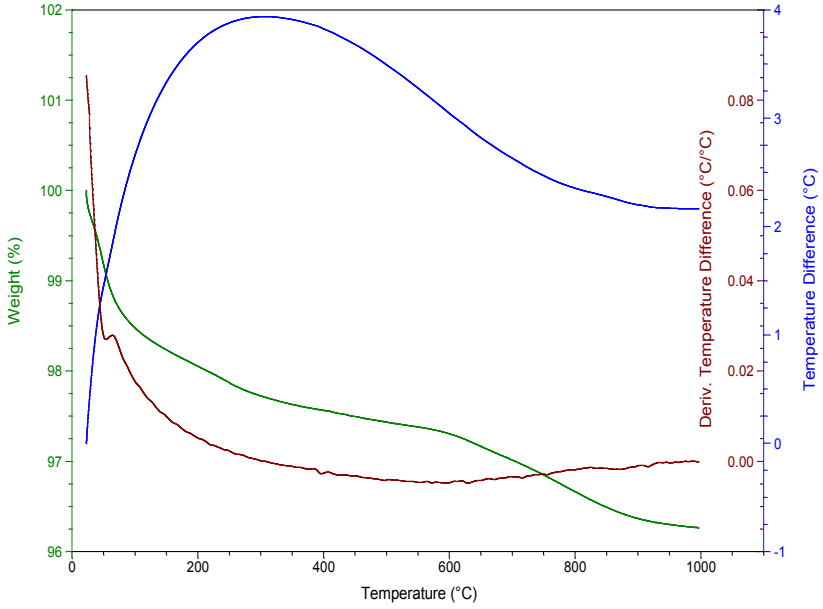

fresh

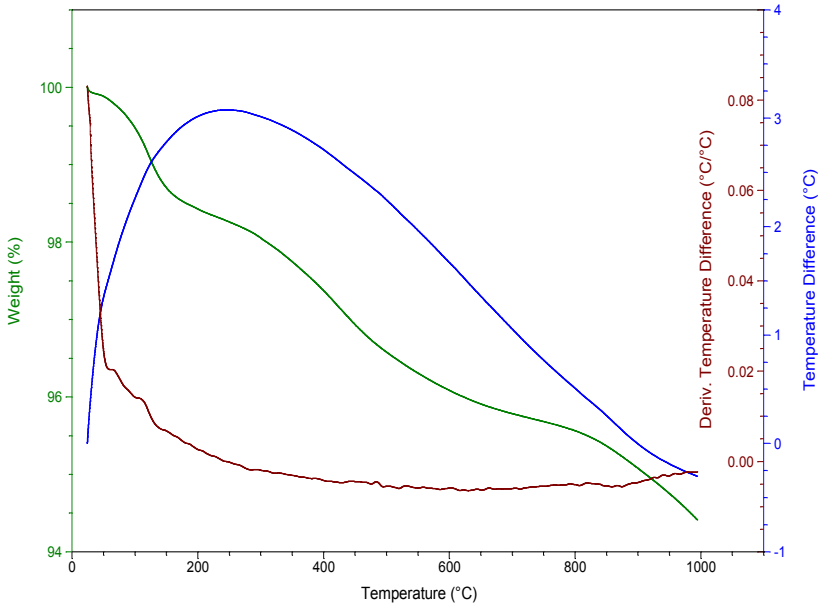

spent

Figure 18 TGA results in nitrogen environment for the fresh and spent Ir/ZrO_2 in guaiacol HDO at 250℃ and total pressure of 30 bar.

For 10 wt.% Ni/ZrO_2 catalyst the mass loss difference from the fresh to the spent catalyst after HDO of guaiacol at 250℃ and 30 bar is relatively small (2 %) in nitrogen environment (images in Figure 19). Endothermic peak can be observed in the spent catalyst at ca. 275℃.

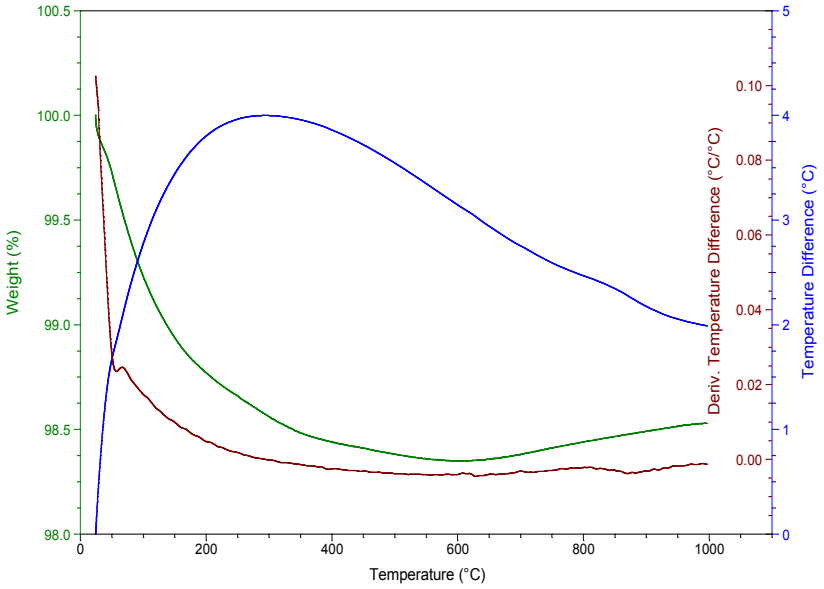

fresh

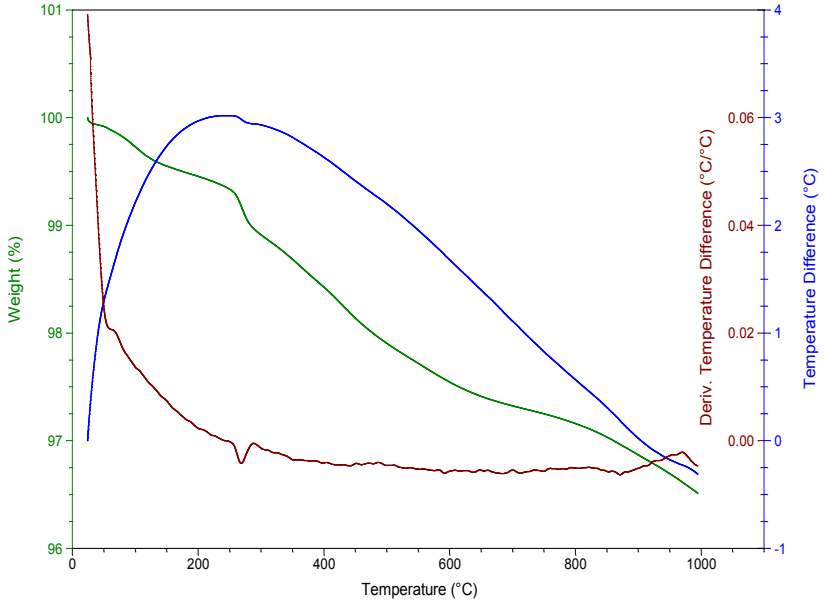

spent

Figure 19 TGA results in nitrogen environment for the fresh and spent 10 wt.% Ni/ZrO_2 in guaiacol HDO at 250℃ and total pressure of 30 bar.

4.1.6 Size exclusion chromatography (SEC)

Size exclusion chromatography was utilized for analysis of IrRe/Al_2O_3-Impr1. The result is presented below using sitosterol as a standard showing that the molecular weight in the sample (M_w=164 g/mol) is much higher than that of sitosterol (M_w=415 g/mol) (indicated as a dark blue line) (Figure 20).

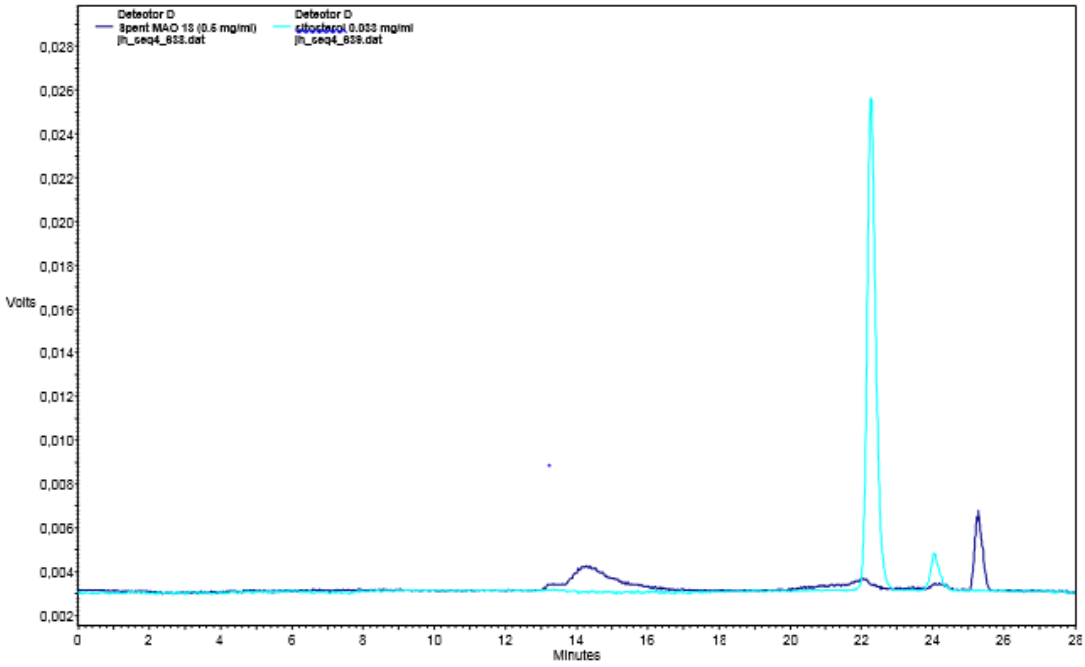

Figure 20 SEC analysis of the spent IRA-Impr1 from HDO of isoeugenol 250℃ and 30 bar total pressure. Sitosterol was used as a standard.

Concentration of the sample in SEC was 0.5 mg/ml using tetrahydrofuran as a solvent. The concentration of sitosterol was 0.033 mg/ml. A large peak belongs to sitosterol at retention time 22.3 min, while a smaller peak corresponds to an impurity at 24.1 min. As can be seen from Figure 20, the total peak area for the peaks in the sample is ca. half of the peak area for sitosterol, making exact quantification challenging.

Comparing retention times with polystyrene (Appendix V), presence of monomer, tetramers and hexa-mers was found. The heaviest oligomer belongs to the peak at retention time of 14.3 min, which was not identified.

4.1.7 X-ray photoelectron spectroscopy (XPS)

According to XPS results for IRA-DP, IRA-Impr2 and IRA-Impr2 (graphs combined in Figure 21), iridium was present with the binding energies 61.7, 61.2 and 62.1 eV

for the fresh IRA catalysts series respectively, corresponding to the valence state of 4+. In Figure 22 for the spent IRA-DP and IRA-Impr2 catalysts the binding energies were increased by 0.2 eV, while for the spent IRA-Impr1 the binding energy was dropped by 0.2 eV. Therefore, a non-significant change was occurred for the catalysts after isoeugenol HDO indicating the same valence state of 4+. Based on the Freakley et al. [68], the mean binding energy of 61.9 eV (±0.7) corresponds to IrO_2. Furthermore, absence of metallic Ir of 60.8 eV binding energy can be observed in both fresh and spent IRA catalysts (Figures 21 and 22), based on [68].

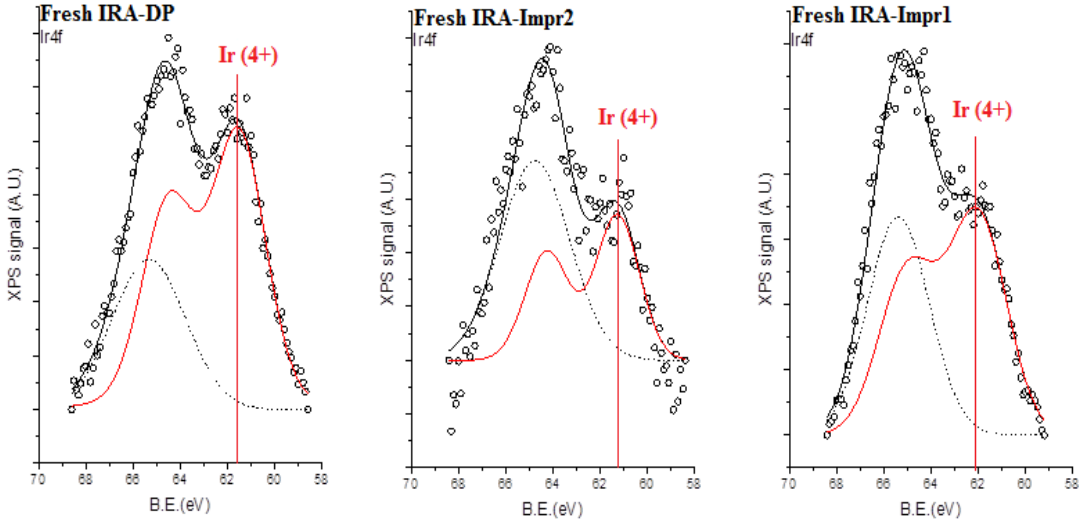

Figure 21 XPS results indicating iridium valence state for the fresh IRA catalysts series.

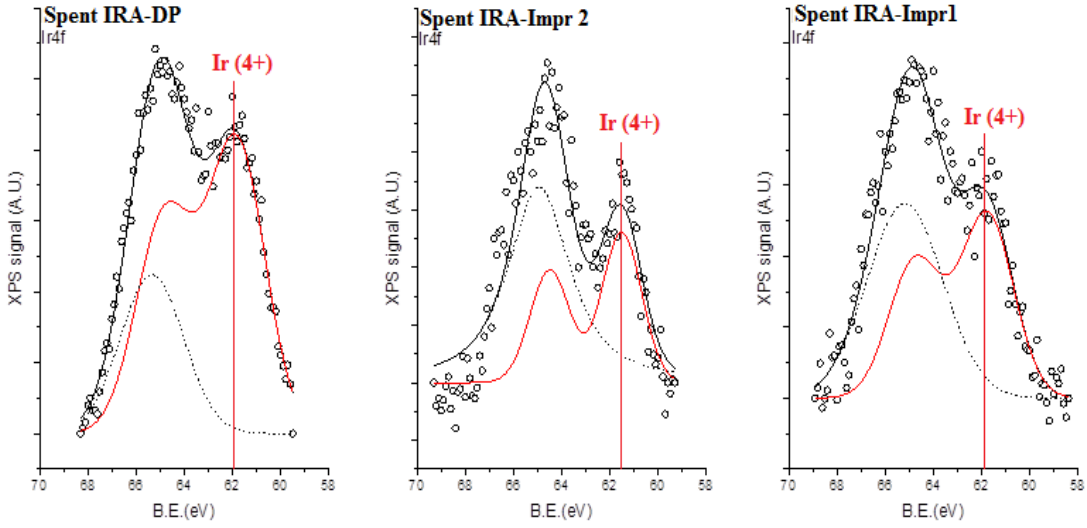

Figure 22 XPS results indicating iridium valence state for the spent IRA catalysts series obtained after isoeugenol HDO at 250℃ and 30 bar.

Presence of different rhenium valence states was found in IRA series catalysts with the major valence state being 7+. Rhenium 7+ corresponds to the binding energy between 46.2-46.8 eV seen in both fresh and spent catalysts, in agreement with [69]. The valence state 6+ in the range between 44.2-44.8 eV was also present in the fresh and spent catalysts [69], except for the spent IRA-Impr1. The fresh IRA-DP catalyst exhibited not only 7+ and 6+ valence states but also 4+ at the binding energy 41.8 eV (Figure 23), similar to Rozmysłowicz et al. [70]. However, the valence state 4+ for rhenium was absent in the spent IRA-DP being used in isoeugenol HDO at 250°C and 30 bar (Figure 24). No metallic Re can be observed in the fresh and spent IRA catalysts as there are no peaks in binding energy of 40.5-40.7 eV, according to [69].

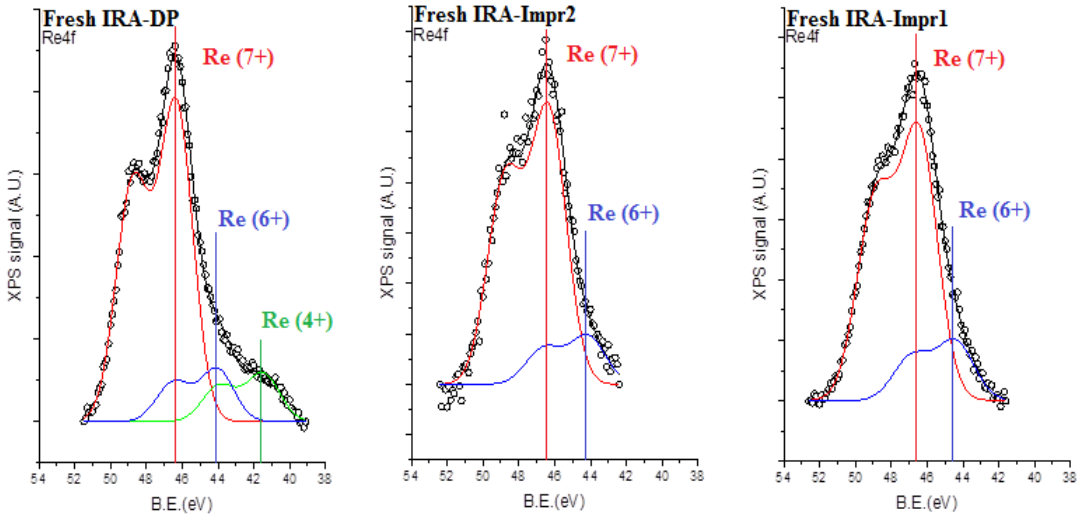

Figure 23 XPS results indicating rhenium valence states for the fresh IRA series catalysts.

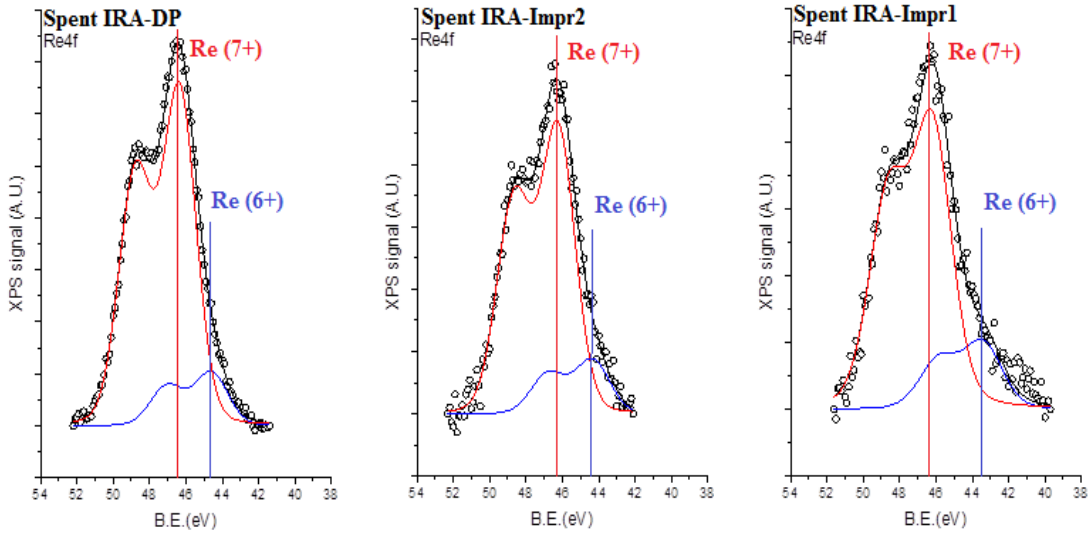

Figure 24 XPS results indicating rhenium valence states for the spent IRA series catalysts obtained after isoeugenol HDO at 250℃ and 30 bar.

Overall, based on all characterization techniques, useful and important results for HDO discussion are coming from nitrogen physisorption, SEM-EDX, CHNS, XPS, TGA (for guaiacol HDO specifically).

4.2 HDO

A range of catalysts was investigated in hydrodeoxygenation of isoeugenol (Appendix XI). The most interesting results are presented below while a more detailed list with the key catalytic data can be found in Appendix XI.

4.2.1 Thermal isoeugenol HDO

Blank experiments were performed for hydrodeoxygenation of isoeugenol at 200℃ and 250℃ and 30 bar total pressure using isoeugenol as a reactant and dodecane as a solvent with the length of experiment being four hours. The reactor was cleaned using glass bead blast polishing prior to experiments. The temperatures were chosen based on preliminary catalytic experiments using alumina and zirconia supported catalysts (Sections 4.2.2.1.1 and 4.2.3.1.1). As can be seen from Figure 25, complete conversion of isoeugenol in both thermal experiments at 200℃ and 250℃ and 30 bar total pressure was observed. Conversion of isoeugenol increased at 200℃ during the first hour from 90 % to 100 %, while isoeugenol at 250℃ was converted completely already during the first minute. In both cases, the gas chromatography based sum of the amounts of

reactants and products in the liquid phase analysis (GCLPA) demonstrated more than 93 and 90 % of the balance respectively at 200℃ and 250℃. By combining results of GC and GC-MS isoeugenol (95 %) and trans-eugenol (5 %) were identified, being lumped into isoeugenol. In the initial sample at 0 minute the presence of hexane, heptane and octane was confirmed by GC and GC-MS (not included into the GCLPA calculations).

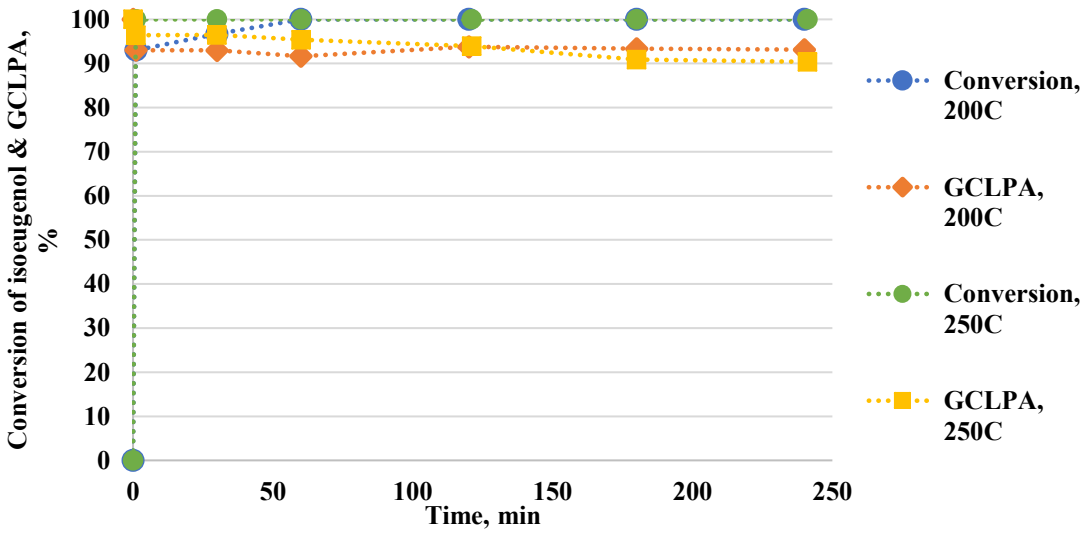

Figure 25 Conversion of isoeugenol and GCLPA versus time in the thermal isoeugenol HDO at 200℃ (mao39) and 250℃ (mao33) and 30 bar total pressure.

Mainly dihydroeugenol (99 %) and minor propylcyclohexane amounts (<1 %) were obtained after four hours of HDO as detected by GC and GC-MS for reactions at both 200℃ and 250℃. Isoeugenol was completely converted into products at 250℃ and 30 bar (Figure 26).

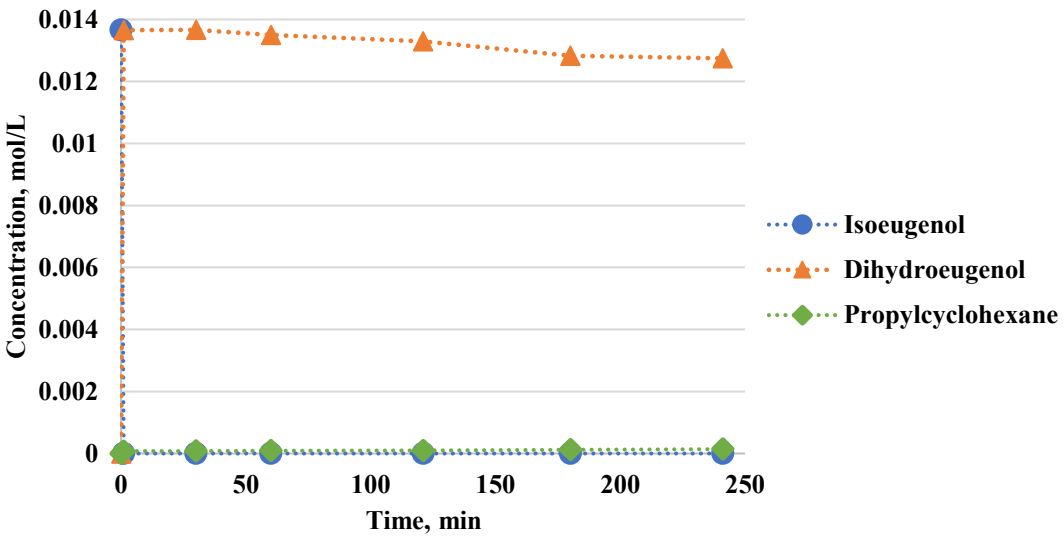

Figure 26 Concentration of the reactant and products according to GC in thermal isoeugenol HDO at 250℃ and 30 bar total pressure (mao33).

These results are in agreement with Bjelic et al. [15], who reported that isoeugenol transformations at 250ºC under 30 bar total pressure in hydrogen resulted in rapid hydrogenation of isoeugenol even in the absence of any catalyst (as mentioned in Section 1.3.1).

4.2.2 Isoeugenol HDO with metal catalysts supported on Al_2O_3

4.2.2.1 Temperature effect

In order to investigate isoeugenol HDO and the reaction pathways, it was decided to explore the influence of temperature and selectivity to hydrodeoxygenated products at 30 bar total pressure and 200℃ and 250℃. The list of tested catalysts and conditions is presented in Appendix IX.

4.2.2.1.1 Ir and Re catalysts supported on alumina

At 200℃ and 30 bar the catalysts presented in Figure 27 were tested in isoeugenol HDO. Complete conversion of isoeugenol in HDO was obtained with all catalysts. As can be seen from Figure 27, the GCLPA is higher at 200℃ than at 250℃ with the magnitude of the difference depending on the particular case. The highest GCLPA was accounted for Re/Al_2O_3 being 89 % and the lowest was 64 % for $IrRe/Al_2O_3$-Impr2. A decrease of ca. 19-27 % in GCLPA was observed in isoeugenol HDO tests at 250℃ compared with 200℃. An explanation for lower GCLPA at higher reaction

temperatures is in higher formation of gaseous products as confirmed also by the gas phase analysis (see below).

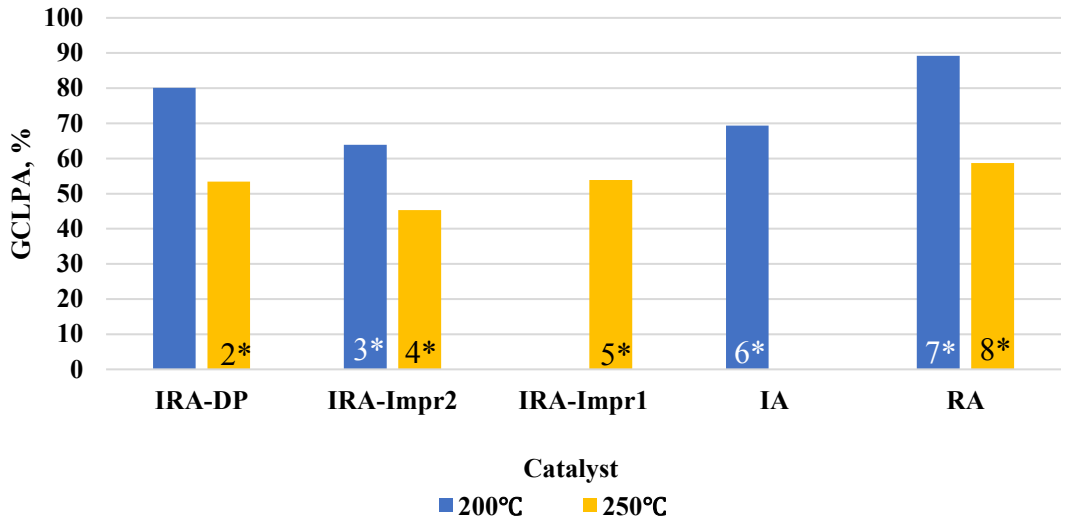

Figure 27 GCLPA after four hours of reaction in isoeugenol HDO at 200 and 250℃ and 30 bar over iridium and rhenium catalysts supported on alumina. Notation: 1- mao9; 2*- mao38; 3*- mao31; 4*- mao41; 5*- mao13; 6*- mao11; 7*- mao10; 8*- mao22.*

The gas phase analysis by GC-MS for isoeugenol HDO at 250℃ and 30 bar using IRA-DP and IRA-Impr1 catalysts confirmed presence of high amounts of methane and especially ethane, followed by propane and butane (Figures 28, 29). It should be noted that the quantity of propane was higher in the presence of IRA-Impr1 compared with IRA-DP. Hexane, heptane and octane were present in both gaseous samples using IRA-DP and IRA-Impr1. Moreover, the main reaction product propylcyclohexane was also present in the gas phase. Propylcyclohexane was observed appearing at RT 15.8 and 6.4 min in Figures 28 and 29 respectively.

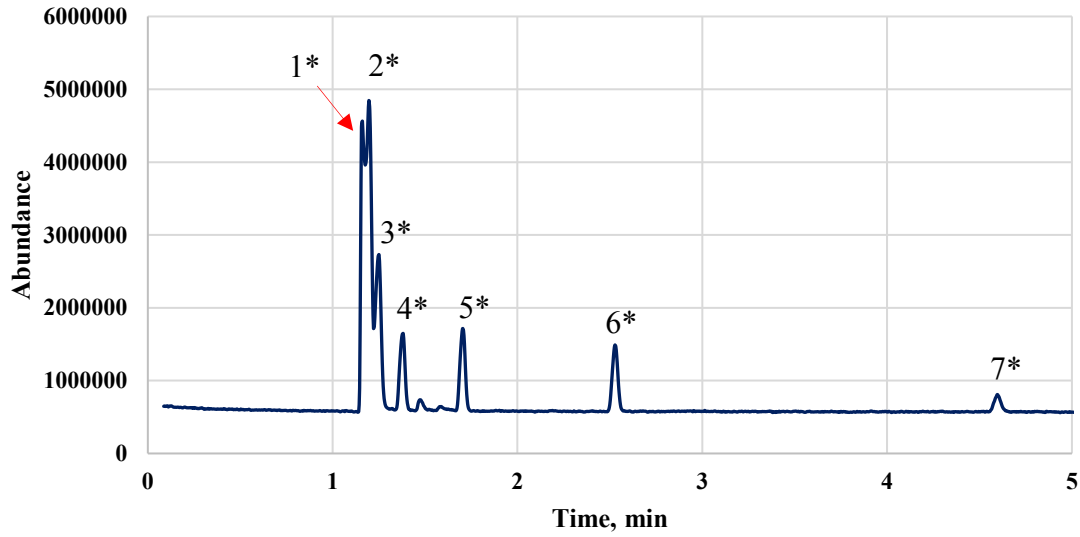

Figure 28 GC-MS analysis of the gas sample after four hours in isoeugenol HDO at 250℃ and 30 bar over IrRe/Al_2O_3-DP (mao38) (representation of 5 minutes). Notation: 1- methane (1.16 min), 2*- ethane (1.2 min), 3*- propane (1.22 min), 4*- butane (1.38 min), 5*- pentane (1.7 min), 6*- hexane (2.5 min), 7*- heptane (4.6 min).*

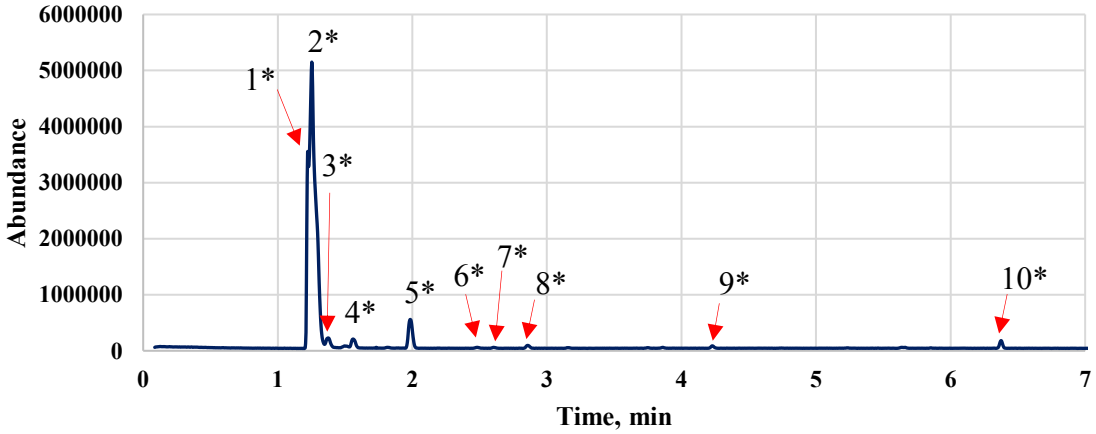

Figure 29 Gas sample analysis by GC-MS after two hours in isoeugenol HDO at 250℃ and 30 bar over IrRe/Al_2O_3-Impr1 (mao32) (representation of 7 minutes). Notation: 1- methane (1.2 min), 2*- ethane (1.25 min), 3*- propane (1.36 min), 4*- pentane (1.59 min), 5*- hexane (1.97 min), 6*- cyclohexane (2.46 min), 7*- 2-methylhexane (2.66 min), 8*- heptane (2.9 min), 9*- octane (4.2 min), 10*- propylcyclohexane (6.4 min).*

As can be seen from Figure 30, bimetallic catalysts performed better than monometallic alumina supported catalysts. The highest concentration of propylcyclohexane was observed for IrRe/Al_2O_3-Impr2 being approximately 0.001 mol/L, followed by IrRe/Al_2O_3-DP (0.0004 mol/L) and Ir/Al_2O_3 (ca. 0.0003 mol/L). The lowest concentration was observed over Re/Al_2O_3 catalyst being almost close to zero.

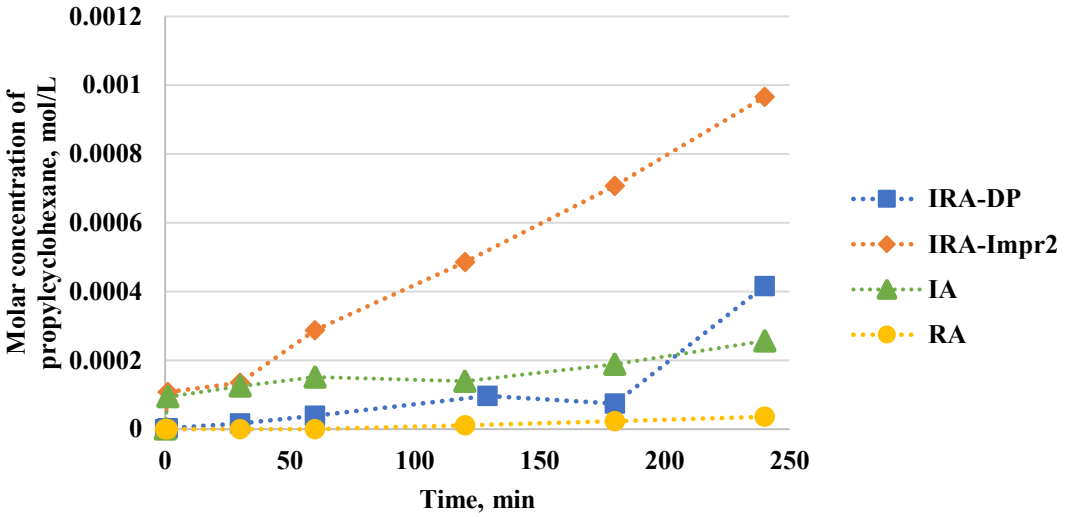

Figure 30 Molar concentration of propylcyclohexane vs reaction time in isoeugenol HDO at 200℃ and 30 bar over IrRe/Al_2O_3-DP (mao9), IrRe/Al_2O_3-Impr2 (mao31), Ir/Al_2O_3 (mao11) and Re/Al_2O_3 (mao10) catalysts.

In addition, concentration of dihydroeugenol as a function of time was considered for isoeugenol HDO at 200℃ and 30 bar for above mentioned alumina supported catalysts (Figure 31). As can be seen (Figure 31), some reactivity of dihydroeugenol can be observed for IRA-Impr2, while IRA-DP and monometallic catalysts such as IA and RA were even less active. Interesting enough, these catalysts demonstrated at 1 min concentration of dihydroeugenol below the initial value, with IrRe/Al_2O_3-DP and IrRe/Al_2O_3-Impr2 dihydroeugenol conversion was 20 and 35 % respectively, while Ir/Al_2O_3 and Re/Al_2O_3 displayed 7 and 5 % respectively. Overall conversion of dihydroeugenol is significantly higher over bimetallic catalysts than over monometallic ones in isoeugenol HDO at 200℃ and 30 bar total pressure.

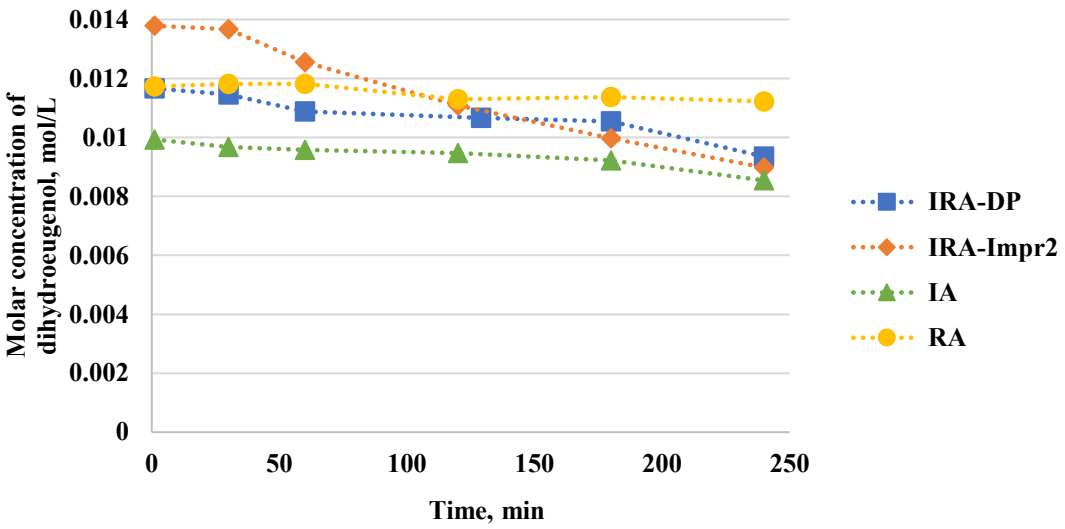

Figure 31 Molar concentration of dihydroeugenol as a function of time starting from 1 min sample in isoeugenol HDO at 200℃ and 30 bar total pressure over IrRe/Al_2O_3-DP (mao9), IrRe/Al_2O_3-Impr2 (mao31), Ir/Al_2O_3 (mao11) and Re/Al_2O_3 (mao10) catalysts.

For isoeugenol HDO at 250℃ and 30 bar the main product was propylcyclohexane with the decreasing yield as follows: IRA-DP > IRA-Impr1 ≥ IRA-Impr2. IrRe/Al_2O_3-DP allowed the highest yield 0.009 mol/L which can be explained by the rhenium valence state 4+. According to literature [71], Re at higher valence states such as 6+ and 7+ is not efficient in saturation of aromatics in comparison with the valence states 2+, 3+ and 4+. Other two bimetallic catalysts demonstrated lower product concentration being 0.0063 mol/L and 0.0057 mol/L for IRA-Impr1 and IRA-Impr2, respectively. As can be seen from Figure 32, IRA-Impr2 catalyst was not as active at 250℃ (0.0057 mol/L) as at 200℃ (0.001 mol/L) (Figure 30), which is related to the coke formation at a higher reaction temperature. More coke in the amounts of ca. 25 % was present in the spent catalyst compared to the fresh one according to CHNS analysis (Section 4.1.4). Despite almost the same synthesis method for IRA-Impr1 and IRA-Impr2, the former showed a higher activity and relative 2 wt.% minor coking from the fresh to the spent determined by CHNS.

By comparing the concentrations of the formed propylcyclohexane with the ratio of Re to Ir obtained via EDX analysis in different IRA catalysts (Section 4.1.3.2), it can be concluded that higher weight ratios between these metals resulted in higher concentrations of the main product. IRA-DP exhibited a high weight ratio of Re/Ir being 4.4, IRA-Impr1 and IRA-Impr2 had 2.7 and 1.4 respectively. According to Liu

et al. [20], the weight ratio of Re to Ir played a significant role in hydrodeoxygenation of high carbon furylmethane forming alkanes (>82 %) for the aviation jet fuel, with the Re/Ir ratio of 2 giving the best results.

While the product concentration using Re/Al_2O_3 was 10 times smaller than for $IrRe/Al_2O_3$-DP catalyst at 250℃ and 30 bar (Figure 32), it was still higher than in isoeugenol HDO at 200℃ and 30 bar (Figure 30).

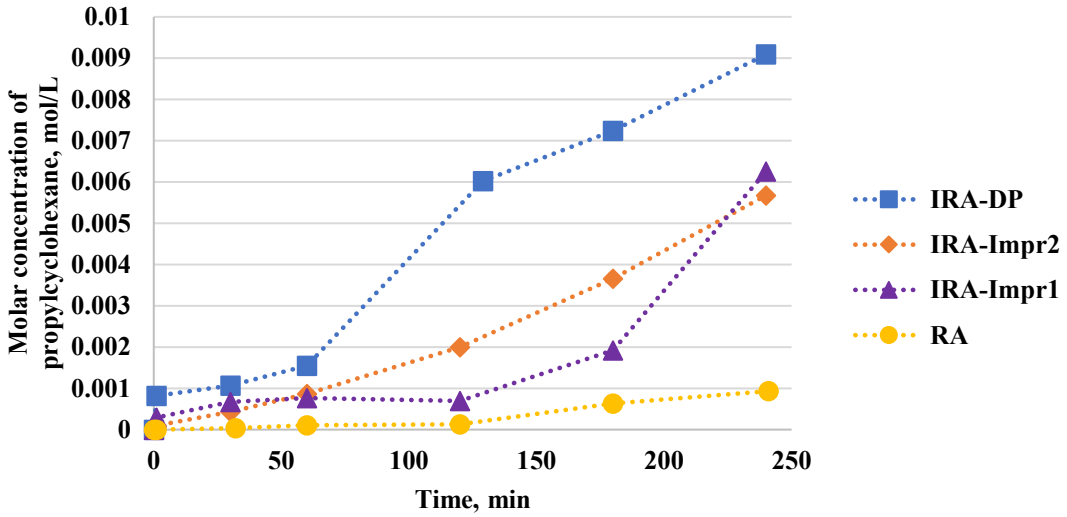

Figure 32 Molar concentration of propylcyclohexane vs reaction time in isoeugenol HDO at 250℃ and 30 bar total pressure over $IrRe/Al_2O_3$-DP (mao38), $IrRe/Al_2O_3$-Impr2 (mao41), $IrRe/Al_2O_3$-Impr1 (mao13) and Re/Al_2O_3 (mao22) catalysts.

As Figure 33 demonstrates, dihydroeugenol was completely converted after four hours at 250℃ and 30 bar using IRA-DP catalyst. Other IRA series catalysts such as IRA-Impr2 and IRA-Impr1 also demonstrated a high conversion of dihydroeugenol being almost 93 and 88 % respectively. On the other hand, Re/Al_2O_3 catalyst showed only 35 % conversion of dihydroeugenol. Therefore, 250℃ is a suitable temperature based on the molar concentration of propylcyclohexane while the most selective catalyst towards propylcyclohexane in isoeugenol HDO at 250℃ and 30 bar of total pressure among the tested ones was $IrRe/Al_2O_3$-DP.

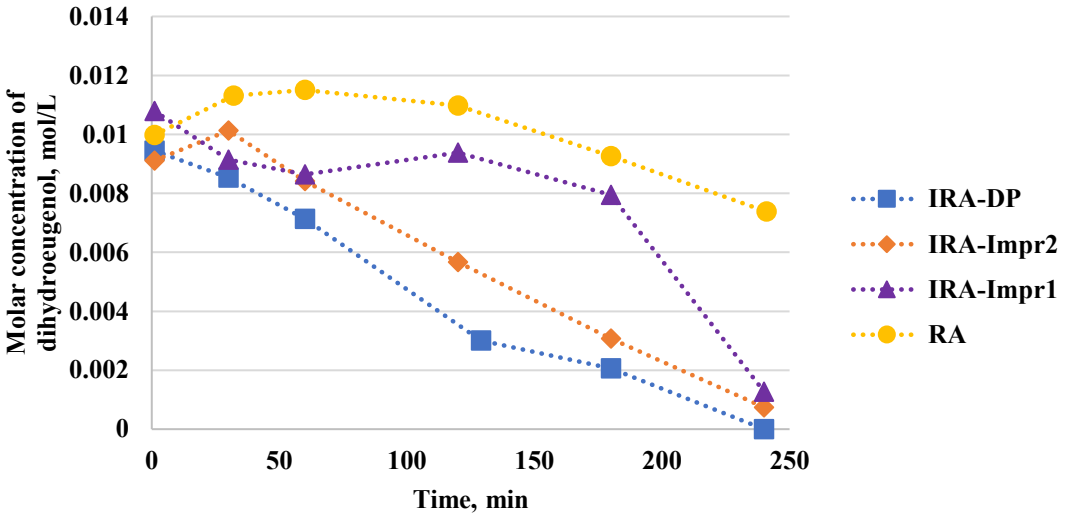

Figure 33 Molar concentration of dihydroeugenol as a function of time starting from 1 min sample in isoeugenol HDO at 250℃ and 30 bar total pressure over IrRe/Al_2O_3-DP (mao38), IrRe/Al_2O_3-Impr2 (mao41), IrRe/Al_2O_3-Impr1 (mao13) and Re/Al_2O_3 (mao22) catalysts.

4.2.2.1.2 Platinum and rhenium catalysts supported on alumina

In the current work, alumina supported platinum and rhenium catalysts (3 wt.% Pt-3 wt.% Re/Al_2O_3 and Pt/Al_2O_3) were investigated in isoeugenol HDO at 250℃ and 30 bar. Figure 34 shows GCLPAs for PRA-33, PA and RA catalysts after four hours of the reaction. The bimetallic catalyst displayed 45 % of GCLPA while PA and RA – 76 and 59 %, respectively, demonstrating that in the presence of rhenium the GCLPA drops at a high temperature. These observations can be rationalized considering formation of gaseous products over the bimetallic catalyst being in line with GC analysis of the liquid sample giving rather high amounts of hexane (0.003 mol/L), heptane (0.004 mol/L) and octane (0.008 mol/L). In addition, conversion of dihydroeugenol was 100 % using the bimetallic catalyst, while in the presence of monometallic ones the conversion of dihydroeugenol was only 14 and 36 % for Pt and Re respectively.

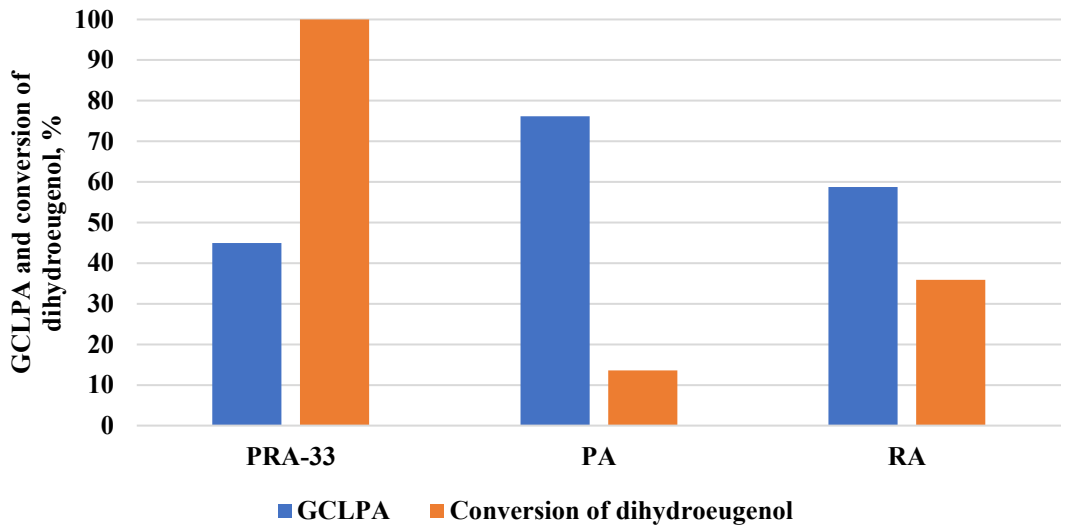

Figure 34 GCLPA and conversion of dihydroeugenol after four hours of reaction in isoeugenol HDO at 250℃ and 30 bar over alumina supported catalysts such as 3 wt.% Pt-3 wt.% Re/Al_2O_3 (mao14), Pt/Al_2O_3 (mao16) and Re/Al_2O_3 (mao22).

In Figure 35 the concentration of propylcyclohexane vs the reaction time is plotted for PRA-33 and PA showing a higher activity of PRA-33 catalyst in comparison with PA and RA in isoeugenol HDO at 250℃ and 30 bar. The final concentration of propylcyclohexane using PRA-33 turned out to be 0.007 mol/L (the initial concentration of isoeugenol is 0.012 mol/L). It is known that platinum is a catalytically active noble metal with deoxygenating ability [72], while Re demonstrates high selectivity towards aromatic ring hydrogenation [71].

Monometallic PA and RA catalysts demonstrated a low concentration of propylcyclohexane with RA being more active (0.0009 mol/L) than PA (0.0003 mol/L). According to Deepa and Dhepe [9], Pt-Al_2O_3 in eugenol HDO at 250℃ and 30 bar resulted mainly in formation of dihydroeugenol and absence of propylcyclohexane. In this work Pt/Al_2O_3 also showed low selectivity to propylcyclohexane.

Therefore, presence of Re in combination with Pt has a positive effect for selectivity towards propylcyclohexane.

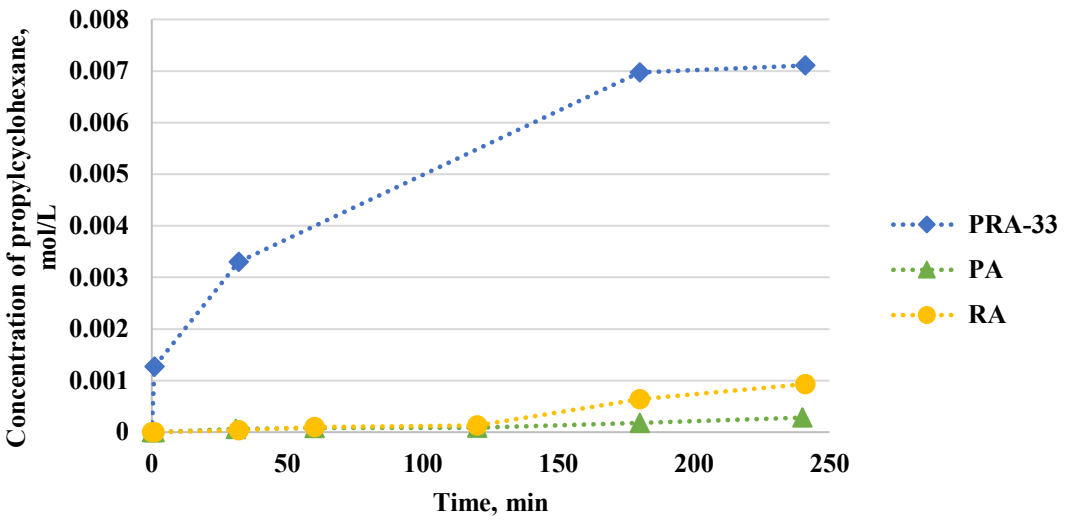

Figure 35 Molar concentration of propylcyclohexane vs reaction time in isoeugenol HDO at 250℃ and 30 bar total pressure over 3 wt.% Pt-3 wt.% Re/Al_2O_3 (mao14), Pt/Al_2O_3 (mao16) and Re/Al_2O_3 (mao22) catalysts.

Therefore, bimetallic alumina supported catalysts containing Ir, Pt and Re resulted in high conversion of dihyroeugenol and a high concentration of propylcyclohexane in isoeugenol HDO at 250℃ and 30 bar. A suitable temperature for hydrodeoxygenation is 250℃. The most efficient among alumina supported catalysts was IrRe/Al_2O_3-DP catalyst which resulted in complete conversion of dihydroeugenol and a high concentration of propylcyclohexane (0.009 mol/L). Superior performance of this catalyst was due to the presence of rhenium in the valence state 4+ and a high weight ratio of Re/Ir being 4.4 (the highest one) in comparison with IRA-Impr2 and IRA-Impr1.

4.2.2.2 Pressure effect over IRA-DP and IRA-Impr1

Based on the results in the temperature series two catalysts namely IrRe/Al_2O_3-DP and IrRe/Al_2O_3-Impr1 were selected for the pressure influence tests in isoeugenol HDO at 250℃.

Figure 36 represents the gas chromatography based sum of the reactant and the products from the liquid phase analysis (GCLPA) as a function of pressures. A minor decrease in GCLPA with a pressure increase can be observed.

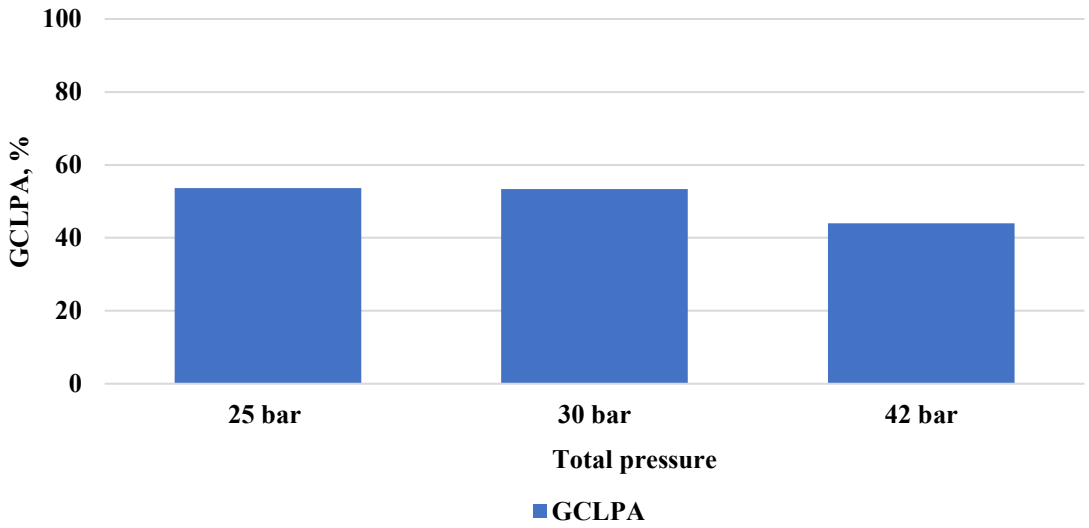

Figure 36 GCLPA after four hours of in isoeugenol HDO at 250℃ and 25 (mao52), 30 (mao38) and 42 (mao40) bar total pressure over IrRe/Al_2O_3-DP.

As can be seen from Figure 37, concentration of propylcyclohexane was the highest at 30 bar (0.009 mol/L) compared to 25 or 42 bar (0.0077 and 0.008 mol/L respectively).

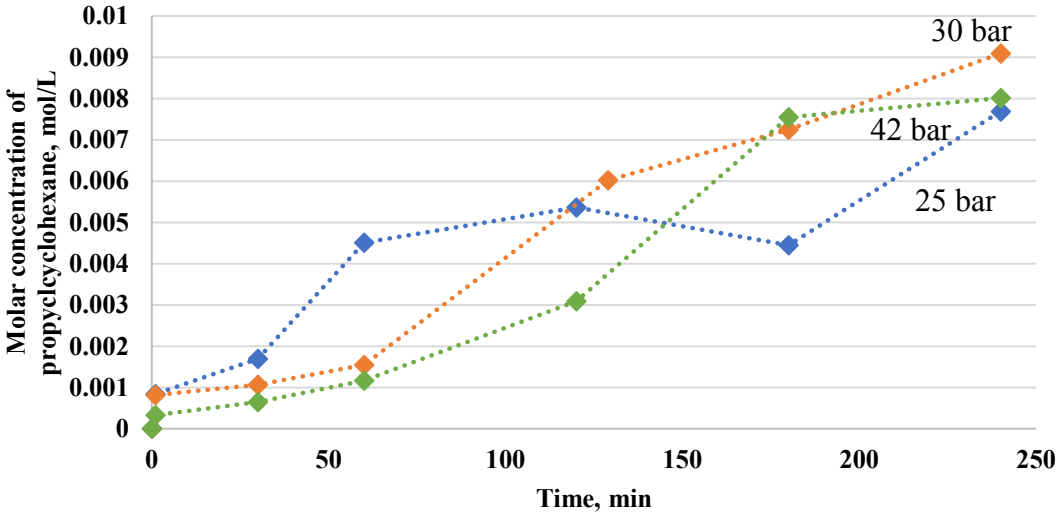

Figure 37 Molar concentration of propylcyclohexane vs reaction time in isoeugenol HDO at 250℃ and 25 (mao52), 30 (mao38) and 42 (mao42) bar total pressure over IrRe/Al_2O_3-DP.

The effect of hydrogen pressure in the range of 17-40 bar was also investigated using IRA-Impr1 catalyst in isoeugenol HDO at 250℃. The GCLPA was 84 % at 40 bar (Figure 38), which corresponds to the literature data [15].

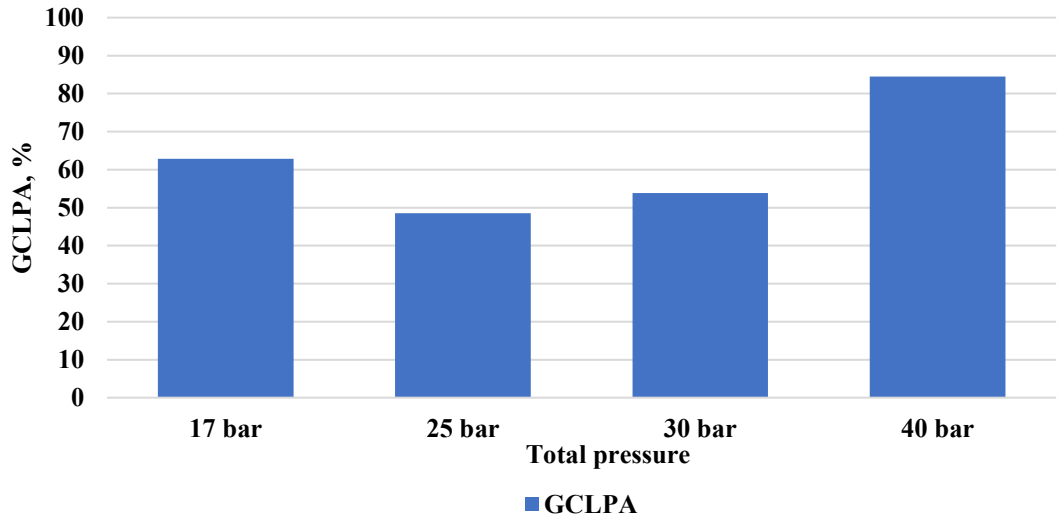

Figure 38 GCLPA after four hours of isoeugenol HDO at 250℃ and 17 (mao18), 25 (mao25), 30 (mao30) and 40 (mao37) bar total pressure over IrRe/Al_2O_3-Impr1.

Over IrRe/Al_2O_3-Impr1 in isoeugenol HDO at 250℃ and 40 bar propylcyclohexane formation was favored significantly in comparison with other pressures (Figure 39). There was a clear delay of HDO at the lowest pressure of 17 bar while a higher total pressure apparently prevents catalyst deactivation. After prolonged reaction times dihydroeugenol was completely converted at higher pressures, while a part of dihydroeugenol was still present at 25 bar even after 240 min.

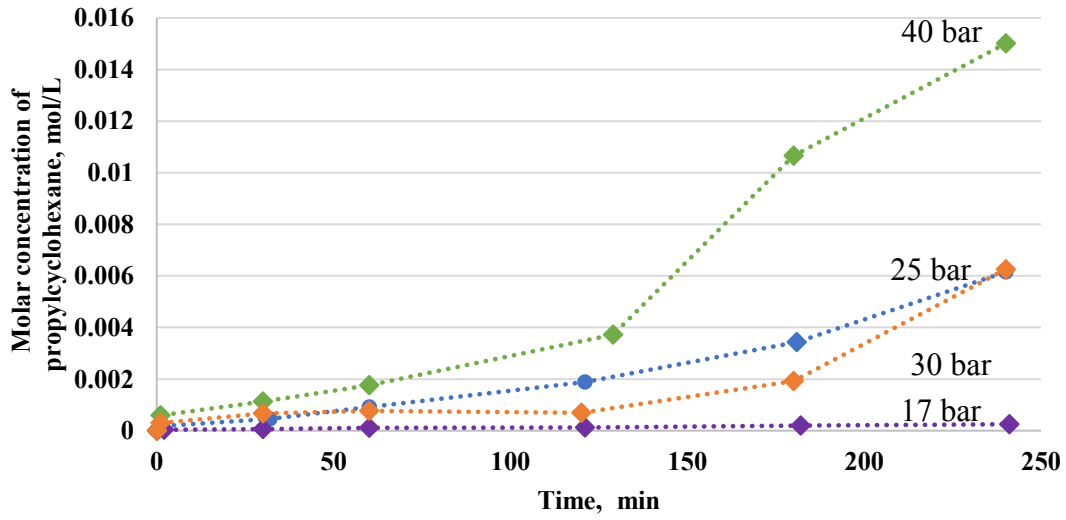

Figure 39 Molar concentration of propylcyclohexane vs reaction time in isoeugenol HDO at 250℃ and 17 (mao18), 25 (mao25), 30 (mao13) and 40 (mao37) bar total pressure over IrRe/Al_2O_3-Impr1.

Overall, differences in the pressure do not affect the reaction pathways as dihydroeugenol and propylcyclohexane were mainly produced, however, a higher

pressure influenced the HDO rate giving higher conversion. In the case of isoeugenol HDO over IRA-DP no big differences were seen with varying pressure except at 30 and 40 bar giving complete conversion of dihydroeugenol. In the case of IRA-Impr1 isoeugenol HDO at 40 bar showed the highest concentration of propylcyclohexane with the highest GCLPA of 84 %.

4.2.2.3 Reproducibility tests of the alumina supported catalysts

Repeatability tests were performed for isoeugenol HDO over IrRe/Al_2O_3-DP and IrRe/Al_2O_3-Impr2 at 250℃ and 30 bar.

From Figure 40, good repeatability can be confirmed based on the concentration of propylcyclohexane throughout the whole reaction course. In the first run the initial concentration of isoeugenol was 0.013 mol/L being selective to propylcyclohexane (0.0086 mol/L), while in the second experiment a slightly higher than 0.013 mol/L of isoeugenol was used to form 0.009 mol/L. Propylcyclohexane was formed as the main product with complete conversion of dihydroeugenol after four hours. Propylbenzene, 1,2,4-trimethylbenzene, 1-methyl-propylcyclohexane and cyclohexane were formed in small quantities, according to GC analysis of the liquid phase (Appendix XI). In the initial liquid sample for the 1st and 2nd runs, presence of hexane, heptane and octane was observed. Concentration of hexane, heptane and octane was as following 0.005 mol/L, 0.004 mol/L and 0.006 mol/L, respectively after 4 h. The second test had no hexane and octane, while heptane was formed (0.001 mol/). These compounds are coming from dodecane which was confirmed in Section 4.2.3.1.2.

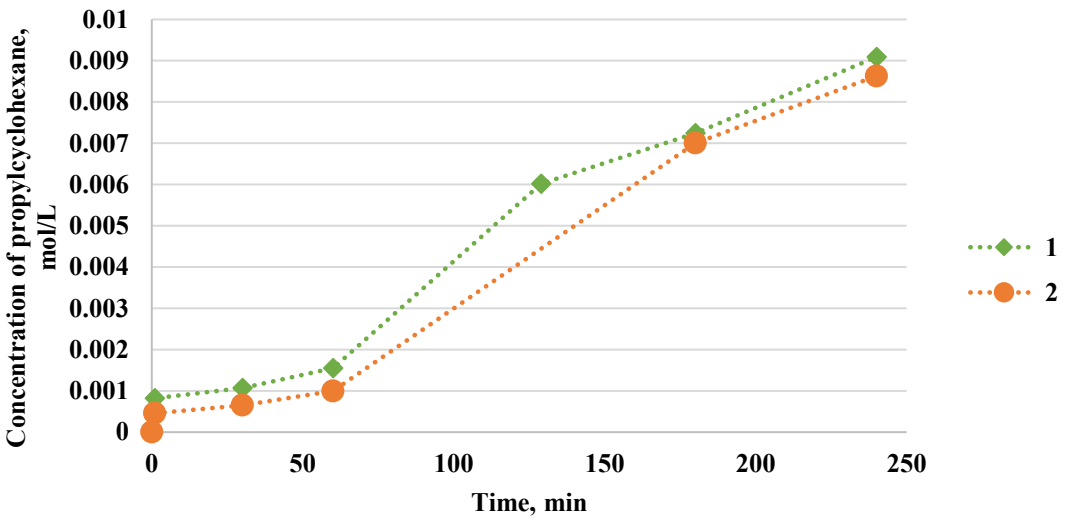

Figure 40 Concentration of propylcyclohexane vs reaction time for isoeugenol HDO at 250℃ and 30 bar total pressure over IrRe/Al_2O_3-DP in repeatability tests (1-mao38 and 2-mao17).

IrRe/Al_2O_3-Impr2 catalyst was used three times in isoeugenol HDO at 250℃ and 30 bar total pressure. Almost similar yields of propylcyclohexane can be seen in Figure 41 over IRA-Impr2 catalyst. The initial concertation for the first and second tests were 0.0121 mol/L and 0.0127 mol/L correspondingly, resulting in concentration of propylcyclohexane equal 0.0059 and 0.0057 mol/L respectively. The same products were present as in the case of IRA-DP catalyst, namely propylbenzene and 1,2,4-trimethylbenzene as well as 1-methylpropylcyclohexane, cyclopentane and cyclohexane in minor increasing amounts. Only low quantities of heptane (for the 1st test) and octane (for the 1st and 2nd ones) were observed.

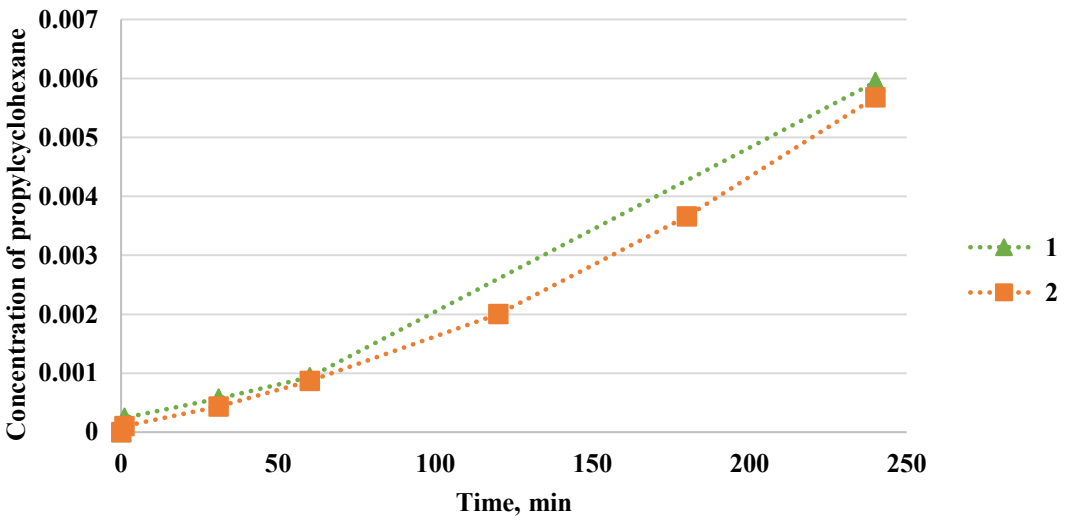

Figure 41 Concentration of propylcyclohexane vs reaction time for isoeugenol HDO at 250℃ and 30 bar total pressure over IrRe/Al_2O_3-Impr2 in repeatability tests (mao41 and mao26).

Overall, the use of both catalysts IrRe/Al_2O_3-DP and IrRe/Al_2O_3-Impr2 demonstrated good repeatability performance in isoeugenol HDO at 250℃ and 30 bar total pressure in the presence of hydrogen based on the concentration of propylcyclohexane.

4.2.2.4 Stability tests of the best IRA series catalysts

IrRe-Al_2O_3-DP and IrRe/Al_2O_3-Impr1 were used for reproducibility tests based on the concentration of propylcyclohexane (0.009 mol/L and 0.006 mol/L respectively).

4.2.2.4.1 IRA-DP

For the reproducibility test of IRA-DP 0.4 mg of the catalyst and 0.8 mg of the reactant were utilized. As can be seen from Figure 42, mainly propylcyclohexane was produced (97 % selectivity based on the molar products concentrations). As the initial concentration of isoeugenol was estimated to be 0.06 mol/L the catalyst was very selective towards propylcyclohexane yield (0.06 mol/L).

During this reaction, dihydroeugenol, 1-methyl-propylcyclohexane and cyclohexane were present after four hours of isoeugenol HDO (Figure 42). Dihydroeugenol was not completely converted, whereas, propylbenzene and 1,2,4-trimethylbenzene appeared at one minute sampling and vanished almost after two hours of the reaction, the former one leading to hydrogenated product propylcyclohexane. These results can be explained by a higher reaction rate obtained with a higher initial isoeugenol

concentration. During this test, hexane, heptane and octane were obtained in the concentration of ca. 0.02 mol/L each and in total ca. 0.006 mol/L (which were not included into GCLPA calculations).

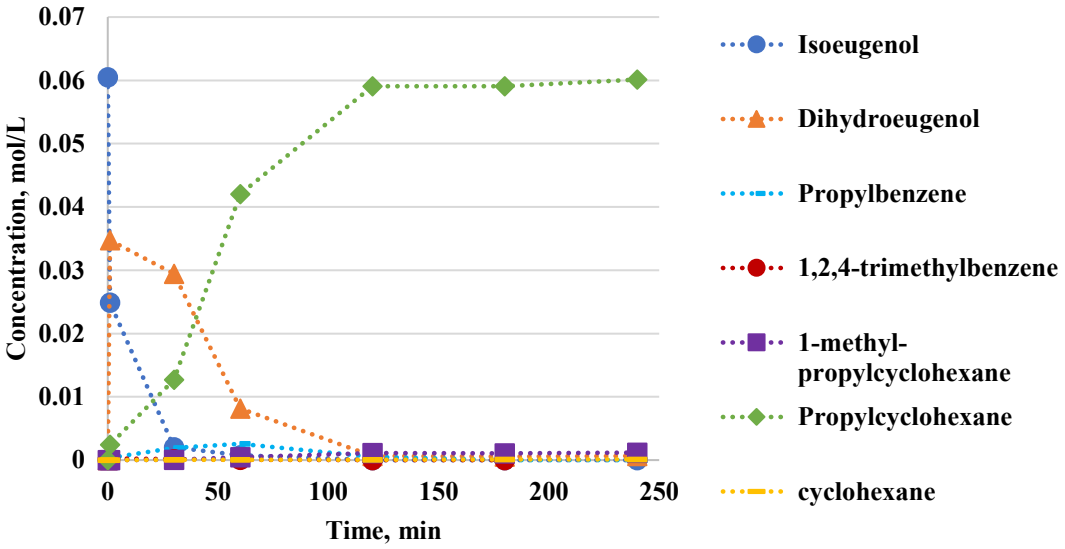

Figure 42 Concentration of isoeugenol and products vs reaction time in isoeugenol HDO at 250℃ and 30 bar total pressure over the fresh IrRe/Al_2O_3-DP catalyst (mao53).

The spent catalyst was characterized by N_2 physisorption, showing the specific surface area of 101 m^2/g, being the same as for the fresh one (Table 16).

After the first reaction the spent catalyst was regenerated using the temperature program described in Section 3.1.4 (T_{max}=400℃). As can be seen from Figure 43, this time isoeugenol (0.01 mol/L) HDO was not so selective towards propylcyclohexane (ca. 0.004 mol/L) over regenerated IrRe/Al_2O_3-DP, and moreover high amounts of dihydroeugenol (ca. 0.003 mol/L) were observed. As mentioned earlier, the spent catalyst does not possess rhenium valence state of 4+ anymore after isoeugenol HDO at 250℃ and 30 bar (Section 4.1.7), diminshing the reaction rate of isoeugenol and transformations of intermediates into propylcyclohexane. Low amounts of cyclohexane and 1-methylpropylcyclohexane were observed after four hours of the reaction. High concentrations of hexane, heptane and octane were obtained for isoeugenol HDO over the regenerated IrRe/Al_2O_3-DP (0.014, 0.012 and 0.018 mol/L respectively). Consequently in the presence of the deposited-precipitated Ir and Re metals on alumina support high amounts of gaseous products can be obtained.

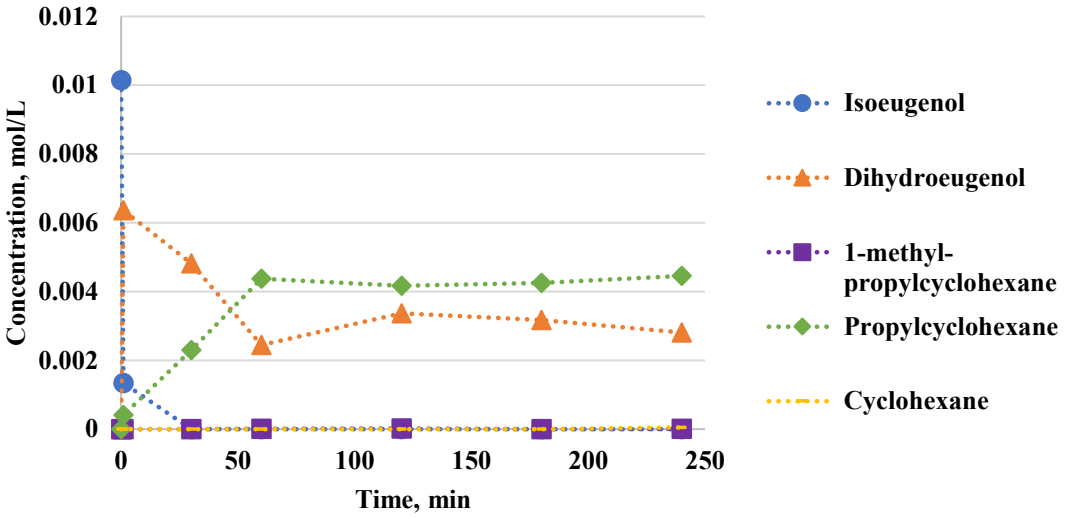

Figure 43 Concentration of isoeugenol and products vs reaction time in isoeugenol HDO at 250℃ and 30 bar total pressure over the regenerated IrRe/Al_2O_3-DP catalyst (mao54).

At a higher concentration of the reactant and IRA-DP catalyst with the same weight ratio of 2), a more prominent formation of propylcyclohexane was observed in isoeugenol HDO. The fresh IrRe/Al_2O_3-DP catalyst demonstrated almost complete selectivity towards propylcyclohexane, while the regenerated one resulted in ca. 40 % selectivity of propylcyclohexane which can be related to the absence of rhenium in 4+ valence state.

4.2.2.4.2 IRA-Impr1

IrRe-Al_2O_3-Impr1 was also utilized for stability tests too. From Figure 44, substantial conversion of dihydroeugenol can be seen between 1 and 2 h, accelerating formation of 1-methyl-propylcyclohexane and propylcyclohexane. Propylbenzene and 1,2,4-trimethylbenzene were also formed being present after four hours of isoeugenol HDO. In this reaction hexane, heptane and octane were not observed after four hours of the reaction in comparison with IrRe/Al_2O_3-DP catalyst.

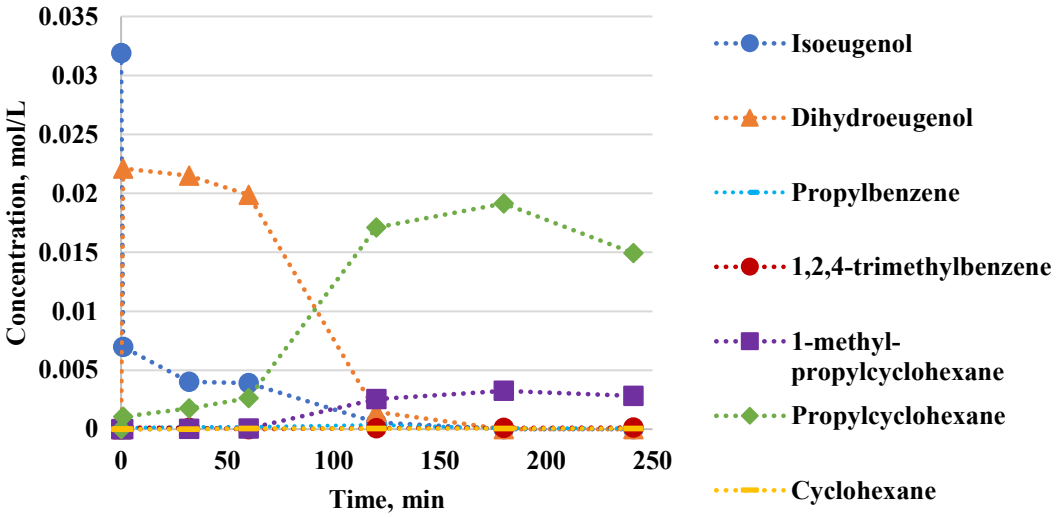

Figure 44 Concentration of isoeugenol and products vs reaction time in isoeugenol HDO at 250℃ and 30 bar total pressure over the fresh IrRe/Al_2O_3-Impr1 catalyst (mao27).

The spent catalyst was characterized by N_2 physisorption, showing the specific surface area being 203 m^2/g, almost the same as for the fresh one (Table 16), i.e. apparently no coking in isoeugenol HDO at 250℃ and 30 bar was present.

The regenerated IrRe/Al_2O_3-Impr1 (0.117 mg) and the reactant (0.234 mg) were utilized resulting in the same product distribution as for the fresh one in isoeugenol HDO at 250℃ and 30 bar (Figure 44). As can be seen from Figure 45, isoeugenol was converted to propylcyclohexane (0.016 mol/L). A constant concentration of 1-methyl-propylcyclohexane can be observed from two to four hours of the reaction. Formation of hexane, heptane and octane in gas phase was high for the regenerated catalyst being approximately 0.003 mol/L each (the sum ca. 0.009 mol/L). It can be therefore concluded that the fresh catalyst was more active than the regenerated one since mainly light alkanes such as methane and ethane were produced in high quantities (Figure 29), furthermore, C_6H_{14}, C_7H_{16} and C_8H_{18} after four hours of the reaction in isoeugenol HDO at 250℃ and 30 bar were absent for the fresh catalyst.

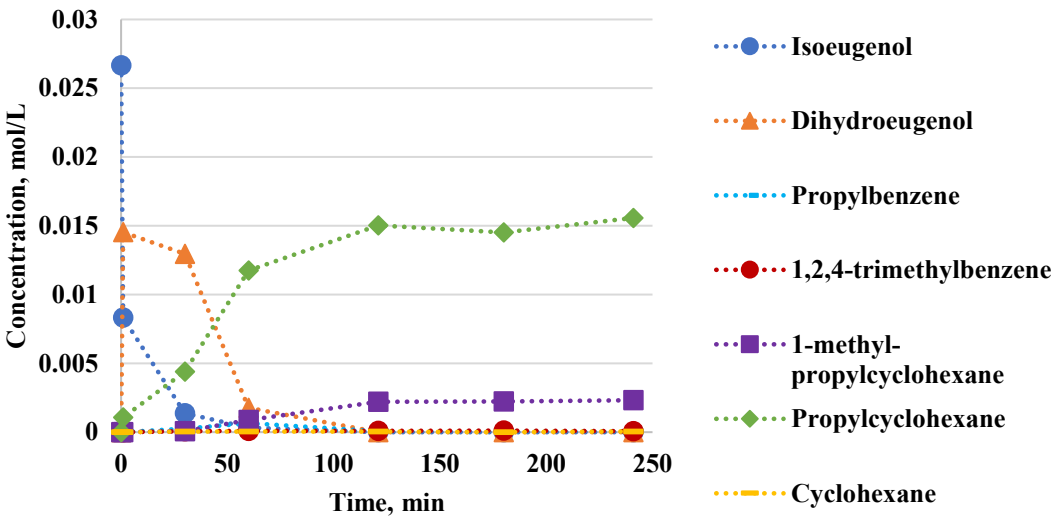

Figure 45 Concentration of isoeugenol and products vs reaction time in isoeugenol HDO at 250℃ and 30 bar total pressure over the regenerated IrRe/Al_2O_3-Impr1 catalyst (mao32).

The regenerated catalyst was characterized by N_2 physisorption showing a small decrease in the specific surface area (Table 16).

Overall, IrRe/Al_2O_3-Impr1 demonstrated good stability being completely converted in the presence of the regenerated catalyst in isoeugenol HDO at 250℃ and 30 bar. The same product distribution was observed after regeneration. The yields of propylcyclohexane in both cases were significant (0.015 mol/L and 0.016 mol/L for the fresh and the regenerated catalysts respectively). In the presence of the fresh catalyst light alkanes were formed, while for the regenerated IrRe/Al_2O_3-Impr1 hexane, heptane and octane were observed.

4.2.2.5 Optimization of isoeugenol HDO

In the current work isoeugenol HDO was performed with a higher quantity of the reactant at 250℃ and 30 bar with IrRe/Al_2O_3-DP. One gram of the reactant and 0.1 g of the catalyst were used with the weight ratio of 10 between isoeugenol and IRA-DP, which was even larger than in a typical experiment.

As can be seen from Figure 46 showing a comparison of two isoeugenol HDO tests with 0.1 g IRA-DP catalyst isoeugenol reacted faster than in case of 0.05 g. This is typically a sign of more prominent catalyst deactivation at lower catalyst loadings.

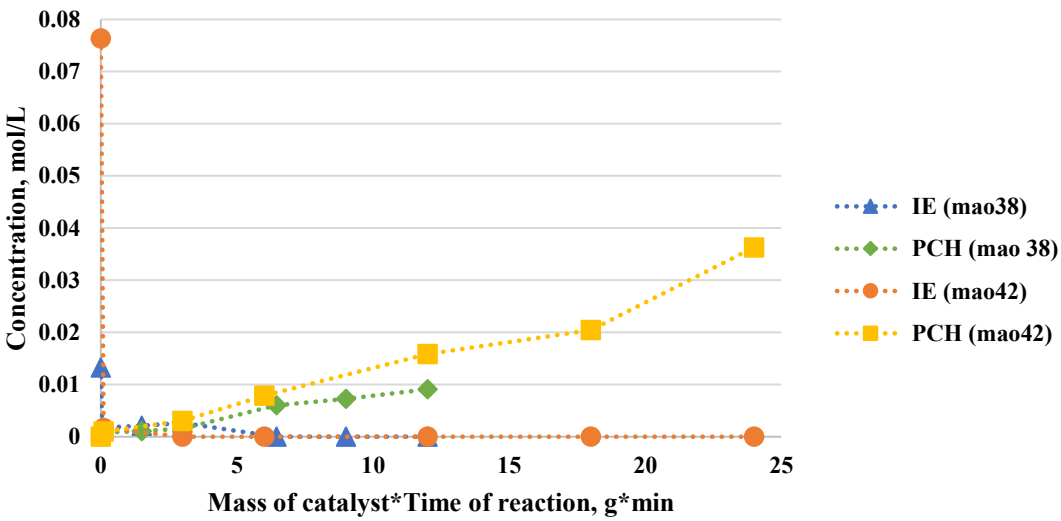

*Figure 46 Concentration of isoeugenol (IE) and propylcyclohexane (PCH) vs mass of catalyst applied in isoeugenol HDO * reaction time using IRA-DP catalyst (mao38 and mao42).*

As seen in Figure 47 the initial concentration of isoeugenol was 0.076 mol/L according to GC liquid phase analysis. Only ca. 47 % yield of propylcyclohexane (0.036 mol/L) was obtained. Dihydroeugenol was gradually converted at a low catalyst loading, being present even after 4 hours of the reaction (0.008 mol/L). In addition, propylbenzene concentration was increasing moderately throughout 4 hours. Among other products 1-methyl-propylcyclohexane, propylcyclopentane and cyclohexane were seen in minor amounts increasing with time, while 1,2,4-trimethylbenzene concentration was decreasing. Production of hexane, heptane and octane was insignificant.

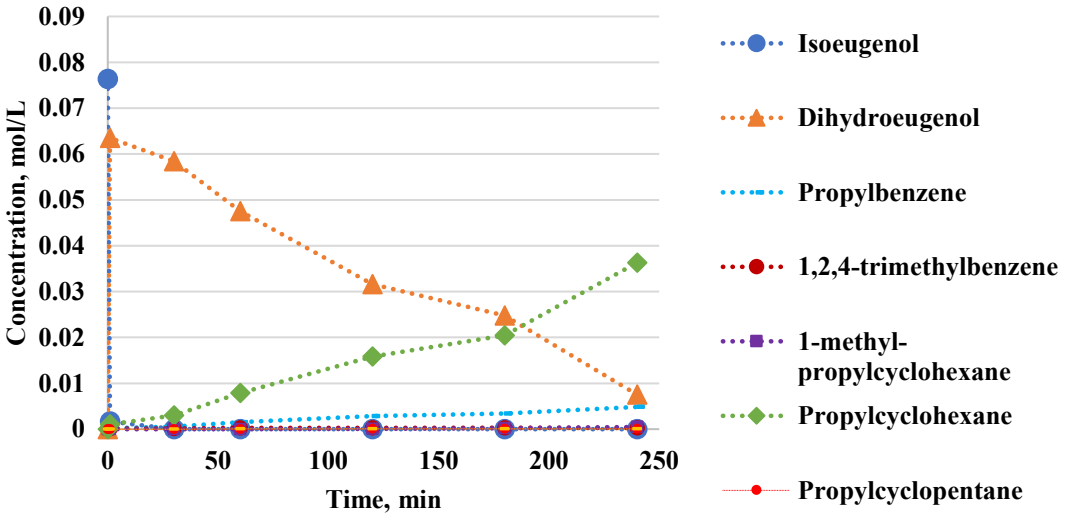

Figure 47 Concentration of isoeugenol and products vs reaction time in isoeugenol HDO at 250℃ and 30 bar total pressure over IrRe/Al_2O_3-DP catalyst (mao42).

In isoeugenol HDO at 250℃ and 30 bar (Appendix XI), when the initial concentration of isoeugenol was 0.013 mol/L, 0.009 mol/L of propyclohexane was obtained (69 % yield), while for a higher concentration of isoeugenol (0.069 mol/L) and a lower catalyst mass of catalyst (0.1 g), 47 % of propylcyclohexane was yielded.

4.2.2.6 Concluding remarks using alumina supported catalysts in isoeugenol HDO

Preferable conditions for isoeugenol HDO over alumina supported catalysts were 250℃, total pressure of 30 bar and bimetallic catalysts. The best alumina supported catalyst under these conditions was IrRe/Al_2O_3-DP being highly selective towards propylcyclohexane (0.009 mol/L). Despite almost similar impregnation synthesis method of IrRe/Al_2O_3-Impr2 and IrRe-Al_2O_3-Impr1, the latter was more selective towards propylcyclohexane than the former one. The spent IrRe/Al_2O_3-Impr2 had a significant coke formation confirmed via CHNS and EDX analysis in comparison with the spent IrRe/Al_2O_3-Impr1. Good reproducibility for tests were demonstrated over IrRe/Al_2O_3-DP and IrRe/Al_2O_3-Impr2 in isoeugenol HDO at 250℃ and 30 bar. Stability tests demonstrated that over IRA-Impr1 the fresh catalyst was more active towards cracking giving methane and ethane than the regenerated one resulting also in C_6H_{14}-C_8H_{18}. Hexane, heptane and octane were mainly formed over the bimetallic alumina supported catalysts such as IRA-DP, IRA-Impr2, IRA-Impr1 and PRA-33. The reaction rate is directly proportional not only to isoeugenol concentration but also to catalyst mass, as in the case of IRA-DP catalyst.

4.2.3 Catalysts with zirconia as a support

4.2.3.1 Isoeugenol HDO

4.2.3.1.1 Temperature effect

Zirconia supported catalysts such as Ir/ZrO_2 and 10 wt.% Ni/ZrO_2 were utilized to study the temperature effect in isoeugenol HDO by performing catalytic reaction at 150℃, 200℃ and 250℃ for 4 hours. As discussed above conversion of isoeugenol to dihydroeugenol occurred even in the absence of any catalyst.

In Figure 48 a gradually decrease of GCLPA using Ir/ZrO_2 catalyst can be seen with temperature increase. In case of 10 wt. % Ni/ZrO_2 catalyst a sharp decrease of GCLPA can be observed (Figure 48). A higher reaction temperature resulted in a more prominent GCLPA decrease, e.g. at 250℃ GCLPA was 15 and 23 % for 10 wt.% Ni/ZrO_2 and Ir/ZrO_2 respectively, while at a lower reaction temperature GCLPA was higher, namely 99 and 69 % at 150℃, respectively. These results were in agreement with a more prominent adsorption of reactants and formation of gaseous products at a higher reaction temperature.

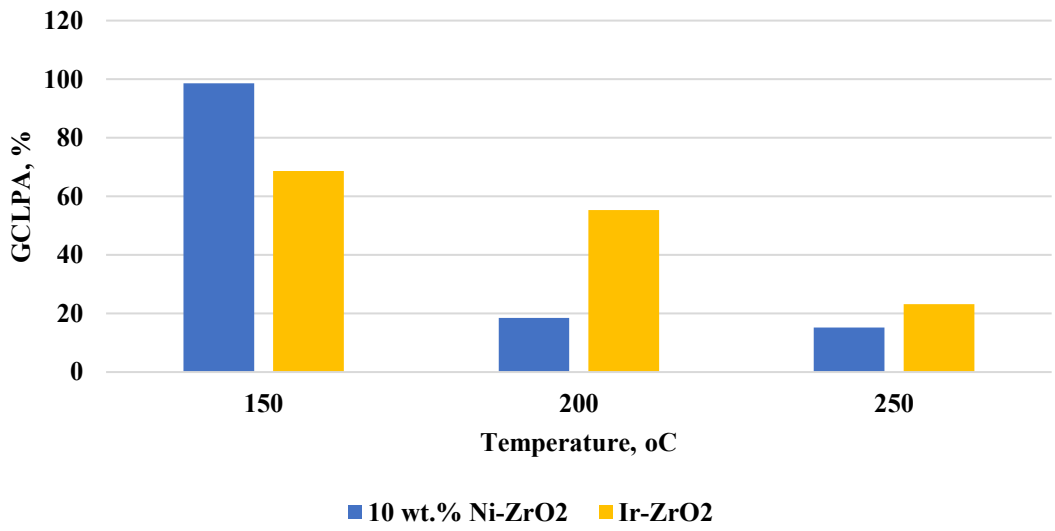

Figure 48 GCLPA after four hours of isoeugenol HDO at 150 (mao4 and 5 resp.), 200 (mao20 and 8 resp.) and 250℃ (mao21 and 19 resp.) and 30 bar of total pressure over 10 wt.% Ni/ZrO_2 and Ir/ZrO_2.

Furthermore, as seen in Figure 49 dihydroeugenol was converted almost completely at 250℃ and 30 bar of total pressure for both catalysts being around 95 and 94 % for 10 wt.% Ni/ZrO_2 and Ir/ZrO_2, respectively, while at lower temperatures the

conversions were significantly low. Therefore, a higher conversion of dihydroeugenol was related to larger formation of propylcyclohexane, as noted by Deepa and Dhepe [9].

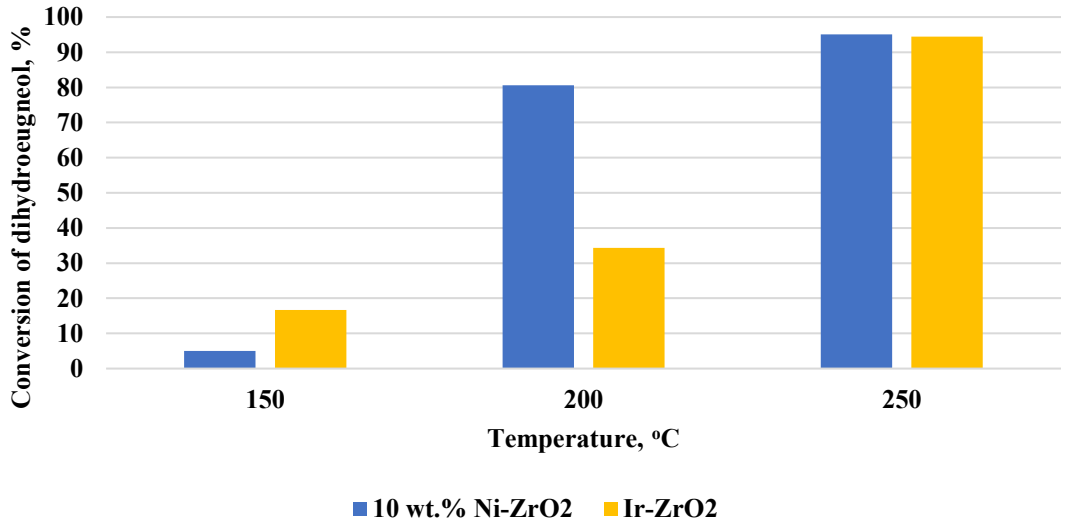

Figure 49 Conversion of dihydroeugenol after four hours of the reaction vs temperature for isoeugenol HDO at 150, 200 and 250℃ and 30 bar of total pressure over 10 wt.% Ni/ZrO_2 and Ir/ZrO_2.

As one of the aims of this work was to obtain hydrodeoxygenated compounds such as propylcyclohexane, the influence of the reaction temperature on the concentration of propylcyclohexane during 4 hours of the reaction is plotted (Figure 50). Considering the initial concentration of isoeugenol (0.012 mol/L), the highest concentration of propylcyclohexane was observed at 250℃ where 0.0028 mol/L of the product was formed. At 150℃ and 200℃ the concentration of propylcyclohexane was 0.0002 and 0.0005 mol/L respectively. Therefore, a seven fold increase for the concentration of propylcyclohexane from 150℃ to 250℃ was observed by increasing the temperature. According to the literature [73], it was noted that zirconia support activates the oxy-compounds on the surface favoring deoxygenated compounds.

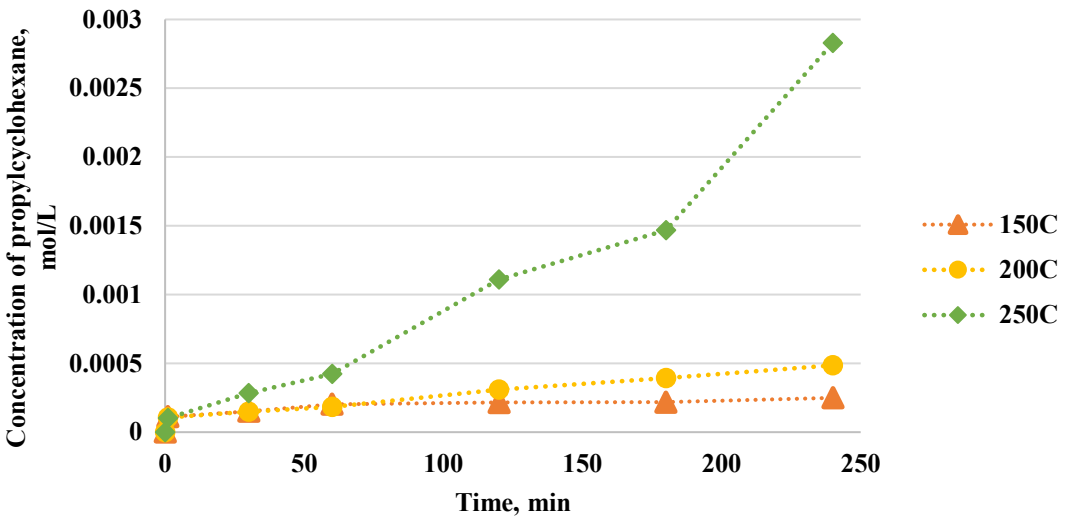

Figure 50 Concentration of propylcyclohexane vs time obtained in isoeugenol HDO at 150, 200 and 250℃ and 30 bar of total pressure over Ir/ZrO_2.

In case of 10 wt.% Ni/ZrO_2 catalyst there was a slight difference in the distribution of the deoxygenated productdepending on temperature. At 150℃ there was formation of 1,2,4-trimethylbenzene, while at 200 and 250℃ propylcyclohexane was observed (Figure 51). Consequently, low temperature is not sufficient enough even at high pressure of 30 bar to hydrogenate the phenyl ring.

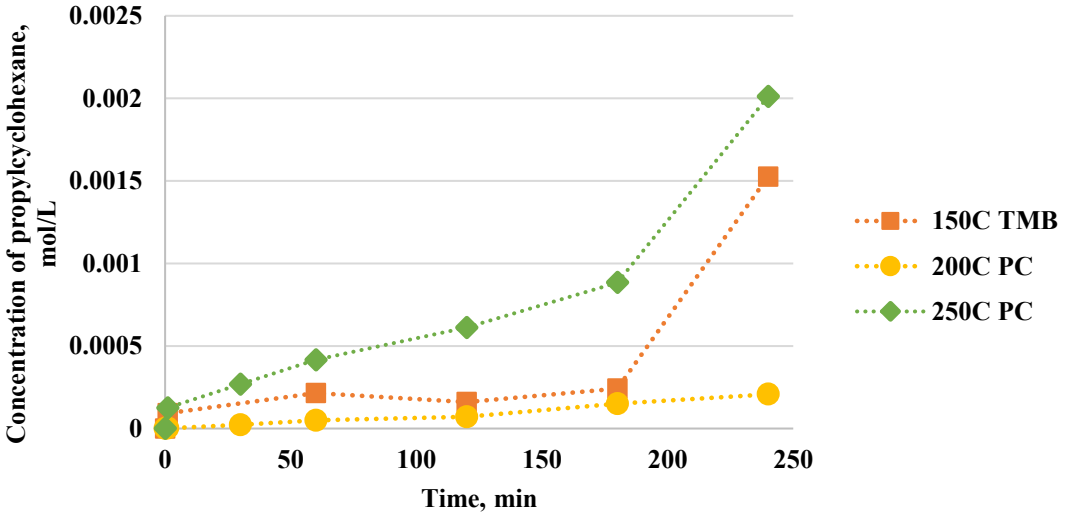

Figure 51 Concentration of propylcyclohexane vs time obtained via isoeugenol HDO at 150, 200 and 250℃ and 30 bar of total pressure over 10 wt.% Ni/ZrO_2.

4.2.3.1.2 Transformations of solvent over Ir/ZrO_2

Hydrodeoxygenation test was performed without any model compound at 250℃ and 30 bar total pressure over Ir/ZrO_2 catalyst allowing to investigate the influence of the

solvent dodecane (Figure 52). The amount of such alkanes as hexane, heptane and octane was increased significantly in the absence of isoeugenol. As mentioned earlier, the initial molar concentration of isoeugenol was 0.012 mol/L, while hexane, heptane and octane concentration were 0.018, 0.017 and 0.024 mol/L, respectively, after four hours in the absence of isoeugenol. On the other hand in the presence of isoeugenol concentration of hexane, heptane and octane was zero.

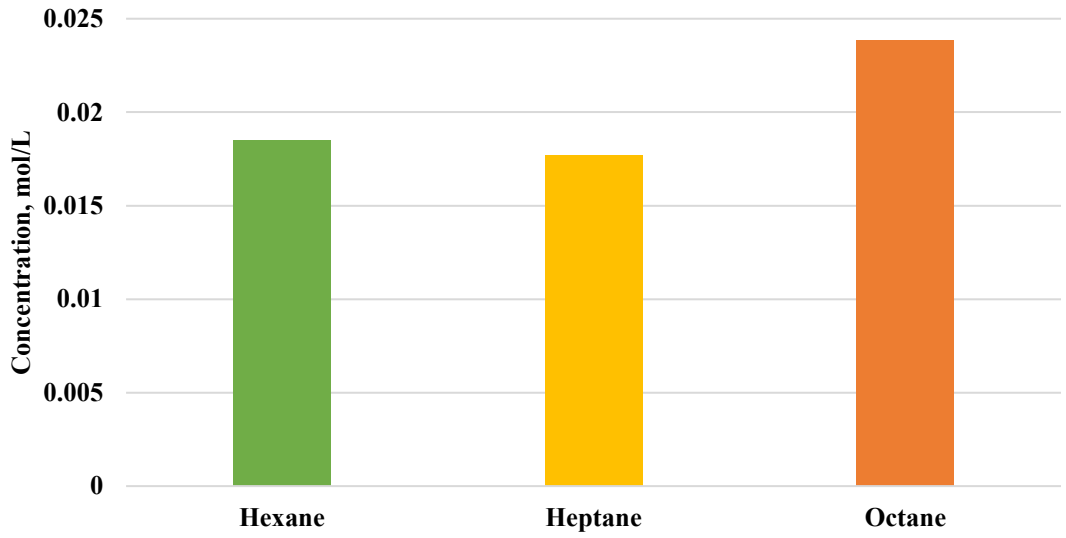

Figure 52 Concentrations of hexane, heptane and octane in HDO at 250℃ and 30 bar total pressure in the absence of isoeugenol as a reactant.

4.2.3.2 Guaiacol HDO

Hydrodeoxygenation of guaiacol was performed over Ir/ZrO_2 and 10 wt.% Ni/ZrO_2 at 250℃ and 30 bar total pressure. Cyclohexanol and 2-methoxycyclohexanone were mainly formed with minor quantities of cyclohexane and methoxycyclohexane. Complete conversion of guaiacol was obtained over both catalysts, however, GCLPA was different being 43 and 54 % for Ir/ZrO_2 and 10 wt.% Ni/ZrO_2 respectively.

During these experiments the gas samples were taken and analyzed both by GC and GC-MS after four hours of the reaction. Methane was the main compound present in GC while ethane, propane, butane and other gases were detected for both reactions over zirconia supported catalysts in GC-MS in addition to methane. Comparing the first three minutes of retention time in GC-MS for both catalysts, it can be stated that more gases were formed for Ir/ZrO_2 catalyst in comparison with 10 wt.% Ni/ZrO_2. Over Ir/ZrO_2 catalyst more CH_4 was produced than over 10 wt.% Ni/ZrO_2 (Figure 53).

Ethane exhibited the highest peak at RT of 1.2 min for both catalysts (Figure 53). Formation of a larger amounts of gaseous products over Ir/ZrO_2 compared to 10 wt.% Ni/ZrO_2 could explain a low GCLPA (43 %).

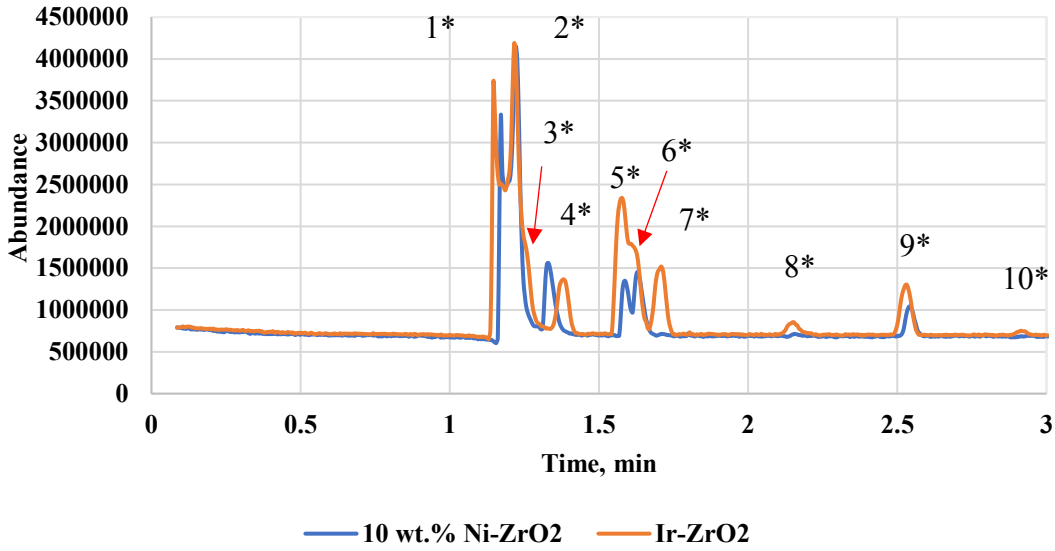

Figure 53 Gas samples taken after four hours of guaiacol HDO at 250℃ and 30 bar total pressure over Ir/ZrO_2 and 10 wt.% Ni/ZrO_2 catalysts via GC-MS.
Notation: 1- methane (1.15 and 1.2 min), 2*- ethane (1.22 min), 3*- propane (1.26 min), 4*- butane (1.33 and 1.4 min), 5* and 6*- 2-propanone and 2-propanol (1.58 and 1.62 min), 7*- pentane (1.71 min), 8*- cyclopentane (2.14 min), 9*- hexane (2.54 min), 10*- methylcyclopentane (2.91 min).*

Considering Ir/ZrO_2 catalyst distribution of the reactant and products in terms of the molar concentration vs the reaction time in guaiacol HDO is presented in Figure 54. The initial concentration of guaiacol was 0.015 mol/L. As can be seen from Figure 54 the concentration of the formed products is almost twofold lower than the initial reactant concentration. The main products were cyclohexanol, cyclohexane and 2-methoxycyclohexanone. According to Zhang et al. [74], methoxy group restrains deoxygenation, which explains presence of a low amount of 1-methoxycyclohexane throughout the reaction. Formation of methoxycyclohexanol from guaiacol was not observed. On the other hand, the hydrogenated product such as 2-methoxycyclohexanone was formed having the highest peak at ca. 2 h at 250℃ and then decreased gradually. Consequently, this product reacted further by hydrogenation and hydrogenolysis giving cyclohexanol (0.004 mol/L) and cyclohexane (0.002 mol/L). With formation of hydrodeoxygenated compounds such propylcyclohexane

(0.002 mol/L), Ir/ZrO_2 was active in hydrodeoxygenation. Iridium is known to catalyze hydrogenation [20], while zirconia is efficient in deoxygenation [62].

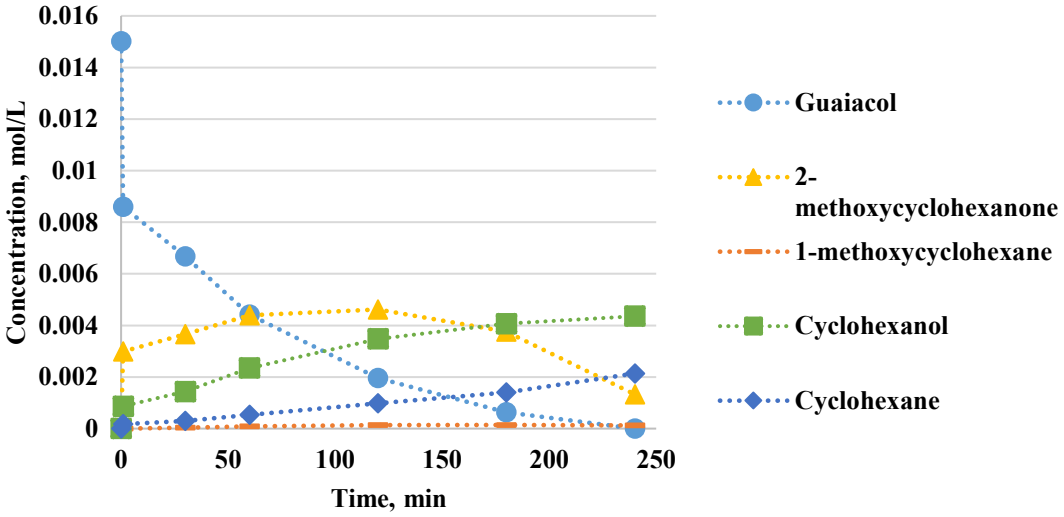

Figure 54 Concentration of the reactant and products vs reaction time in guaiacol HDO at 250℃ and 30 bar total pressure in the presence of hydrogen over Ir/ZrO_2.

Over 10 wt.% Ni/ZrO_2 catalyst in HDO at 250℃ and 30 bar guaiacol was converted completely after 3 h when the initial concentration was ca. 0.018 mol/L (Figure 55). The formed products were the same as in the case of iridium on the same support, however, the product distribution was different. Mainly cyclohexanol and 2-methoxycyclohexanone were formed (0.006 and 0.004 mol/L respectively). Very low amounts of cyclohexane and 1-methoxycyclohexane were obtained. According to Mortensen et al. [25], 5 wt.% Ni/ZrO_2 displayed the best performance among catalysts tested in hydrodeoxygenation of phenol yielding 80 mol % of cyclohexane and 10 mol % of cyclohexanol. In the works of Mortensen et al. [25] and Zhang et al. [30], where guaiacol was used as the reactant, cyclohexane was present with selectivity of 30 and 75 % respectively to 5 wt. % and 10 wt. % metal loadings of Ni/ZrO_2.

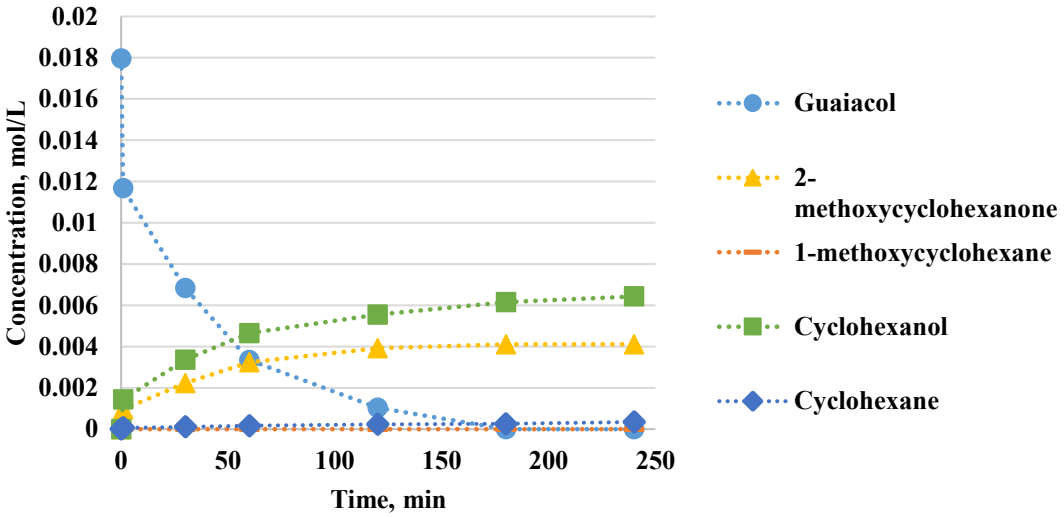

Figure 55 Concentration of reactant and products vs reaction time in guaiacol HDO at 250℃ and 30 bar total pressure in the presence of hydrogen over 10 wt. % Ni/ZrO₂.

Concluding it can be stated that in guaiacol HDO over Ir/ZrO_2 and 10 wt. % Ni/ZrO_2 complete conversion of guaiacol was observed. Ir/ZrO_2 catalyst was more active as it catalyzed guaiacol HDO not only to formation of alcohol but also cyclohexane (0.002 mol/L), while insignificant amounts of 0.0003 mol/L were obtained over 10 wt. % Ni/ZrO_2. Despite a higher activity of Ir/ZrO_2 GCLPA was lower (48 %) compared to 10 wt. % Ni/ZrO_2 (57 %) due to more prominent formation of gaseous products.

4.2.3.3 Vanillin HDO

Thermal vanillin HDO was investigated demonstrating formation of vanillin alcohol and incomplete conversion of vanillin at 100℃ and 30 bar total pressure with GCLPA of 91 % (Entry mao45 in Appendix XI). Using Ir/ZrO_2 and 10 wt. % Ni/ZrO_2 hydrodeoxygenation of vanillin was further performed at 100℃ and 30 bar total pressure in the presence of hydrogen with water as a solvent. Figure 56 displays that conversion of vanillin was almost complete being 99 % for Ir/ZrO_2 and 94 % for 10 wt. % Ni/ZrO_2. According to Zhang et al. [75], carbonyl group restrains hydrodeoxygenation of phenolic compounds, consequently, lowering conversion of vanillin. GCLPA was the highest over 10 wt. % Ni/ZrO_2 being 92 %. Over Ir/ZrO_2 GCLPA was 78 % in line with guaiacol HDO.

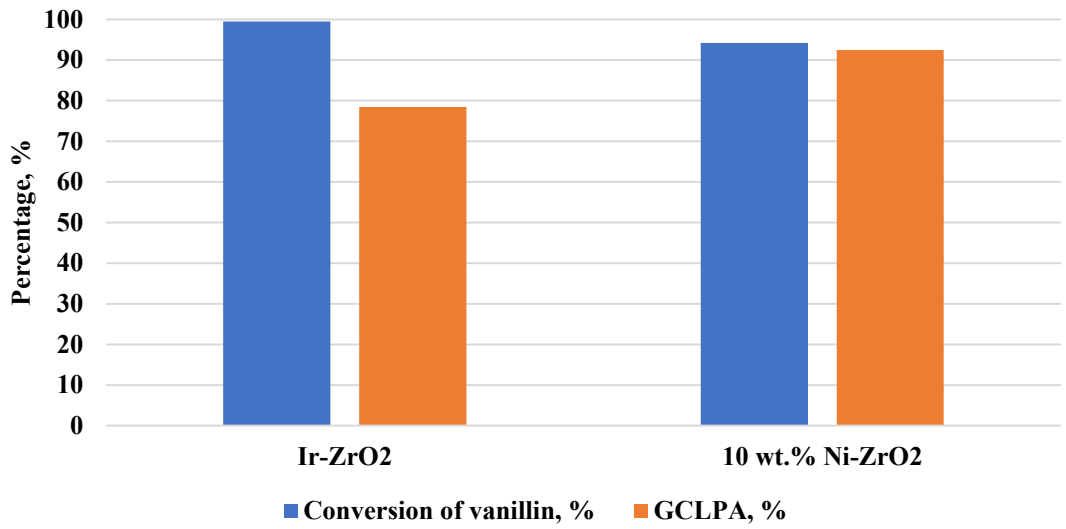

Figure 56 Conversion of vanillin and GCLPA after four hours of vanillin HDO at 100℃ and 30 bar total pressure in the presence of hydrogen over Ir/ZrO_2 and 10 wt. % Ni/ZrO_2.

As can be seen from Figure 57 for the initial concentration of vanillin (0.0077 mol/L) vanillyl alcohol (0.0059 mol/L) was formed as the main product over Ir/ZrO_2. No any other products were identified in HPLC. The same result in terms of selectivity was achieved in the absence of any catalyst (thermal test mao45).

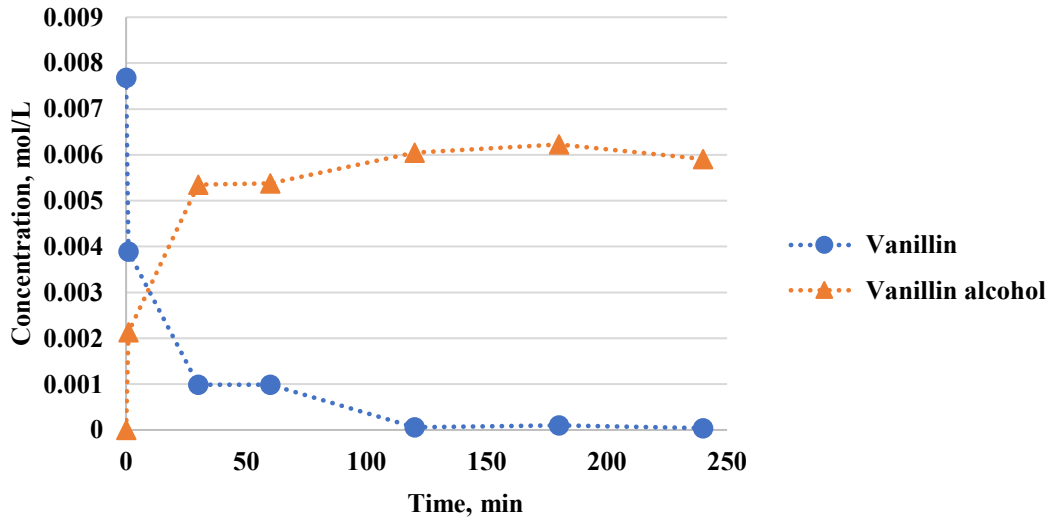

Figure 57 Concentration of the reactant and product versus time in vanillin HDO at 100℃ and 30 bar total pressure in the presence of hydrogen over Ir/ZrO_2.

Using 10 wt. % Ni/ZrO_2 catalyst the same results were observed for vanillin HDO as in the case of Ir/ZrO_2 (Figure 58). The main product was vanillin alcohol with 0.0059 mol/L concentration after four hours. Unconverted vanillin concentration was 0.0004

mol/L. No any other products were seen in HPLC similar to results in the absence of any catalyst (thermal test mao45).

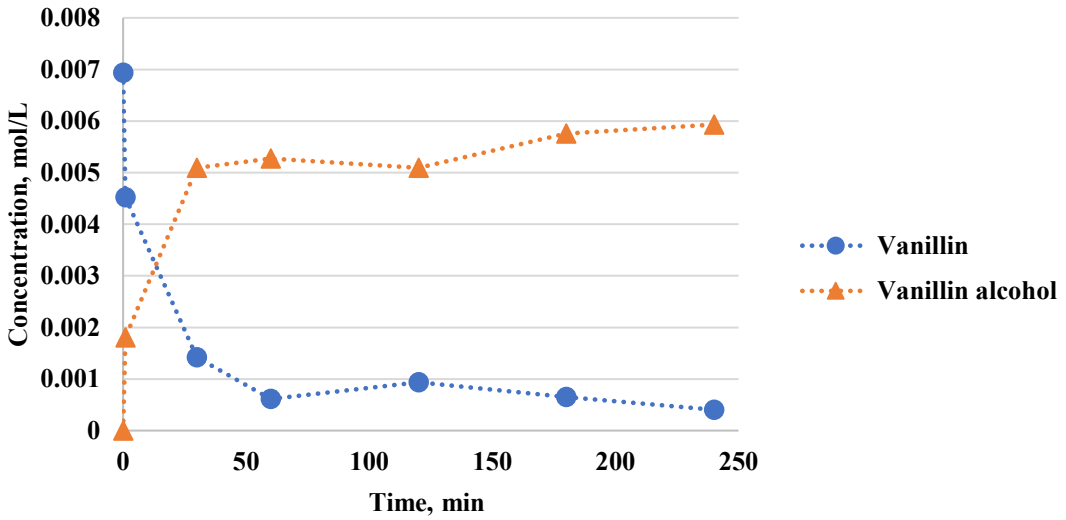

Figure 58 Concentration of the reactant and the product versus time in vanillin HDO at 100℃ and 30 bar total pressure in the presence of hydrogen over 10 wt. % Ni/ZrO₂.

Figure 59 demonstrates that after four hours of the reaction at 100℃ and 30 bar, similar concentrations of the product vanillin alcohol were obtained for both catalysts. No other products such as p-cresol or p-creosol were observed in vanillin HDO in both cases.

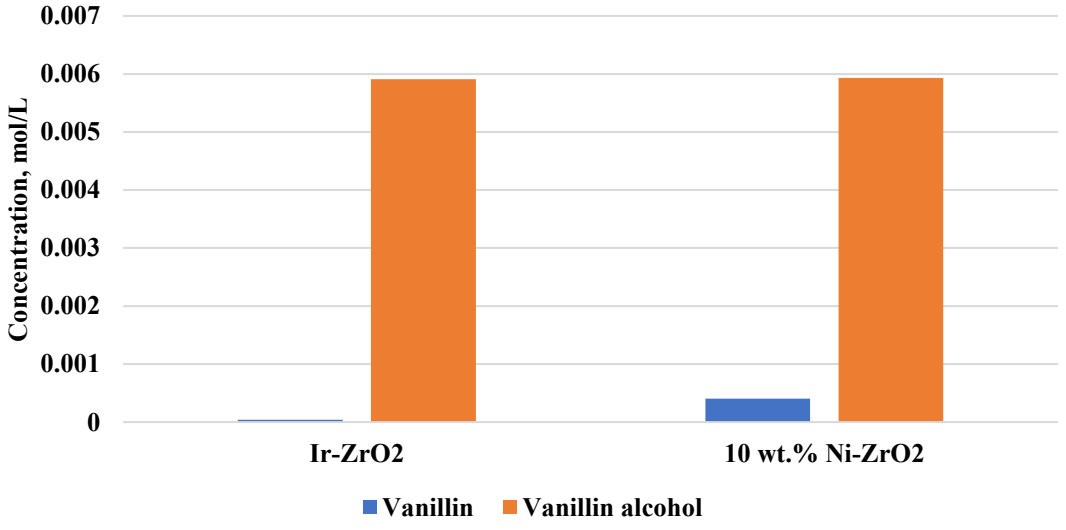

Figure 59 Concentration of vanillin and vanillin alcohol after four hours of the reaction in vanillin HDO at 100℃ and 30 bar total pressure in the presence of hydrogen over Ir/ZrO₂ and 10 wt. % Ni/ZrO₂ catalysts.

Overall, Ir/ZrO_2 and 10 wt. % Ni/ZrO_2 catalysts did not give hydrodeoxygenated products in vanillin HDO giving only vanillyl alcohol in the case of the thermal test. High GCLPA was obtained for both reactions in vanillin HDO being 78 and 94 % for Ir/ZrO_2 and 10 wt. % Ni/ZrO_2 catalysts respectively.

4.2.3.4 Comparison of results

From results described in Sections 4.2.3.1, 4.2.3.2 and 4.2.3.3, it can be concluded that different phenolic compounds, e.g. isoeugenol, guaiacol and vanillin gave rise to different products over Ir/ZrO_2 and 10 wt. % Ni/ZrO_2. In the case of guaiacol and vanillin HDO mainly alcohol compounds were obtained, while in the case of isoeugenol HDO mainly a hydrodeoxygenated compound was obtained over both catalysts (namely, propylcyclohexane). However, complete conversion of the reactant was obtained for isoeugenol and guaiacol HDO, while vanillin HDO was incomplete. On the other hand, hydrodeoxygenation of vanillin demonstrated higher GCLPA over Ir/ZrO_2 (78 %) and 10 wt.% Ni/ZrO_2 (94 %) in comparison with HDO of isoeugenol (17 and 25 % respectively) and guaiacol (48 and 57 % respectively). The most successful degree of hydrodeoxygenation was accounted for isoeugenol in the presence of Ir/ZrO_2 and 10 wt.% Ni/ZrO_2 catalysts.

4.2.4 Catalysts on carbon support

4.2.4.1 Isoeugenol HDO

4.2.4.1.1 Temperature effect

Carbon supported catalysts were also utilized in isoeugenol HDO at 200 and 250℃ under 30 bar. The bimetallic catalysts such as PtRe/C-31 (PRC-31) were tested in isoeugenol HDO at 200 and 250℃ while PtRe/C-13 (PRC-13) was applied only at 250℃.

As can be seen from Figure 60 the concentration of propylcyclohexane was elevated at a higher operating temperature in isoeugenol HDO over PRC-31 catalyst than at lower one. The increase in concentration was ca. 29 % when temperature increased from 200℃ to 250℃. Mainly dihydroeugenol and propylcyclohexane were formed with dihydroeugenol completely transforming to propylcyclohexane. Only at 250℃ hexane, heptane and octane were formed. These compounds were not included into

GCLPA calculations, being already present in low concentrations in the initial sample of dodecane. Throughout these tests no propylbenzene and 1,2,4-trimethylbenzene were seen in GC analysis of the liquid samples.

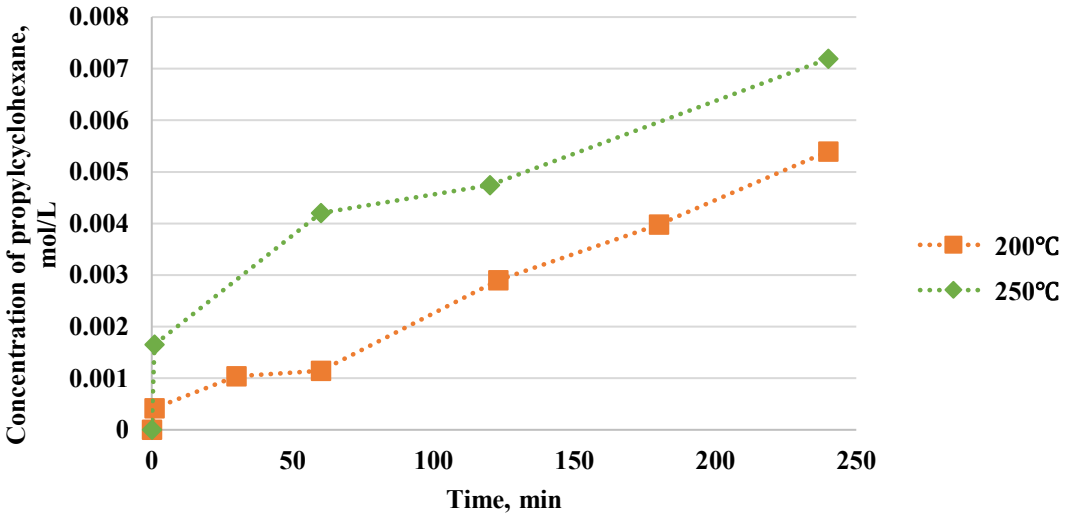

Figure 60 Concentration of propylcyclohexane vs reaction time in isoeugenol HDO at 200 and 250℃ and 30 bar using PtRe/C-31 catalyst (mao30 and mao15 respectively in Appendix XI).

The results for PRC-31 and PRC-13 catalysts are compared in isoeugenol HDO at 250℃ and 30 bar in Figure 61. The difference between these catalysts is in the metals loadings. As identified by EDX analysis the fresh PtRe/C-31 catalyst possesses 1.5 wt. % of platinum and 0.9 wt. % of rhenium, while PtRe/C-13 catalyst has a much higher loadings of metals (5.8 wt. % of Pt and 6.4 wt. % of Re). As can be seen from Figure 60, the use of a catalyst with higher Pt and Re loadings (PRC-13) resulted in a higher concentration of propylcyclohexane in comparison with lower metals loadings in PRC-31 catalyst. The initial concentration of isoeugenol for both catalysts was 0.012 mol/L. There was also a difference in GCLPA being 57 % for PRC-13 and 44 % for PRC-31. In both cases dihydroeugenol was converted completely. Heptane, hexane and octane concentrations were almost twofold in isoeugenol HDO over PRC-13 (Re/Pt=1.1) than over PRC-31 (Re/Pt=0.6).

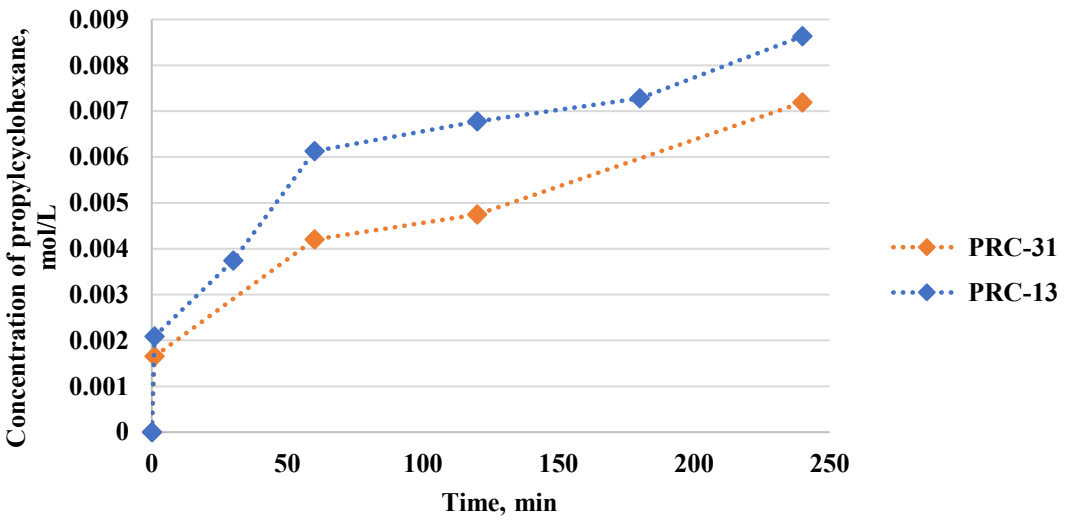

Figure 61 Concentration of propylcyclohexane vs reaction time in isoeugenol HDO at 250℃ and 30 bar using PtRe/C-31 (mao15) and PtRe/C-13 (mao51) catalysts.

4.2.4.1.2 Solventless HDO with Ir-C catalyst

Solventless HDO of isoeugenol in the presence of Ir/C catalyst was also investigated. Some precautions were taken during these reactions in terms of operating conditions. As known, isoeugenol contains of methoxy and hydroxy groups which upon reactant cracking under high temperature can lead to high vapour pressure. In Table 20, the vapor pressures of water and methanol are presented at 150, 200 and 250℃. As can be seen already at 150℃ the pressure of compounds is ca. 18.3 bar. Therefore, a lower pressure was chosen for isoeugenol HDO namely 11.6 and 11 bar respectively at 150 and 200℃. The catalyst mass and isoeugenol were respectively 0.58 g and 57.6 g.

Table 20 Partial pressure of water and methanol at different temperatures and pressures

Temperature, ℃	Partial vapor pressure of water[1], bar	Partial vapor pressure of methanol, bar	Sum of partial pressures, bar
250	40.1	-	> 40.1
200	15.5	38.9[2]	54.4
150	4.7	13.6[2]	18.3

1 – the partial vapor pressure of water (boiling point=100℃) was calculated using [76].
2 - the partial vapor pressure of methanol (boiling point=64.7℃) was calculated using [77].

The first test was performed with the initial temperature of 150℃ increasing it gradually to 200℃. For the first 218 min of the reaction the process was made in a

semi-batch mode with hydrogen gas pressure of ca. 11.6 bar, followed by pressure increase to 20 bar to avoid the back flow of water and methanol to the hydrogen supply line. At the beginning of heating, a drop in the total pressure was observed from 10.6 to 9.5 bar, indicating a significant consumption of hydrogen during the pre-start stage. Bjelic et al. [15] during the heating stage also observed intensive hydrogen consumption which led to formation of hydrogenated compounds. In our case dihydroeugenol was produced, confirmed by GC analysis of the liquid sample (Appendix XI). As the desired temperature was reached the pressure was increased to 11.6 bar. In Figure 62 the temperature and pressure program can be seen for solventless isoeugenol HDO, demonstrating that at the operating temperature of 150℃ the set pressure was stable being 11.6 bar. Up to 218 min the temperature was increased by 10℃ at the beginning the first and second hour each, and then every 30 minutes. Throughout the reaction there was a minor pressure increase. No other products were formed after four hours of reaction apart from dihydroeugenol. Therefore, the initial hydrogen pressure was not sufficient enough to promote the reaction towards propylcyclohexane. Water was not observed after cooling. Heptane and octane were identified by GC in very low concentrations, while hexane concentration was 0.005 mol/L. As the temperature reached 25℃ the gas samples were taken and analyzed by GC and GC-MS (Appendix VIII).

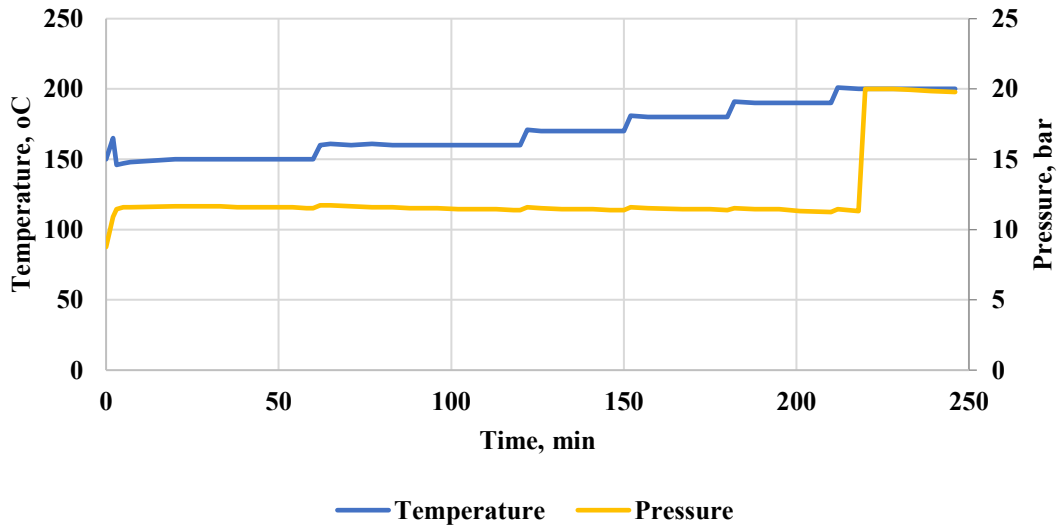

Figure 62 Temperature programmed solventless isoeugenol HDO with Ir/C and starting temperature of 150℃ (up to 200℃) including pressure variation.

Figure 63 shows results for isoeugenol HDO performed at 200℃ and a starting pressure of 10.6 bar in the batch mode. During heating consumption of hydrogen was observed without stirring (at 144℃ the pressure was 8.9 bar). In order to keep the constant pressure during the first three minutes of the reaction, hydrogen was additionally supplied by opening the valve. While temperature was increasing, more hydrogen was added, leading to an increase of the total pressure to 11.1 bar (without hydrogen supply) at ca. 24 min. As can be seen from Figure 63, the total pressure dropped starting from 38 min until the end of the reaction (11 bar to 10.6 bar respectively). Therefore, the batch mode was not effective giving almost dihydroeugenol. Only negligible amounts of propylcyclohexane as well as hexane and octane were observed. The same gas sampling was performed after cooling.

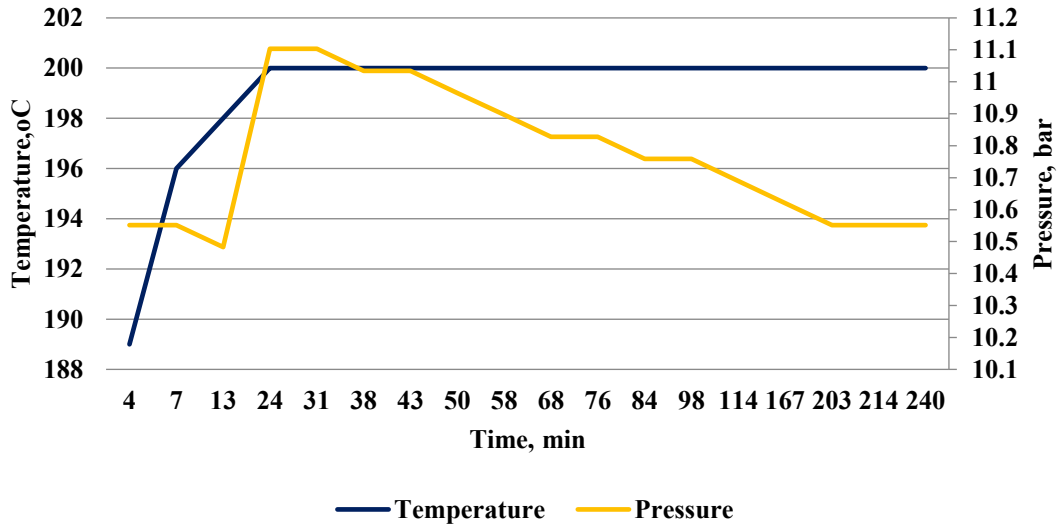

Figure 63 Temperature programmed solventless isoeugenol HDO with Ir/C at 200℃ including pressure variation.

Figure 64 displays results of GC-MS analysis of the gas samples for the first three minutes of retention time. This Figure illustrates some overlapping between methane and ethane. The gas samples at 150 and 200℃ contained methane, ethane and propane. The first three peaks are prominent at 150℃ and 200℃. Other straight chain alkanes such as butane and hexane were also observed in both tests. In addition, propylcyclohexane and dodecane were also present. However, propylcyclohexane at 150℃ was not detected in the liquid sample according to GC, while at 200℃ negligible amounts were detected. In GC analysis of the gas samples, it confirmed the presence of methane and ethane. Other compounds are presented in Appendix VIII.

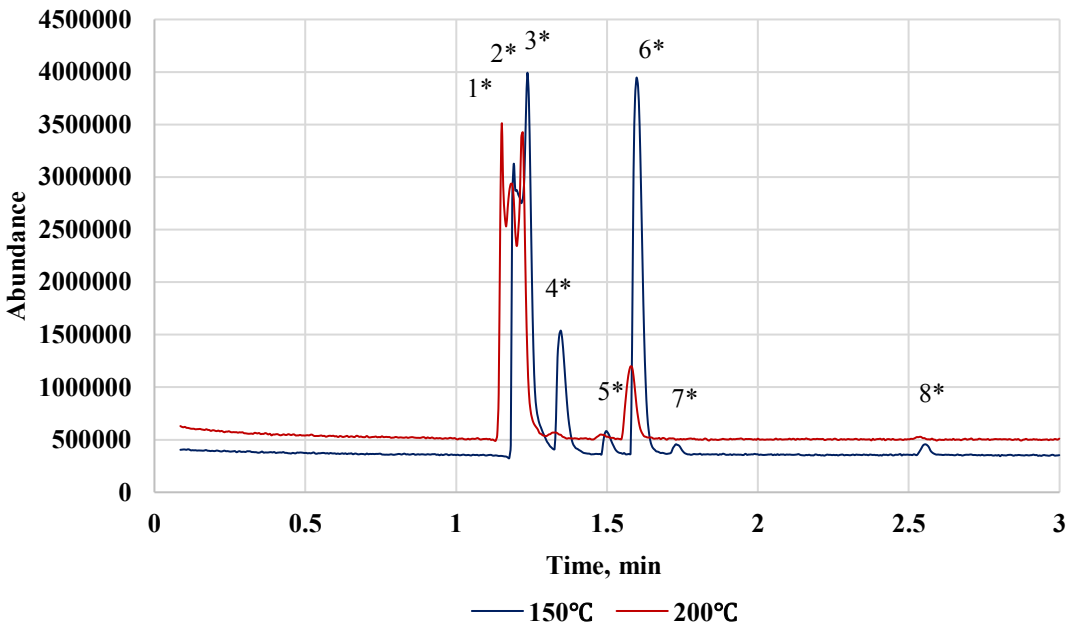

Figure 64 Abundance of gases present after four hours of reaction (including only the first three minutes) for isoeugenol HDO over Ir/C at 150 and 200℃. Notation: 1- methane (1.19 and 1.15 min), 2*- ethane (1.21 and 1.18 min), 3*- propane (1.24 and 1.22 min), 4*- butane (1.34 and 1.32 min), 5* and 6* - ethanol and 2- propanone (impurities), 7* - pentane (1.74 min), 8*- hexane (2.56 and 2.55 min).*

Overall, solventless isoeugenol HDO at 150 and 200℃ did not show any production of propylcyclohexane.

5 Conclusion

Shortage of petroleum and the climate change influenced the current focus of oil refineries on alternative resources such as bio-oil, which is renewable. Due to presence of 40 % of oxygen, high viscosity and acidity it cannot be easily used contrary to petroleum based fuel in engines, therefore, upgrading with zeolites, aqueous phase processing in engines and hydrotreating are utilized to improve the oil to the desired level. The most conventional way is hydrotreating where hydrodeoxygenation takes place. In this work catalytic hydrodeoxygenation of bio-oil model compounds mainly isoeugenol over alumina, zirconia and carbon supported catalysts as well as guaiacol and vanillin over zirconia supported catalysts was investigated.

Prior to isoeugenol HDO, the thermal experiments were performed confirming complete transformation of isoeugenol into predominantly dihydroeugenol and small amounts of propylcyclohexane at 200 and 250℃ under total pressure of 30 bar in the presence of hydrogen.

Isoeugenol HDO was performed at total pressure 30 bar over alumina and carbon supported catalysts at different temperatures showing that the most suitable temperature among the tested ones was 250℃ giving high yields of propylcyclohexane with bimetallic alumina and carbon supported catalysts. Among bimetallic catalysts on alumina, IrRe/Al_2O_3-DP was the best one yielding propylcyclohexane (69 %) at complete conversion of dihydroeugenol. This can be explained by the presence of 4+ rhenium valence state and a high weight ratio of Re/Ir (4.4). However, gas chromatography based sum of the reactants and products in the liquid phase analysis (GCLPA) over all these catalysts was mediocre implying high formation of gaseous products and adsorption of the compounds on the catalyst surface. Comparing bimetallic carbon supported catalysts in isoeugenol HDO at 250℃ and 30 bar it can be concluded that PtRe/C-13 demonstrated a higher yield of propylcyclohexane (72 %) than PtRe/C-31 (58 %).

The initial liquid sample prior to heating already contained hexane, heptane and octane compounds according to GC and GC-MS. Molar concentrations of these compounds during HDO at 250℃ and 30 bar varied depending on the catalyst type. They were not included in the calculation of GCLPA. With IrRe/Al_2O_3-Impr1 and IrRe/Al_2O_3-Impr2

the above mentioned compounds were absent after four hours of the reaction, while over IrRe/Al_2O_3-DP, PtRe/Al_2O_3-33, PtRe/C-31 and PtRe/C-13 they were enhanced notably being in total 0.015, 0.015, 0.009 and 0.018 mol/L, respectively.

The pressure effect in isoeugenol HDO at 250℃ over IrRe/Al_2O_3-DP and IrRe/Al_2O_3-Impr1 was investigated. In the case of IRA-DP catalyst, the reaction pressures such as 25, 30 and 42 bar did not result in changes of propylcyclohexane molar concentration. Complete conversion of dihydroeugenol was observed at 30 and 42 bar. In the case of IrRe/Al_2O_3-Impr1, the highest yield was achieved at 40 bar giving propylcyclohexane concentration of 0.015 mol/L from initial molar concentration of isoeugenol 0.015 mol/L. In addition, gas chromatography based sum of the reactants and products in the liquid phase analysis (GCLPA) was the highest at 40 bar being 84 %, while at 30 bar it was 54 %.

Reaction temperature and pressure changes gave the same products differing in selectivity.

IrRe/Al_2O_3-DP and IrRe/Al_2O_3-Impr2 catalysts demonstrated good reproducibility based on the gas chromatography based sum of the reactants and products in the liquid phase analysis (GCLPA) and concentration of propylcyclohexane in isoeugenol HDO at 250℃ and total pressure of 30 bar in the presence of hydrogen.

Stability tests were performed over IrRe/Al_2O_3-DP and IrRe/Al_2O_3-Impr1 in isoeugenol HDO at 250℃ and 30 bar, where higher catalyst amounts were taken at the reactant to catalyst ratio equal to 0.5. In isoeugenol HDO over the fresh IrRe/Al_2O_3-DP, the reaction rate was higher at a high concentration of isoeugenol. The regenerated IrRe/Al_2O_3-DP demonstrated a low concentration of propylcyclohexane due to the absence of Re in the valence state 4+. IrRe/Al_2O_3-Impr1 showed good stability based on the concentration of propylcyclohexane. Cracking ability of the regenerated catalyst was lower with formation of hexane, heptane and octane in comparison with the fresh one, where in high quantities methane and ethane were formed according to the gas phase analysis. The spent catalysts had almost the same specific surface area as the fresh ones.

At 250℃ over Ir/ZrO_2 and 10 wt. % Ni/ZrO_2 in isoeugenol HDO conversion of the intermediate dihydroeugenol was rather high (94 and 95 %, respectively) giving the concentration of propylcyclohexane of 0.0028 and 0.002 mol/L, correspondingly. However, GCLPA dropped significantly at 250℃ to 25 % (Ir/ZrO_2 including TGA) and 17 % (10 wt. % Ni/ZrO_2 including TGA), because of gas phase products formation and adsoption of the compounds on the catalyst surface. Hexane, heptane and octane were absent after four hours of the reaction.

Guaiacol HDO was performed at 250℃ and 30 bar demonstrating different distribution of the products. Mainly alcohols such as cyclohexanol and 2-methoxycyclohexanone were formed over both catalysts. However, in the presence of Ir over zirconia the yield of cyclohexane (13 %) was larger than in the case of 10 wt. % Ni/ZrO_2 catalyst. Gas chromatography based sum of the reactants and products in the liquid phase analysis was low in both cases of guaiacol HDO tests in comparison with vanillin HDO results, where more than 91 % was obtained. However, vanillin was not fully converted at 100℃ and 30 bar producing only vanillyl alcohol, i.e. both Ir/ZrO_2 and 10 wt. % Ni/ZrO_2 catalysts were not effective in hydrodeoxygenation.

GC analysis of the gas samples after four hours of isoeugenol and guaiacol HDO at 250℃ and 30 bar over alumina and zirconia supported catalysts, showed high amounts of ethane and methane. Methane was observed for zirconia supported catalysts in guaiacol HDO at 250℃ and 30 bar also by GC-MS. These results point out on hydrogenolysis.

Transformations of dodecane over Ir/ZrO_2 at 250℃and 30 bar showed hydrogenolysis of the solvent. Hexane, heptane and octane concentrations were formed with the combined concentration of 0.052 mol/L. Interestingly, in the presence of isoeugenol these compounds were not observed.

Optimization tests were performed for isoeugenol HDO over IRA-DP by changing the reactant to catalyst ratio and using solventless conditions over Ir/C. As expected a lower catalysts amount resulted in less propylcyclohexane. Isoeugenol (57.62 g) HDO at 150 or 200℃ (semi-batch and batch modes, correspondingly) and the total pressure of ca. 11 bar over Ir/C (0.576 g) afforded only dihydroeugenol formation. No other

products were observed in the liquid phase even if methane and ethane was present in the gas phase according to GC analysis.

It might be useful to investigate isoeugenol HDO in the future with bimetallic catalysts on alumina and carbon supports at higher temperatures (>250℃) and pressures (>30 bar). Solventless reactions over Ir/C can be carried out at a pressure exceeding 20 bar. Gases such as methane, ethane, propane and butane, should be calibrated in GC-MS.

Overall, this thesis work is a contribution into global research efforts of the transformations of bio-oil into bio-fuels.

6 References

[1] Xiu, S. and Shahbazi, A. Bio-oil production and upgrading research: A review. *Renew. Sustain. Energy Rev.* **(2012)**, 16, 4406-4414.

[2] Demirbas, A. Current technologies for the thermo-conversion of biomass into fuels and chemicals. *Energy Sources* **(2004)**, 26, 715-730.

[3] Mohan, D., Pittman, C.U. and Steele, P.H. Pyrolysis of wood/biomass for bio-oil: A critical review. *Energy and Fuels* **(2006)**, 20, 848-889.

[4] Czernik, S. and Bridgwater, A.V. Overview of application of biomass fast pyrolysis oil. *Energy and Fuels* **(2004)**, 18, 590-598.

[5] Wang, H., Male, J. and Wang, Y. Recent advances in hydrotreating of pyrolysis bio-oil and its oxygen-containing model compounds. *ACS Catal.* **(2013)**, 3, 1047-1070.

[6] Mullen, C.A. and Boateng, A.A. Chemical composition of bio-oils produced by fast pyrolysis of two energy crops. *Energy & Fuels* **(2008)**, 22, 2104-2109.

[7] Tran, N.T.T., Uemura, Y., Chowdhury, S. and Ramli, A. Vapor-phase hydrodeoxygenation of guaiacol on Al-MCM-41 supported Ni and Co catalysts. *Appl. Catal. A Gen.* **(2016)**, 512, 93-100.

[8] Shafaghat, H., Rezaei, P.S. and Daud, W.M.A.W. Catalytic hydrodeoxygenation of simulated phenolic bio-oil to cycloalkanes and aromatic hydrocarbons over bifunctional metal/acid catalysts of Ni/HBeta, Fe/HBeta and NiFe/HBeta. *J. Ind. Eng. Chem.* **(2016)**, 35, 268-276.

[9] Deepa, A.K. and Dhepe, P.L. Function of metals and supports on the hydrodeoxygenation of phenolic compounds. *Chempluschem* **(2014)**, 79, 1573-1583.

[10] Lyu, G., Wu, S. and Zhang, H. Estimation and comparison of bio-oil components from different pyrolysis conditions. *Front. Energy Res.* **(2015)**, 3, 1-11.

[11] Lampman, G. M. and Sharpe, S. D. A phase transfer catalyzed permanganate oxidation: preparation of vanillin from isoeugenol acetate. *Journal of Chemical Education* **(1983)**, 60(6), 503.

[12] Atsumi, T., Fujisawa, S. and Tonosaki, K. A comparative study of the antioxidant/prooxidant activities of eugenol and isoeugenol with various concentrations and oxidation conditions. *Toxicology in Vitro* **(2005)**, 19(8), 1025–1033.

[13] Sharma, S. K., Srivastava, V. K. and Jasra, R. V. Selective double bond isomerization of allyl phenyl ethers catalyzed by ruthenium metal complexes. *Journal of Molecular Catalysis A: Chemical* **(2006)**, 245(1–2), 200–209.

[14] Bomont, L., Alda-Onggar, M., Fedorov, V., Aho, A., Peltonen, J., Eränen, K., Peurla, M., Kumar, N., Wärnå, J., Russo, V., Mäki-Arvela, P., Grenman, H., Lindblad, M. and Murzin, D.Y. Production of cycloalkanes in hydrodeoxygenation of isoeugenol over Pt- and Ir-modified bifunctional catalysts. *Eur. J. Inorg. Chem.* **(2018)**, 24, 2841-2854.

[15] Bjelić, A., Grilc, M. And Likozar, B. Catalytic hydrogenation and hydrodeoxygenation of lignin-derived model compound eugenol over Ru/C: Intrinsic microkinetics and transport phenomena. *Chemical Engineering Journal* **(2018)**, 333, 240–259.

[16] Trueba, M. and Trasatti, S. P. γ-alumina as a support for catalysts: a review of fundamental aspects. *Eur. J. Inorg. Chem.* **(2005)**, 17, 3393–3403.

[17] Zhang, X., Tang, W., Zhang, Q., Wang, T. and Ma, L. Hydrocarbons production from lignin-derived phenolic compounds over Ni/SiO_2 catalyst. *Energy Procedia* **(2017)**, 105, 518 – 523.

[18] Lam, E. and Luong, J. H. T. Carbon materials as catalyst supports and catalysts in the transformation of biomass to fuels and chemicals. *ACS Catalysis*. **(2014)**, *4* (10), 3393–3410.

[19] Li, X., Xing, J., Zhou, M., Zhang, H., Huang, H., Zhang, C., Song, L. And Li, X. Influence of crystal size of HZSM-5 on hydrodeoxygenation of eugenol in aqueous phase. *Catalysis Communications* **(2014)**, 56, 123–127.

[20] Liu, S., Dutta, S., Zheng, W., Gould, N. S., Cheng, Z., Xu, B., Saha, B. and Vlachos, D. G. Catalytic hydrodeoxygenation of high carbon furylmethanes to renewable jet-fuel ranged alkanes over a rhenium-modified iridium catalyst. *ChemSusChem*. **(2017)**, 10(16).

[21] Chen, K., Mori, K., Watanabe, H., Nakagawa, Y. and Tomishige, K. C–O bond hydrogenolysis of cyclic ethers with OH groups over rhenium-modified supported iridium catalysts. *Journal of Catalysis* **(2012)**, 294, 171–183.

[22] Amada,Y., Shinmi, Y., Koso, S., Kubota, T., Nakagawa, Y. and Tomishige, K. Reaction mechanism of the glycerol hydrogenolysis to 1,3-propanediol over Ir–ReO_x/SiO_2 catalyst. *Applied Catalysis B: Environmental* **(2011)**, 105(1-2), 117–127.

[23] Rogers, L. E., Lyon, G. M. and Porter, F. S. Spot test for vanillylmandelic acid and other guaiacols in urine of patients with neuroblastoma. *American Journal of Clinical Pathology* **(1972)**, 58(4), 383–387.

[24] Mäki-Arvela, P. and Murzin, D. Hydrodeoxygenation of lignin-derived phenols: from fundamental studies towards industrial applications. *Catalysts* **(2017)**, 7(9), 265.

[25] Mortensen, P.M., Gardini, D., de Carvalho, H.W.P., Damsgaard, C.D., Grunwaldt, J.-D., Jensen, P.A., Wagner, J.K and Jensen, A.D. Stability and resistance of nickel catalysts for hydrodeoxygenation: carbon deposition and effects of sulfur, potassium, and chlorine in the feed. *Catal. Sci. Technol.* **(2014)**, 4, 3672-3686.

[26] Popov, A., Kondratieva, E., Goupil, J. M., Mariey, L., Bazin, P., Gilson, J. P., Travert, A. And Maugé, F. Bio-oils hydrodeoxygenation: adsorption of phenolic molecules on oxidic catalyst supports. *J. Phys. Chem. C* **(2010)**, 114(37), 15661–15670.

[27] Lee, C.R., Yoon, J.S., Suh, Y.-W., Choi, J.-W., Ha, J.-M., Suh, D.J. and Park, Y.-K. Catalytic roles of metals and supports on hydrodeoxygenation of lignin monomer guaiacol. *Catalysis Communications* **(2012)**, 17, 54–58.

[28] Arce-Ramos, J.-M., Grabow, L.C., Handy, B.E. and Cárdenas-Galindo, M.-G. Nature of acid sites in silica-supported zirconium oxide: a combined experimental and periodic DFT study. *J. Phys. Chem. C* **(2015)**, 119(27), 15150–15159.

[29] De Souza, P.M., Nie, L., Borges, L.E.P., Noronha, F.B. and Resasco, D.E. Role of oxophilic supports in the selective hydrodeoxygenation of m-cresol on Pd catalysts. *Catalysis Letters*, **(2014)**, 144(12), 2005-2011.

[30] Zhang, X., Zhang, Q., Wang, T., Ma, L., Yu, Y. and Chen, L. Hydrodeoxygenation of lignin-derived phenolic compounds to hydrocarbons over Ni/SiO_2–ZrO_2 catalysts. *Bioresource Technology* **(2013)**, 134, 73-80.

[31] Lu, M., Du, H., Wei, B., Zhu, J., Li, M., Shan, Y., Shen, J. and Song, C. Hydrodeoxygenation of guaiacol on Ru catalysts: influence of TiO_2− ZrO_2 composite oxide supports. *Ind. Eng. Chem. Res.* **(2017)**, 56, 12070-12079.

[32] Gutierrez, A., Kaila, R.K., Honkela, M.L., Slioor, R. and Krause, A.O.I. Hydrodeoxygenation of guaiacol on noble metal catalysts. *Catalysis Today* **(2009)**, 147(3–4), 239-246.

[33] Walton, N.J., Mayer, M.J. and Narbad, A. Vanillin. *Phytochemistry* **(2003)**, 63(5), 505-15.

[34] Lee, T., Chen, H.R., Lin, H.Y. and Lee, H.L. Continuous co-crystallization as a separation technology: the study of 1:2 co-crystals of phenazine–vanillin. *Cryst. Growth Des.* **(2012)**, 12(12), 5897-5907.

[35] Fache, M., Boutevin, B. and Caillol, S. Vanillin production from lignin and its use as a renewable chemical. *ACS Sustainable Chem. Eng.* **(2016)**, 4(1), 35–46.

[36] Bindwal, A.B. and Vaidya, P.D. Reaction kinetics of vanillin hydrogenation in aqueous solutions using a Ru/C catalyst. *Energy Fuels* (**2014)**, 28(5), 3357–3362.

[37] Yang, Q., Xu, Q. and Jiang, H.-L. Metal–organic frameworks meet metal nanoparticles: synergistic effect for enhanced catalysis. *Chem. Soc. Rev.* **(2017)**, 46, 4774.

[38] He, L., Qin, Y., Lou, H. and Chen, P. Highly dispersed molybdenum carbide nanoparticles supported on activated carbon as an efficient catalyst for the hydrodeoxygenation of vanillin. *RSC Adv.* (**2015)**, 5, 43141.

[39] Leofanti, G., Padovan, M., Tozzola, G. and Venturelli, B. Surface area and pore texture of catalysts. *Catalysis Today* **(1998)**, 41(1–3), 207-219.

[40] Murzin, D. **(2013)** *Engineering Catalysis.* [e-book] Available at: <http://ebookcentral.proquest.com/lib/abo-ebooks/reader.action?docID=912966&ppg=1> [Accessed on 5 March 2018].

[41] Horiba Scientific **(2017)** *Physisorption Technology.* [online] Available at: <http://www.horiba.com/scientific/products/particle-characterization/technology/surface-area/> [Accessed 5 March 2018].

[42] Barzetti, T., Selli, E., Moscotti, D. and Forni, L. Pyridine and ammonia as probes for FTIR analysis of solid acid catalysts. *J. Chem. Soc., Faraday Trans.* **(1996)**, 92, 1401-1407.

[43] Belskaya, O.B., Danilova, I.G., Kazakov, M.O., Mironenko, R.M., Lavrenov A.V. and Likholobov, V.A. **(2012)** FTIR spectroscopy of adsorbed probe molecules for analyzing the surface properties of supported Pt (Pd) catalysts. *InTech* [pdf] Available at: <http://cdn.intechopen.com/pdfs-wm/36172.pdf>

[44] ATI Mattson **(1995)** *Infinity series FTIR spectrometer user's manual*.

[45] Goldstein, J., Newbury, D., Joy, D., Lyman, C., Echlin, P., Lifshin, E., Sawyer, L. and Michael, J. **(2003)** *Scanning electron microscopy and X-ray microanalysis*. 3rd ed. New York: Springer US.

[46] Swapp, S. **(2017)** Scanning Electron Microscopy (SEM). [online] Available at: <https://serc.carleton.edu/research_education/geochemsheets/techniques/SEM.html> [Accessed on 8 March 2018].

[47] Ebnesajjad, S. and Khaladkar, P.R. **(2004)** Fluoropolymers applications in the chemical processing industries the definitive user's guide and databook. The United States: William Andrew, Inc.

[48] Thompson, M. **(2008)** CHNS Elemental Analysers. [pdf] Available at: <http://www.rsc.org/images/CHNS-elemental-analysers-technical-brief-29_tcm18-214833.pdf> [Accessed on 9 March 2018].

[49] Boyes, W. **(2010)** Instrumentation reference book. Elsevier: Butterworth-Heinemann [pdf] Available at: <http://sarvniroo.ir/wp-content/uploads/Instrumentation%20Reference%20Book_%20Fourth%20Edition.pdf > [Accessed on 9 March 2018].

[50] Anderson Materials Evaluation, Inc. **(2018)** TGA Analysis or thermogravimetric analysis. Available at: <http://www.andersonmaterials.com/tga.html> [Accessed on 9 March 2018].

[51] Abdullah, H.A., Hauser, A., Ali, F.A. and Al-Adwani, A. Optimal conditions for coke extraction of spent catalyst by accelerated solvent extraction compared to Soxhlet. *Energy Fuels* **(2006)**, 20(1), 320–323.

[52] Duca, D. and Deganello, G. Analysis by size exclusion chromatography (SEC) of catalytic materials: the fractal properties and the pore size distribution of pumice. *Journal of Molecular Catalysis A: Chemical*, **(1996)**, 112(3), 413–421.

[53] Wagner, J.M. (Ed.) **(2010)** *X-Ray photoelectron spectroscopy.* Nova Science: Hauppauge.

[54] Thet, K. and Woo, N. **(2015)** Gas chromatography [online] Available at: <https://chem.libretexts.org/Core/Analytical_Chemistry/Instrumental_Analysis/Chromatography/Gas_Chromatography> [Accessed on 21 May 2018].

[55] Wilson, I.D. and Poole, C.F. **(2009)** Handbook of methods and instrumentation in separation science. 1st ed. London: Elsevier.

[56] Johnsen, L. G., Skou, P. B., Khakimov, B. and Bro, R. Gas chromatography – mass spectrometry data processing made easy. *Journal of Chromatography A* **(2017)**, 1503, 57–64.

[57] Armarego, W.L.F. **(2017)** Purification of laboratory chemicals. 8th ed. Butterworth-Heinemann.

[58] Bernas, A., Kumar, N., Mäki-Arvela, P., Kul'kova, N. V., Holmbom, B., Salmi, T., and Murzin, D. Y. Isomerization of linoleic acid over supported metal catalysts. *Applied Catalysis A: General*, **(2003)**, *245*(2), 257–275.

[59] Emeis, C. A. Determination of integrated molar extinction coefficients for infrared absorption bands of pyridine adsorbed on solid acid catalysts. *Journal of Catalysis*, **(1993)**, 141(2), 347–354.

[60] Sulman, A. **(2017)** Hydrodeoxygenation of lignin based model compounds (master's thesis). Åbo Akademi University, Turku, Finland.

[61] Samain, L., Jaworski, A., Edén, M., Ladd, D.M., Seo, D.K., Garcia-Garcia, F.J. and Häussermann, U. Structural analysis of highly porous γ-Al_2O_3. *Journal of Solid State Chemistry* **(2014)**, 217, 1–8.

[62] Mortensen, P. M., Grunwaldt, J. D., Jensen, P. A. and Jensen, A. D. Screening of catalysts for hydrodeoxygenation of phenol as a model compound for bio-oil. *ACS Catalysis* **(2013)**, 3(8), 1774–1785.

[63] Energy research of Centre of Netherlands. **(2010)** Sibunit supported catalysts [pdf] Available at: <https://www.ecn.nl/fileadmin/ecn/units/h2sf/pdf/Sibunit.pdf> [Accessed on 30 March 2018].

[64] Puskás, R., Varga, T., Grósz, A., Sápi, A., Oszkó, A., Kukovecz, Á. and Kónya, Z. Surface science mesoporous carbon-supported Pd nanoparticles with high specific surface area for cyclohexene hydrogenation: Outstanding catalytic activity of NaOH-treated catalysts. *Surface Science* (2016), 648, 114–119.

[65] Morterra, C., Cerrato, G., Bolis, V., Di Ciero, S. and Signoretto, M. On the strength of Lewis and Bronsted-acid sites at the surface of sulfated zirconia catalysts. *J. Chem. Soc., Faraday Trans.* **(1997)**, 93(6), 1179-1184.

[66] Matos, J., Nahas, C., Rojas, L. and Rosales, M. Synthesis and characterization of activated carbon from sawdust of Algarroba wood. 1. Physical activation and pyrolysis. *Journal of Hazardous Materials* **(2011)**, 196, 360– 369.

[67] Peintinger, M. F., Kratz, M. J. and Bredow, T. Quantum-chemical study of stable, meta-stable and high-pressure alumina polymorphs and aluminum hydroxides. *Journal of Materials Chemistry A: Materials for Energy and Sustainability*, **(2014)**, *2*, 13143–13158.

[68] Freakley, S.J., Ruiz-Esquius, J. and Morgan, D.J. The X-ray photoelectron spectra of Ir, IrO_2 and $IrCl_3$ revisited. *Surf. Interface Anal.* **(2017)**, 49, 794-799.

[69] Okal, J., Tylus, W. and Kępiński, L. XPS study of oxidation of rhenium metal on γ-Al_2O_3 support. *Journal of Catalysis* **(2004)**, 225, 498-509.

[70] Rozmysłowicz, B., Kirilin, A., Aho, A., Manyar, H., Hardacre, C., Wärnå, J., Tapio, S. and Murzin, D. Y. Selective hydrogenation of fatty acids to alcohols over highly dispersed ReO_x/TiO_2 catalyst. *Journal of Catalysis*, **(2015)**, 328, 197–207.

[71] Davenport, W. H., Kollonitsch, V. and Kline, C. H. Advances in rhenium catalysts. *Industrial and Engineering Chemistry* **(1968)**, 60(11), 10–19.

[72] Si, Z., Zhang, X., Wang, C., Ma, L. and Dong, R. An overview on catalytic hydrodeoxygenation of pyrolysis oil and its model compounds. *Catalysts* **(2017)**, 7(6), 169.

[73] De Souza, P. M., Rabelo-Neto, R. C., Borges, L. E. P., Jacobs, G., Davis, B. H., Graham, U. M., Resasco, D.E. and Noronha, F. B. Effect of zirconia morphology on hydrodeoxygenation of phenol over Pd/ZrO_2. *ACS Catalysis* **(2015)**, *5*(12), 7385–7398.

[74] Zhang, C., Qi, J., Xing, X., Tang, S.-F., Song, L., Sun, Y., Zhang, C., Xin, H., and Li, X. An investigation on the aqueous-phase hydrodeoxygenation of various methoxy-substituted lignin monomers on Pd/C and HZSM-5 catalysts. *J. Name.* **(2012)**, 00, 1-3.

[75] Zhang, X., Tang, W., Zhang, Q., Wang, T. and Ma, L. Hydrocarbons production from lignin-derived phenolic compounds over Ni/SiO_2 catalyst. In *Energy Procedia* **(2017)**, 105, 518–523.

[76] Endmemo **(2017)** Vapour pressure of water calculator. Available at: <http://www.endmemo.com/chem/vaporpressurewater.php> [Accessed on 5 April 2018].

[77] DDBST **(n.d.)** Saturated vapor pressure. Available at: <http://ddbonline.ddbst.com/AntoineCalculation/AntoineCalculationCGI.exe?component=Methanol> [Accessed on 5 April 2018].

7 Appendix I

Nitrogen physisorption results

Table I. Results of liquid nitrogen physisorption

Catalysts	Specific surface area, m^2/g	Pore volume, cm^3/g
2 wt.% Pt-MM-4MW22-2AI-C (mesoporous)	798	0.64
2 wt.% Ir-MM-BE-4BE-96h-2AI-35-C (microporous)	863	0.56
3 wt.% Ir/C	326	0.12
1 wt.% Ir/SiO_2-EIM (mesoporous)	390	0.63

8 Appendix II

FTIR analysis results

Table II. Acidity of solid catalysts from FTIR spectroscopy with pyridine adsorption/desorption

Catalyst	**Brønsted acid sites**			**Lewis acid sites**		
	250℃	350℃	450℃	250℃	350℃	450℃
2 wt.% Pt-MM-4MW22-2AI-C	86	0	0	57	0	0
2 wt.% Ir-MM-BE-4BE-96h-2AI-35-C	63	31	0	63	18	0
1 wt.% Ir/SiO_2-EIM	1	1	11	6	5	2

9 Appendix III

Metal particle size from TEM analysis

Table IIIA. Metal cluster size from TEM analysis

Catalyst	Particle size of fresh
2 wt.% Pt-MM-4MW22-2AI-C	10.7
2 wt.% Ir-MM-BE-4BE-96h-2AI-35-C	29.6
3 wt.% Ir/C	2.3
1 wt.% Ir/SiO_2-EIM	5.8

TEM images and histograms (if applicable)

TEM images of 10 wt. % Ni-ZrO_2 Ni particle could not be identified (Figure IIIA).

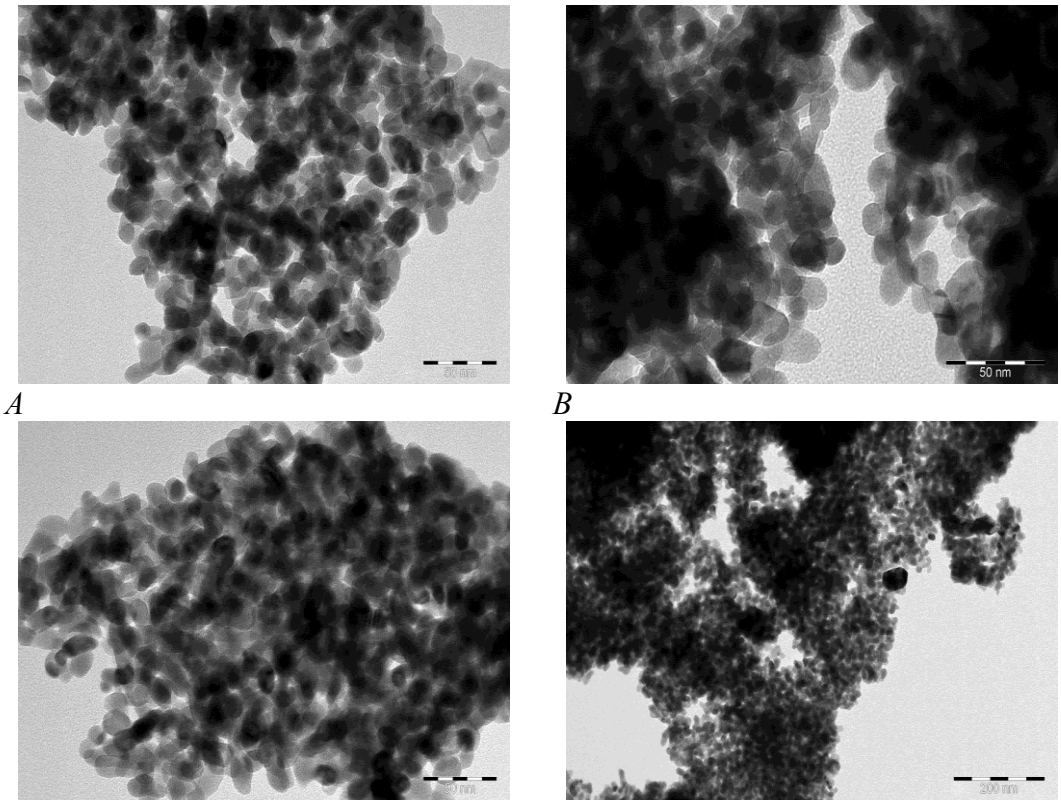

A *B*

C *D*

Figure IIIA. TEM images of the fresh (A and B) and spent (C and D) 10 wt. % Ni/ZrO_2 (mao21) in isoeugenol HDO at 250℃ and total pressure of 30 bar in the presence of hydrogen.

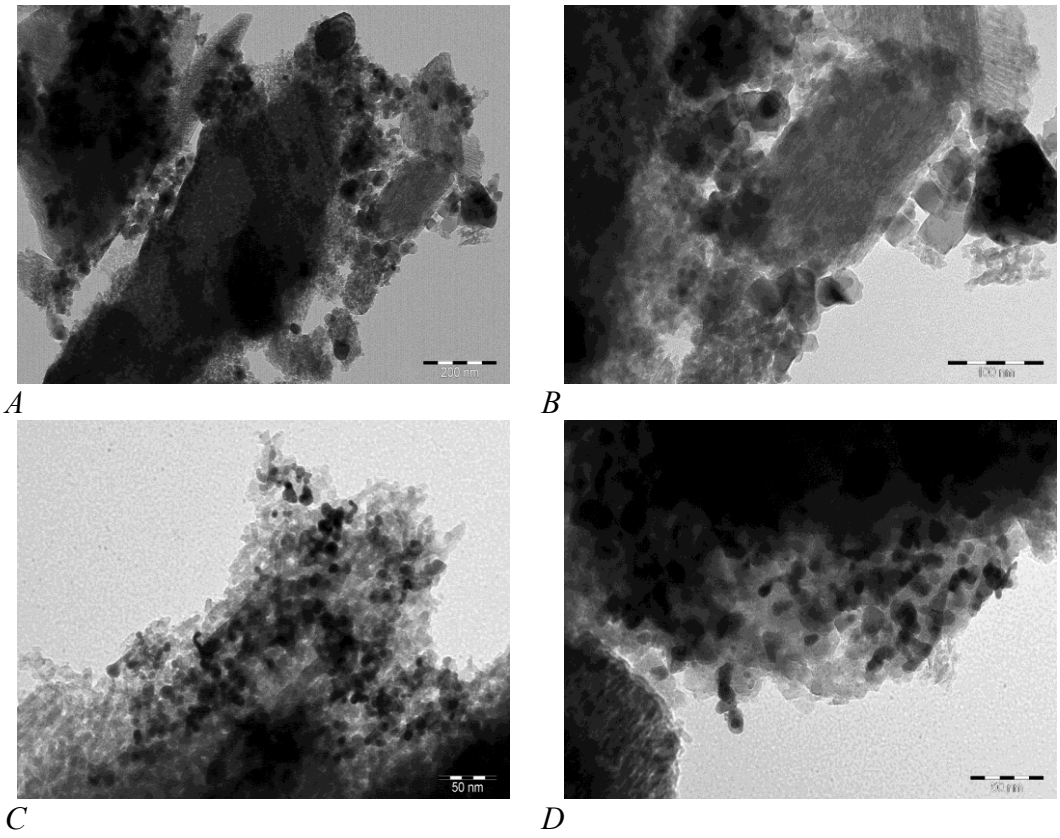

A *B*

C *D*

Figure IIIB. TEM images of the fresh (A and B) and spent (C and D) Pt/Al_2O_3 (mao16) catalysts in isoeugenol HDO at 250℃ and total pressure of 30 bar in the presence of hydrogen.

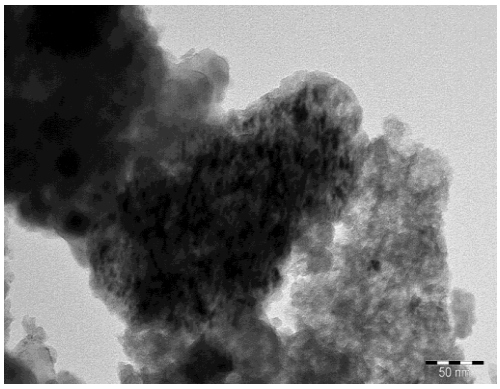

A

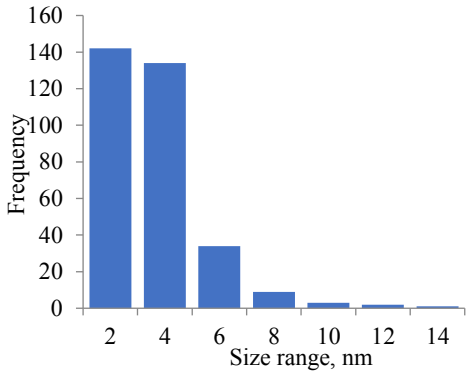

B (average size = 3.6 nm)

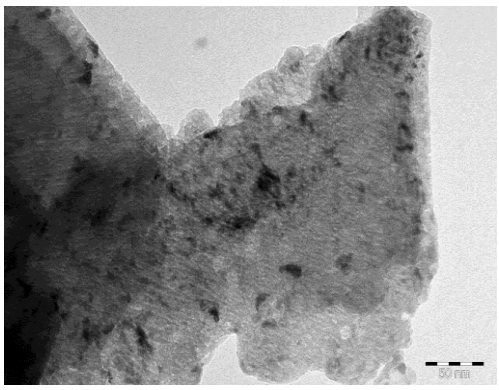

C

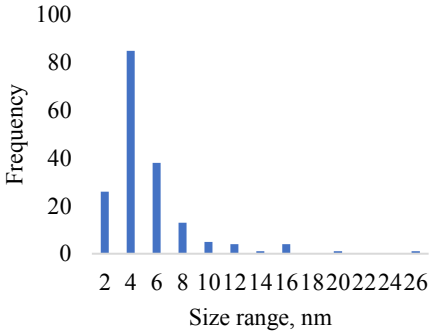

D (average size = 5.3 nm)

Figure IIIC. TEM images and histograms of the fresh (A and B resp.) and spent (C and D resp.) Re/Al_2O_3 (mao22) in isoeugenol HDO at 250℃ and total pressure of 30 bar in the presence of hydrogen.

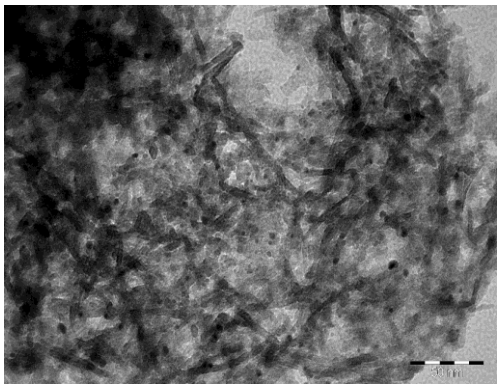

A

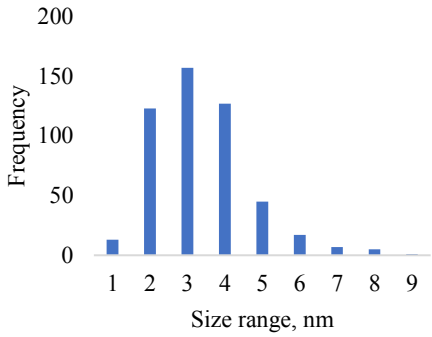

B (average size = 3.4 nm)

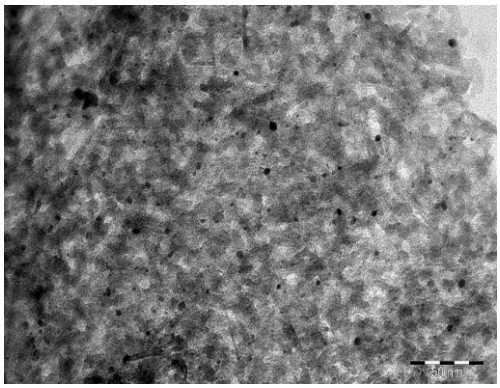

C

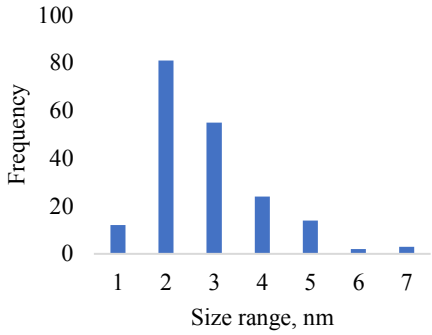

D (average size = 2.8 nm)

Figure IIID. TEM images and histograms of the fresh (A and B resp.) and spent (C and D resp.) 3 wt.% Pt-3 wt.% Re/Al_2O_3 catalysts in isoeugenol HDO at 250℃ and total pressure of 30 bar in the presence of hydrogen.

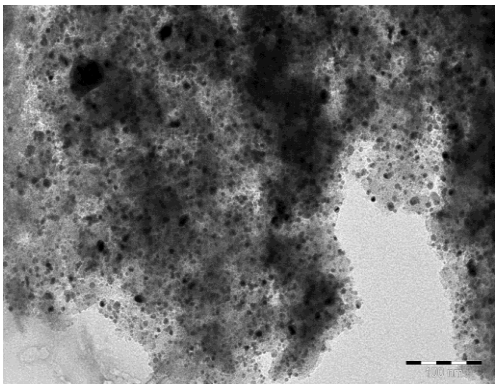

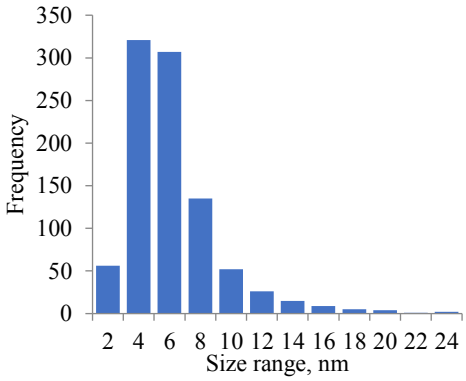

A *B(average size = 6.2 nm)*

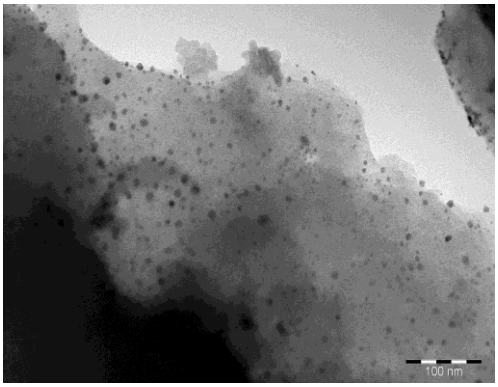

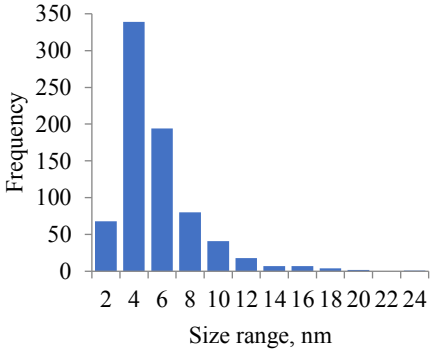

C *D (average size = 5.6 nm)*

Figure IIIE. TEM images and histograms of the fresh (A and B resp.) and spent (C and D resp.) Ir/C (rbb) in isoeugenol HDO at 200℃ and 11 bar (mao43) catalyst.

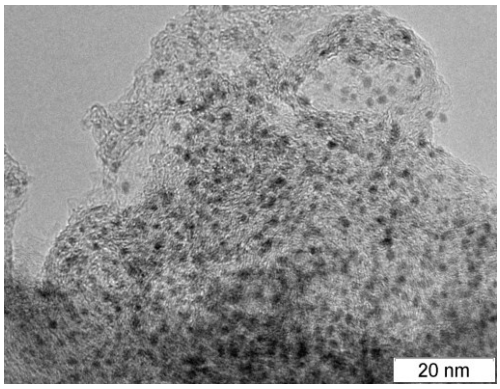

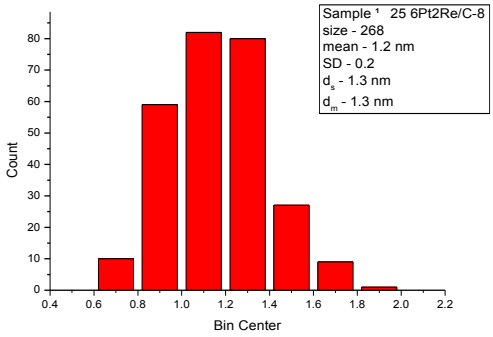

A *B (average size = 1.2 nm)*

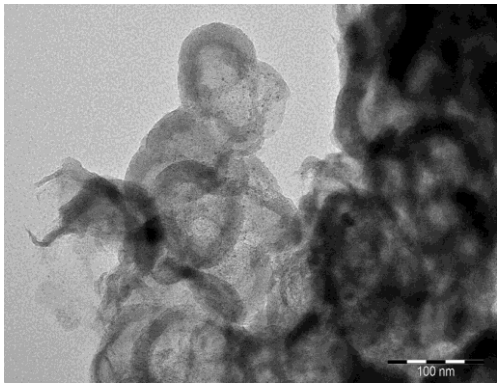

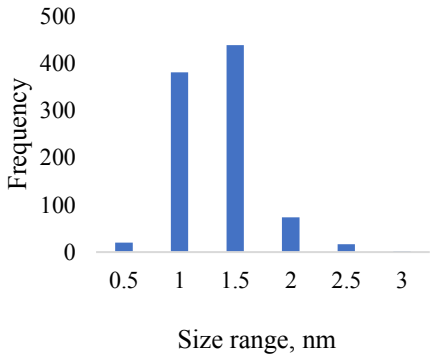

C *D (average size = 1.3 nm)*

Figure IIIF. TEM images and histograms of the fresh (A and B resp. at Boreskov Institute of Catalysis) and spent (C and D resp.) in isoeugenol HDO at 200℃ and 30 bar PtRe/C-31 catalyst.

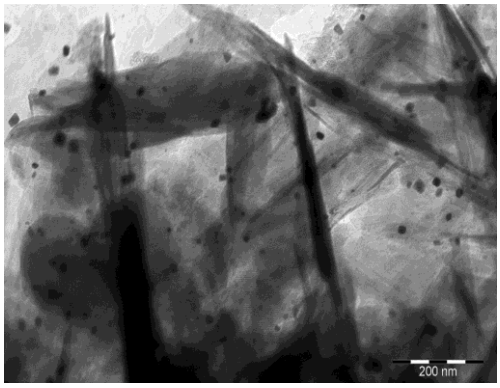

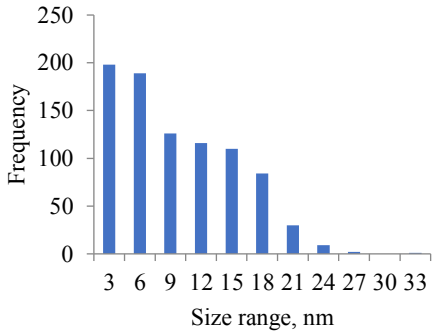

(average size = 9.7 nm)

Figure IIIG. TEM image and the histogram of the fresh 2 wt.% Pt-MM-4MW22-2AI-C catalyst.

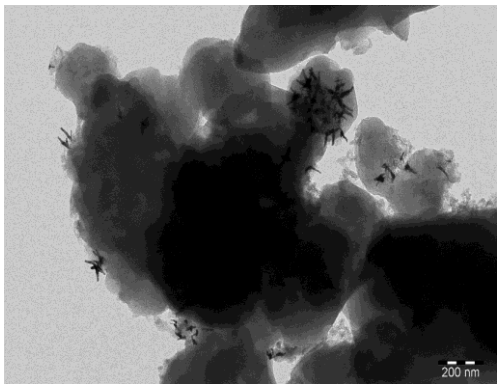

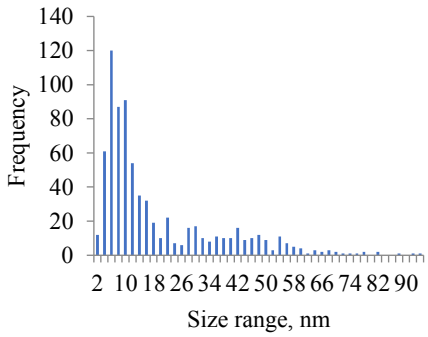

(average size = 20.4 nm)

Figure IIIH. TEM image and the histogram of the fresh 2 wt.% Ir-MM-BE-4BE-96h-2AI-35-C catalyst.

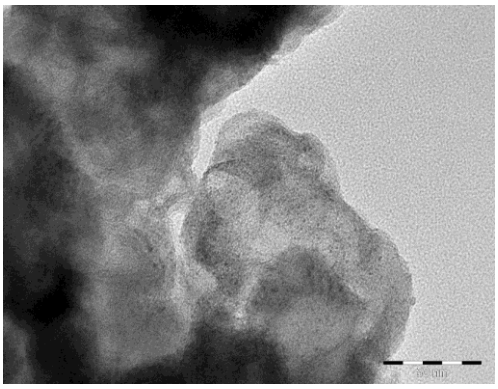

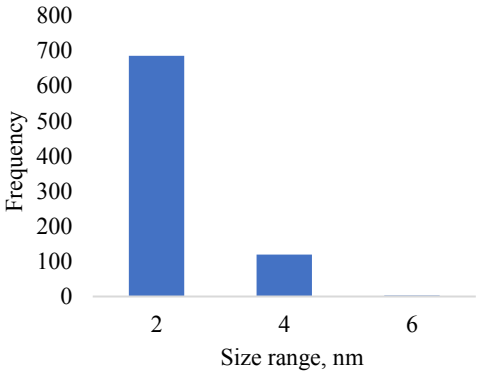

(average size = 2.3 nm)

Figure IIII. TEM image and the histogram of the fresh 3 wt.% Ir/C catalyst.

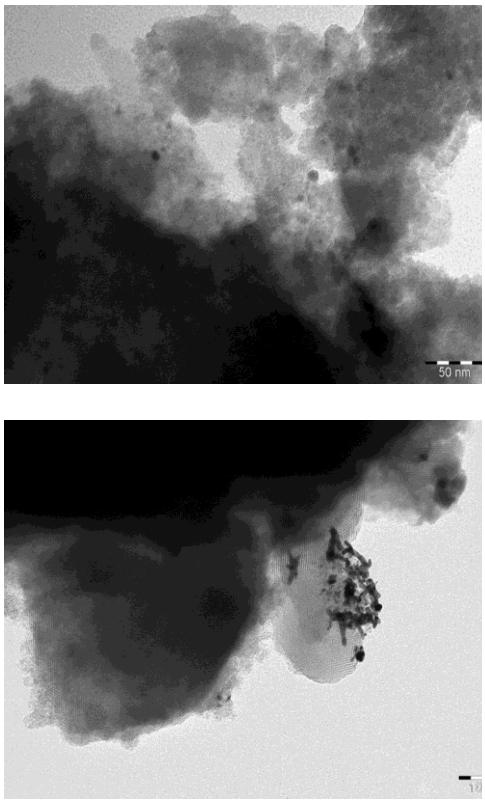

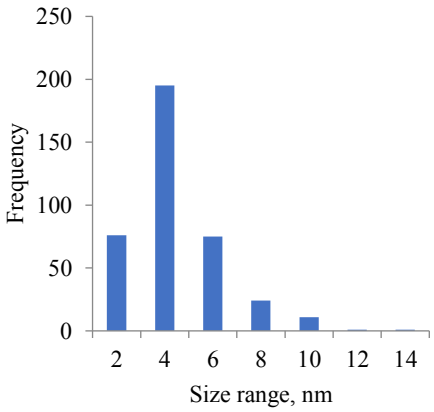

average size = 4.5 nm

Figure IIIG. TEM images and the histogram of the fresh 1 wt.% Ir/SiO_2-EIM catalyst.

10 Appendix IV

SEM-EDX analysis results

Table IVA. Weight percentage of the fresh and spent alumina and carbon supported catalysts constituents via SEM-EDX analysis

Catalyst	Weight %					
	C	O	Al	Re	Ir	Pt
IrRe/Al_2O_3-DP[e]	17.3[a] 15.7[b]	61.4[a] 59.6[b]	16.3[a] 19.1[b]	3.5[a] 4.2[b]	0.8[a] 0.7[b]	-
IrRe/Al_2O_3-Impr2[e]	11.2[a] 17.7[b]	53.9[a] 61.9[b]	25.3[a] 15.6[b]	5.4[a] 3.0[b]	3.8[a] 1.7[b]	-
IrRe/Al_2O_3-Impr1[e]	14.2[a] 16.6[b]	57.8[a] 60.5[b]	21.2[a] 17.2[b]	4.6[a] 3.5[b]	1.7[a] 2.0[b]	-
Re/Al_2O_3[e]	- 13.5[b]	43.5[a] 58.1[b]	45.0[a] 24.0[b]	11.4[a] 4.4[b]	-	-
Pt/Al_2O_3[e]	11.9[a] -	55.7[a] 42.2[b]	27.0[a] 45.7[b]	-	-	5.1[a] 10.1[b]
3 wt.% Pt-3 wt.% Re/Al_2O_3[e]	14.3[a] 13.7[b]	57.5[a] 57.0[b]	21.2[a] 22.6[b]	3.7[a] 3.4[b]	-	2.8[a] 3.0[b]
PtRe/C-31	26.6[a] 26.5[b]	71.0[a] 70.7[b]	-	0.9[a] 1.2[b]	-	1.5[a] 1.6[b]
PtRe/C-13	79.6[a] 80.4[b]	7.8[a] 10.4[b]	-	6.4[a] 5.6[b]	-	5.8[a] 3.3[b]
Ir/C	27.1[a] 27.1[c] 27.1[d]	72.3[a] 72.3[c] 72.3[d]	-	-	0.4[a] 0.3[c] 0.4[d]	-

a* - the fresh state before isoeugenol HDO.

b* - the spent catalyst obtained from isoeugenol HDO 250℃ and 11 bar.

c* - the spent Ir-C catalyst from isoeugenol HDO at 150℃ and 11 bar (mao36).

d* - the spent Ir-C catalyst from isoeugenol HDO at 200℃ and 11 bar (mao43).

e* - carbon is present in alumina supported catalysts due to a carbon coating placed below of the catalyst layer.

Table IVA. Weight percentage of the fresh and spent alumina and carbon supported catalysts' constituents via SEM-EDX analysis

Catalyst	**Weight %**				
	C	**O**	**Ni**	**Zr**	**Ir**
3 wt.%	-	24.4[a]	-	65.4[a]	6.7[a]
Ir/ZrO_2		24.7[b]		65.9[b]	7.0[b]
10 wt.%	-	25.2[a]	10.8[a]	60.6[a]	-
Ni/ZrO_2	10.6[b]	43.8[b]	8.3[b]	37.5[b]	

a* - the fresh state before isoeugenol HDO.

b* - the spent catalyst obtained from isoeugenol HDO 250℃ and 11 bar.

SEM images

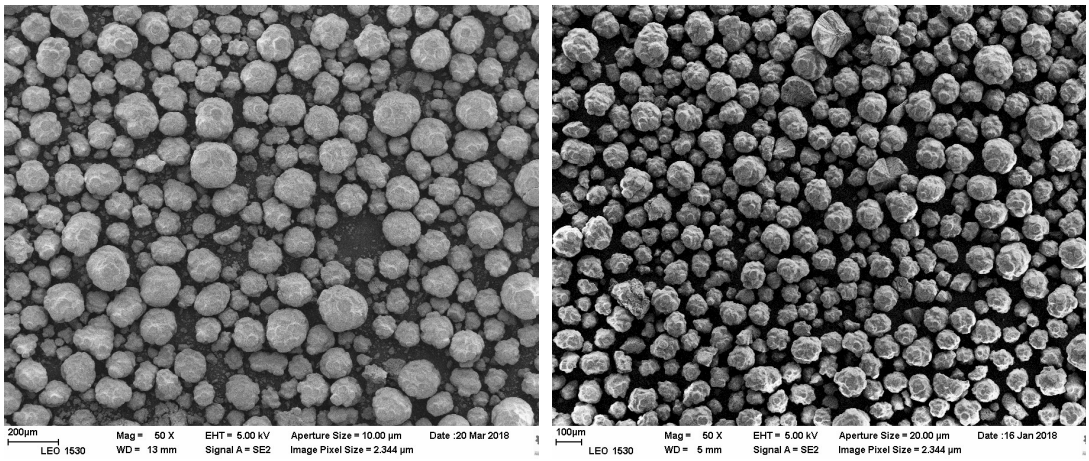

fresh *spent*

Figure IVA. SEM images of the fresh and spent Re/Al_2O_3 (mao22) in isoeugenol HDO at 250℃ and total pressure of 30 bar in the presence of hydrogen.

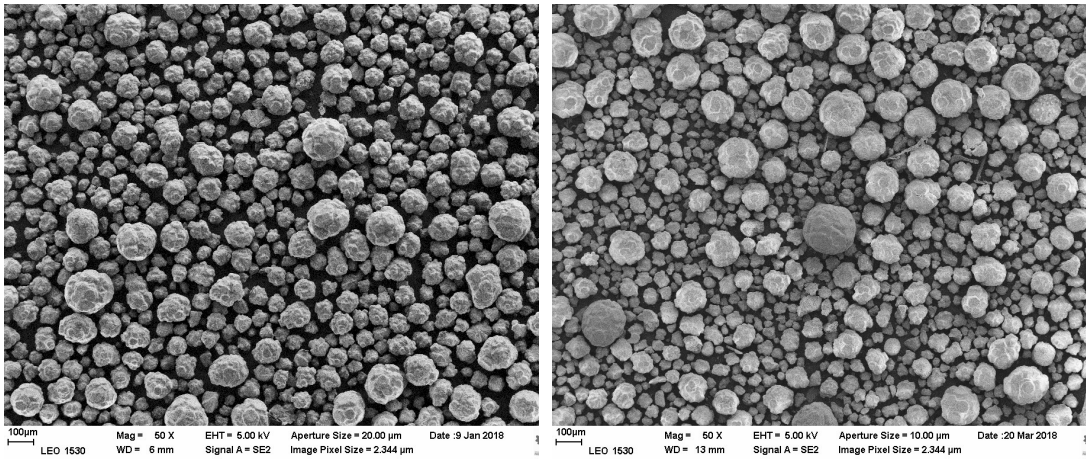

fresh *spent*

Figure IVB. SEM images of the fresh and spent Pt/Al_2O_3 (mao16) in isoeugenol HDO at 250℃ and total pressure of 30 bar in the presence of hydrogen.

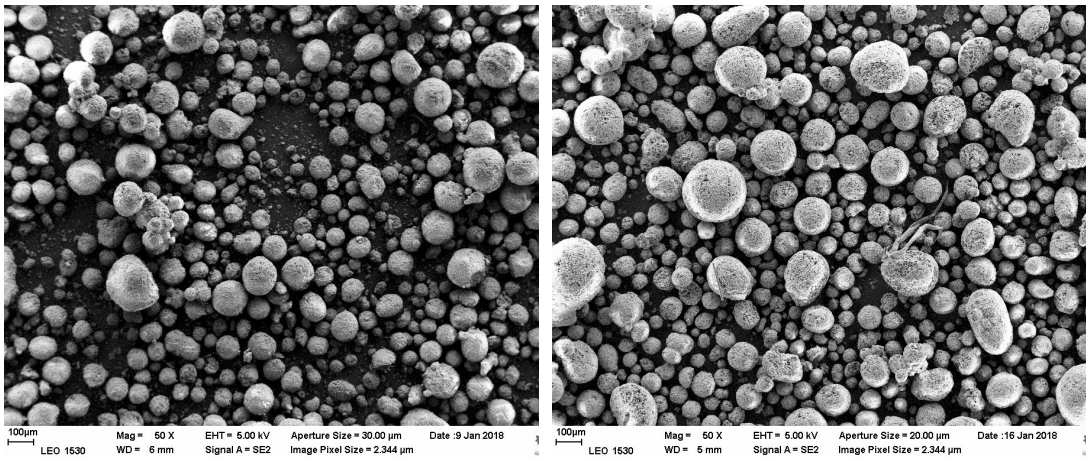

fresh *spent*

Figure IVC. SEM images of the fresh and spent $PtRe/Al_2O_3$ (mao14) in isoeugenol HDO at 250℃ *and total pressure of 30 bar in the presence of hydrogen.*

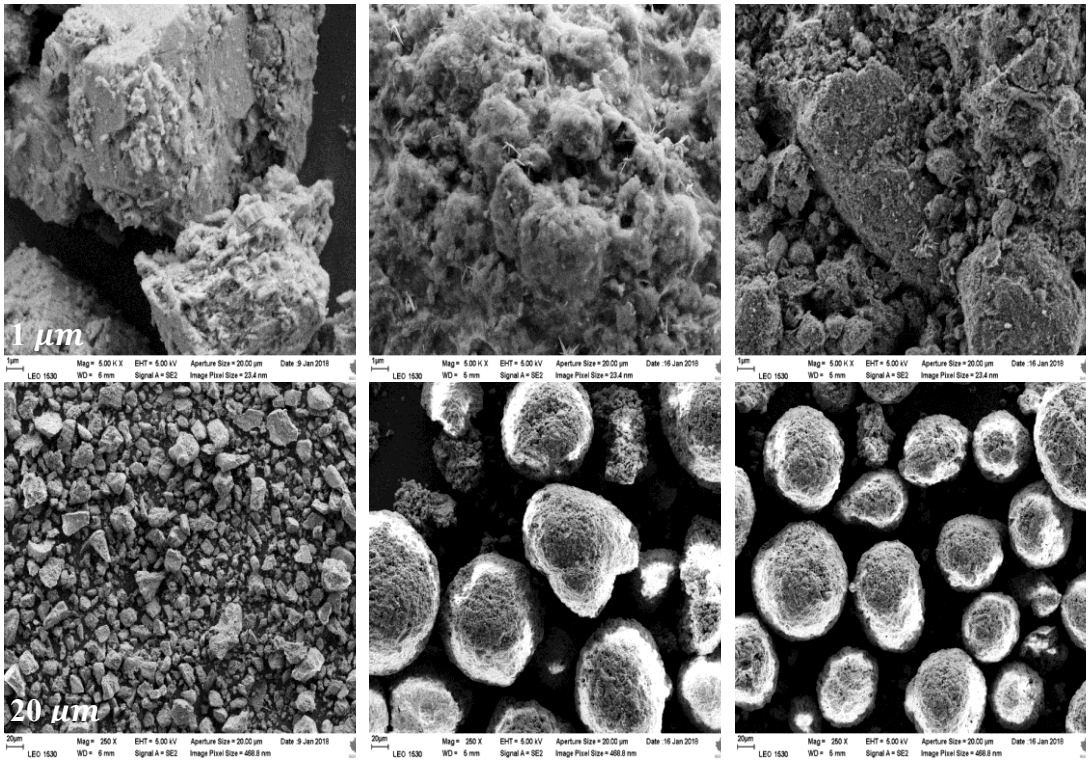

A B C

Figure IVD. SEM images of the spent catalysts in isoeugenol HDO at 250℃ *and total pressure of 30 bar in the presence of hydrogen. A – IRA-DP, B – IRA-Impr2, C –IRA-Impr1.*

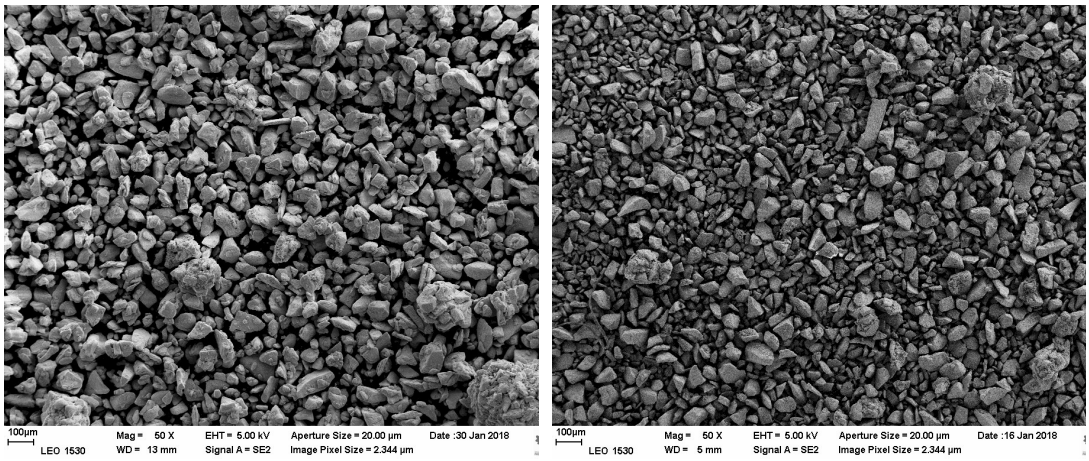

A *B*

Figure IVE. SEM images of the spent catalysts in isoeugenol HDO at 250℃ *and total pressure of 30 bar in the presence of hydrogen. A – Ir/ZrO_2 (mao19), B – 10 wt.% Ni/ZrO_2 (mao21).*

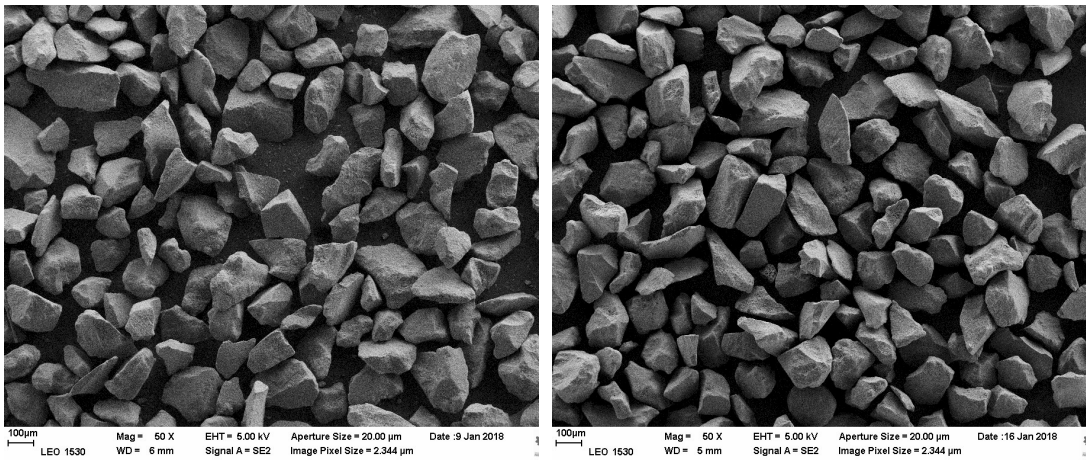

fresh *spent*

Figure IVF. SEM images of the fresh and spent PtRe/C-31 (mao15) in isoeugenol HDO at 250℃ *and total pressure of 30 bar in the presence of hydrogen.*

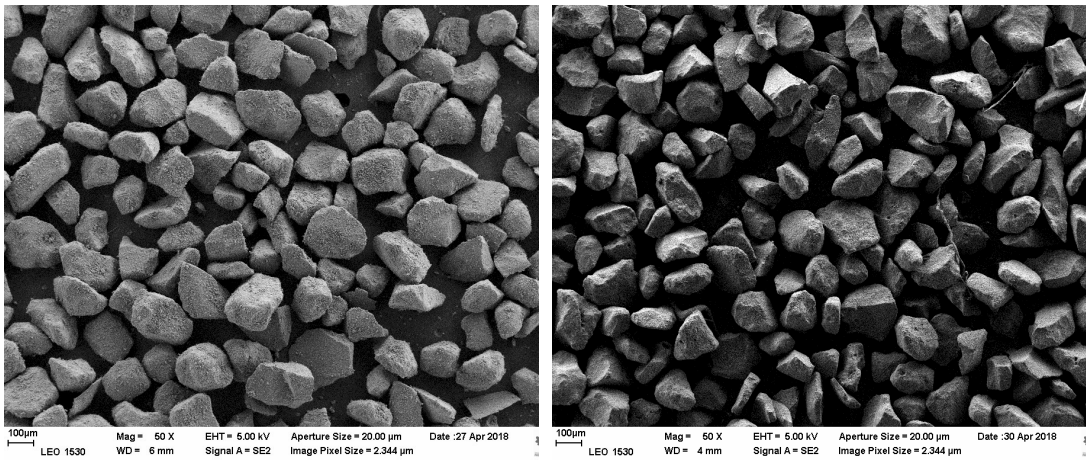

fresh spent

Figure IVG. SEM images of the fresh and spent PtRe/C-13 (mao51) in isoeugenol HDO at 250℃ *and total pressure of 30 bar in the presence of hydrogen.*

11 Appendix V

Size Exclusion Chromatography

Table VA. Retention times of sitosterol as a standard via SEC.

Detector D			
Pk #	**Retention Time**	**Area**	**Area Percent**
1	22.28	388089	92.6
2	24.05	30850	7.4
	Total	**418939**	**100.0**

Table VB. Retention times for IRA-Impr1 in tetrahydrofuran via SEC.

Pk #	Retention Time	Area	Area, %
1	13.25	9018	4.7
2	14.27	84178	43.5
3	21.17	15482	8.0
4	22.06	19511	10.1
5	24.07	12660	6.5
6	25.28	52665	27.2
	Total	**19351**	**100,0**

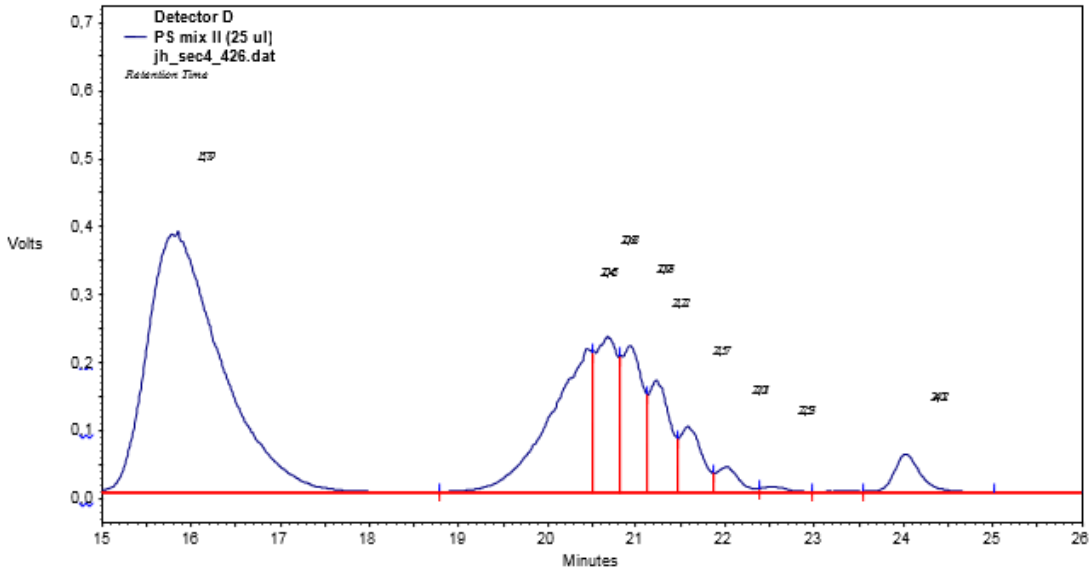

Figure VA. SEC analysis of polystyrene oligomer.

Table VC. Retention times and number of polystyrene units via SEC analysis.

PS oligomer	Molecular weight	Retention Time	Height
n = 9	994	20.45	70517
n = 8	890	20.68	76196
n = 7	786	20.93	71887
n = 6	682	21.22	54846
n = 5	578	21.57	32072
n = 4	474	22.01	12532
n = 3	370	22.53	2797
(n = 2)	(266)	-	-
n = 1	162	24.02	18651

12 Appendix VI

X-ray photoelectron spectroscopy results

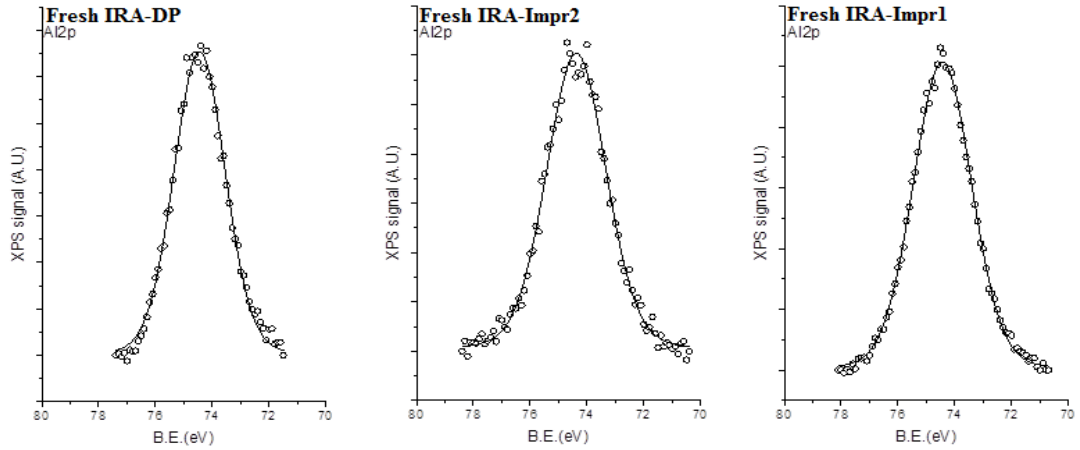

Figure VIA. XPS results indicating aluminum (Al2p) as the reference to account for possible charging for the fresh IRA series catalysts.

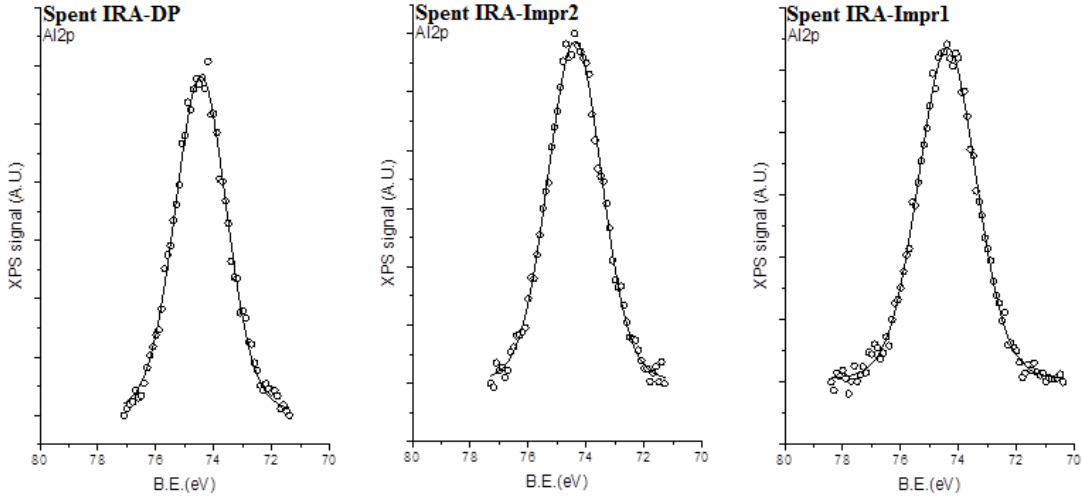

Figure VIB. XPS results indicating aluminum (Al2p) as the reference to account for possible charging for the spent IRA series catalysts.

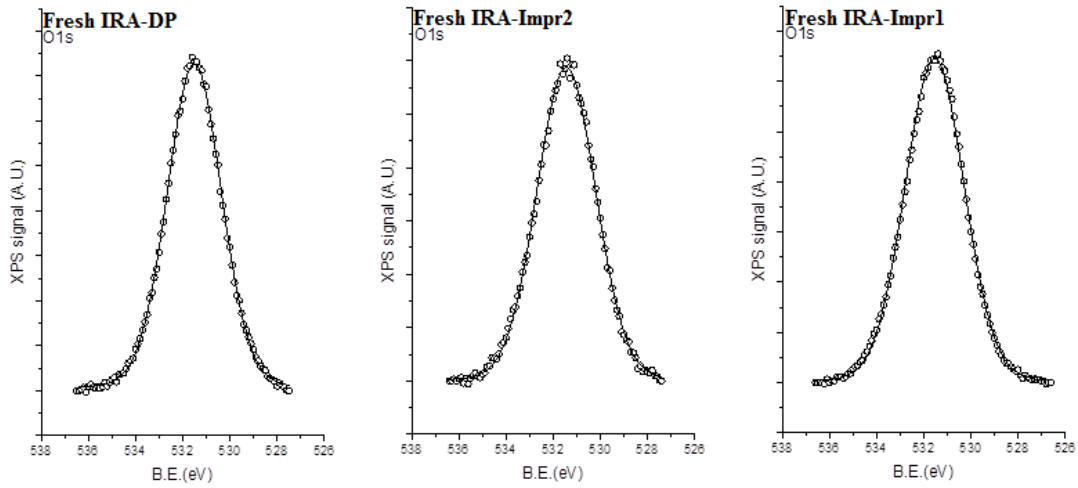

Figure VIC. XPS results indicating oxygen for the fresh IRA series catalysts.

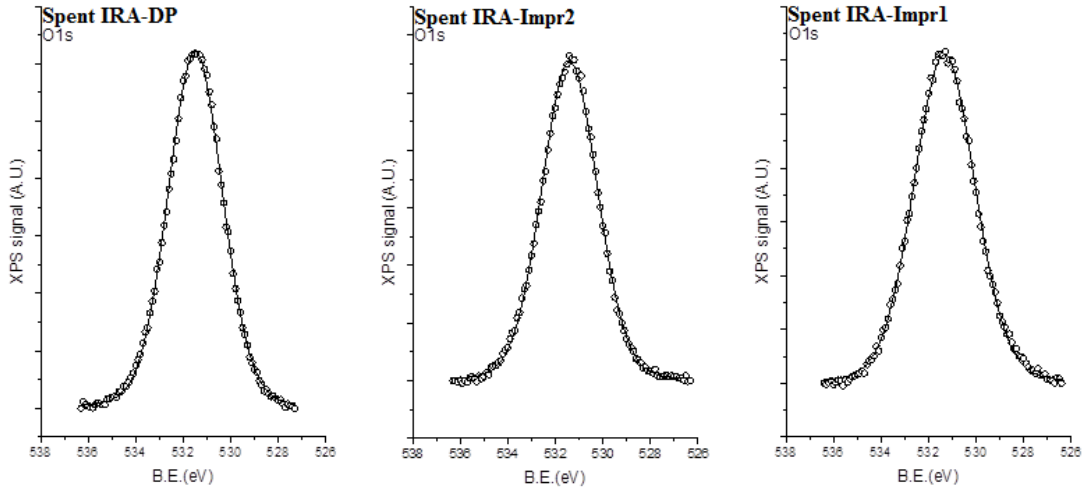

Figure VIC. XPS results indicating oxygen for the spent IRA series catalysts.

13 Appendix VII

X-ray powder diffraction

XRD was provided by Boreskov Institute of Catalysis for IRA-Impr2, proving there was no boehmite.

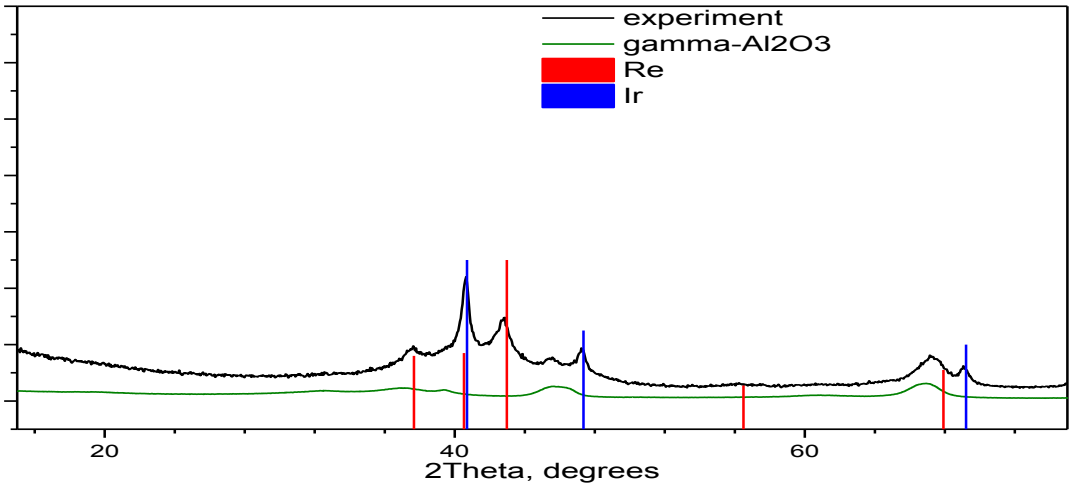

Figure VIIA. XRD analysis of the fresh IRA-Impr2.

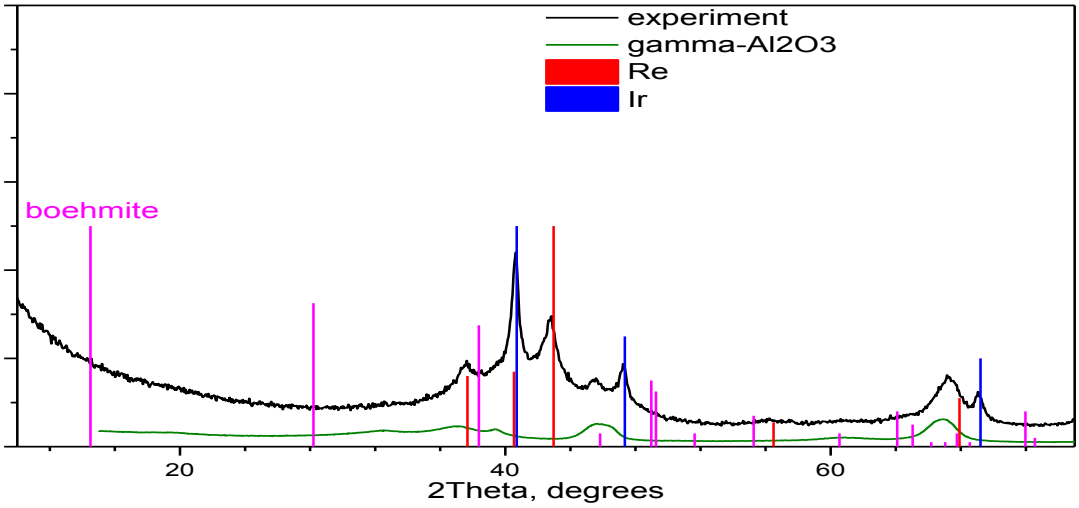

Figure VIIA. XRD analysis of the fresh IRA-Impr2 with addition of boehmite.

14 Appendix VIII

Gas analysis via GC-MS and GC

Table VIIIA. Gas analysis via GC-MS and GC from guaiacol HDO (4 h) at 250℃ and 30 bar with Ir/ZrO_2 and 10 wt.% Ni/ZrO_2

Type	**Results from GC-MS**		**Results from GC**	
	Ir/ZrO_2	**10 wt.% Ni/ZrO_2**	**Ir/ZrO_2**	**10 wt.% Ni/ZrO_2**
matching	Methane, ethane, propane, butane, acetone, 2-propanol, pentane, cyclopentane, cyclohexane, dodecane, dihydroeugenol		Methane RT of 18.8 min (unknown)	
not matching	hexane	Methylcyclo-pentane, heptane	RT of 13.9 min 17.5 min	Ethane iso-butane RT of 12 min 17.5 min 19.4 min

Table VIIIB. Gas sampling results of the solventless temperature programmed reaction with Ir/C (rbb)

Type	**Results from GC-MS**		**Results from GC**	
	150℃ (mao 36)	**200℃ (mao 43)**	**150℃ (mao 36)**	**200℃ (mao 43)**
Matching	Methane, ethane, propane, butane, ethanol, hexane, propylcyclohexane, dodecane		Methane, ethane, RT of 17.5 min (unknown)	
Not matching	Acetone, pentane, heptane, octane, nonane	2-propanol	RT of 16 min	-

15 Appendix IX

The list of catalysts tested in isoeugenol HDO at the specified conditions.

Table IXA. Alumina and carbon supported catalysts tested in isoeugenol HDO at 200℃ or 250℃ and 30 bar total pressure in presence of hydrogen

Entry	Catalyst	T=200℃	T=250℃
1	IrRe/Al_2O_3-DP	+	+
2	IrRe/Al_2O_3-Impr2	+	+
3	IrRe/Al_2O_3-Impr1	-	+
4	Ir/Al_2O_3	+	-
5	Re/Al_2O_3	+	+
6	3 wt.% Pt-3 wt.% Re/Al_2O_3	-	+
7	Pt/Al_2O_3	-	+
8	PtRe/C-31	+	+
9	PtRe/C-13	-	+

16 Appendix XI

Table XIA. List of experiments performed for HDO.
Notation: mass of reactant mainly 0.1 g, volume of dodecane as a solvent – 50 mL, mass of catalyst – 0.05 g and reaction pressure – 30 bar

Entry	Catalyst	Initial concentration of reactant, mol/L	Temperature, ℃	Conversion of isoeugenol & GCLPA, % (4h)	Molar concentration of final products, mol/L	HDO, %	Remarks
mao 2	3 wt.% Ir/C	isoeugenol (0.014)	150	100 & 87 respectively	dihydroeugenol (0.012), propylcyclohexane & 1,2,4-trimethylbenzene (close to 0)	1	
mao 3	2% Pt-MM-4MW22-2Al-C	isoeugenol (0.013)	150	100 & 83 respectively	dihydroeugenol (0.009), 1,2,4-trimethylbenzene (0.002), propylcyclohexane (0.0002)	15	
mao 4	10 wt.% Ni/ZrO_2	isoeugenol (0.013)	150	100 & 99 respectively	dihydroeugenol (0.012), 1,2,4-trimethylbenzene (0.001)	8	"+"
mao 5	Ir/ZrO_2	isoeugenol (0.011)	150	100 & 69	dihydroeugenol (0.008), propylcyclohexane (0.0002)	2	"+"
mao 6	1 wt.% Ir/SiO_2	isoeugenol (0.015)	150	100 & 95 respectively	dihydroeugenol (0.014)	0	
mao 7	2 wt.% Ir-MM-BE-4BE-96h-2Al-35-C	isoeugenol (0.014)	150	100 & 65 respectively	dihydroeugenol (0.009), propylcyclohexane (close to 0)	0	
mao 8	Ir/ZrO_2	isoeugenol (0.014)	200	100 & 55 respectively	dihydroeugenol (0.007), propylcyclohexane (0.0005)	4	"+"
mao 9	IrRe/ Al_2O_3-DP	isoeugenol (0.012)	200	100 & 80 respectively	dihydroeugenol (0.009), propylcyclohexane (0.0004)	3	"+"
mao 10	Re/Al_2O_3	isoeugenol (0.013)	200	100 & 89 respectively	dihydroeugenol (0.011), propylcyclohexane (close to 0)	0	"+"
mao 11	Ir/Al_2O_3	isoeugenol (0.013)	200	100 & 69	dihydroeugenol (0.009), propylcyclohexane (0.0003)	2	"+"
mao 12	IrRe/ Al_2O_3-Impr2	isoeugenol (0.015)	250	100 & 49 respectively	propylcyclohexane (0.007), dihydroeugenol (0.001), 1-methyl-2(3)-propylcyclohexane (0.0007), propylbenzene (0.0001), cyclohexane (close to 0)	86	

Entry	Catalyst	Initial concentration of reactant, mol/L	Temperature, ℃	Conversion of isoeugenol & GCLPA, % (4h)	Molar concentration of final products, mol/L	HDO, %	Remarks
mao 13	IrRe/ Al_2O_3-Impr1	isoeugenol (0.013)	250	100 & 54 respectively	propylcyclohexane (0.006), dihydroeugenol (0.001), 1-methyl-2(3)-propylcyclohexane (0.001), propylcyclopentane and cyclohexane (close to 0)	80	**"+" 4 h after**: hexane (0.001 mol/L), heptane (0.0003 mol/L) and octane (0 mol/L)
mao 14	3 wt.%Pt-3 wt.% Re/ Al_2O_3	isoeugenol (0.014)	250	100 & 35 respectively	dihydroeugenol (0.008), propylcyclohexane (0.002)	14	
mao 15	PtRe/C-31	isoeugenol (0.012)	250	100 & 44 respectively	propylcyclohexane (0.007)	100	**"+" 4 h after:** hexane (0.003 mol/L), heptane (0.002 mol/L) and octane (0.004 mol/L)
mao 16	Pt/Al_2O_3	isoeugenol (0.012)	250	100 & 76 respectively	dihydroeugenol (0.009), propylcyclohexane (0.0003)	3	**"+"**
mao 17	IrRe/ Al_2O_3-DP	isoeugenol (0.013)	250	100 & 53 respectively	propylcyclohexane (0.009),), 1,2,4-trimethylbenzene (0.0001), 1-methyl-2(3)-propylcyclohexane, propylcyclopentane and cyclohexane (close to 0)	100	**"+" 4 h after:** hexane and octane (0 mol/L), heptane (0.001 mol/L)
mao 18	IrRe/ Al_2O_3-Impr1	isoeugenol (0.014)	250	100 & 63 respectively	dihydroeugenol (0.008), propylcyclohexane (0.0002), 1,2,4-trimethylbenzene (0.0001)	2	**"+" Total pressure=17 bar, 4 h after:** hexane, heptane and octane (0 mol/L)
mao 19	Ir/ZrO_2	isoeugenol (0.012)	250	100 & 23 (25 including TGA) respectively	propylcyclohexane (0.003), dihydroeugenol (0.0005)	91	**"+" 4 h after:** hexane, heptane and octane (0 mol/L)
mao 20	10 wt.% Ni/ZrO_2	isoeugenol (0.014)	200	100 & 19 (25 including TGA) respectively	dihydroeugenol (0.002), propylcyclohexane (0.0002)	65	**"+" 4 h after:** hexane, heptane and octane (0 mol/L)
mao 21	10 wt.% Ni/ZrO_2	isoeugenol (0.013)	250	100 & 15 (17 including TGA) respectively	propylcyclohexane (0.002), dihydroeugenol (0.0004)	94	"+" **4 h after:** hexane, heptane and octane (0 mol/L)
mao 22	Re/Al_2O_3	isoeugenol (0.014)	250	100 & 57 respectively	dihydroeugenol (0.007), propylcyclohexane (0.0009)	7	"+" **4 h after:** hexane, heptane and octane (0 mol/L)
mao 23	**no catalyst**	isoeugenol (0.014)	250	100 & 90 respectively	dihydroeugenol (0.012), propylcyclohexane (close to 0)	0	no glass bead blasting of reactor; **thermal test**

Entry	Catalyst	Initial concentration of reactant, mol/L	Temperature, ℃	Conversion of isoeugenol & GCLPA, % (4h)	Molar concentration of final products, mol/L	HDO, %	Remarks
mao 24	**no catalyst**	isoeugenol (0.016)	250	100 & 91 respectively	dihydroeugenol (0.015), propylcyclohexane (close to 0)	0	no glass bead blasting of reactor; **thermal test**
mao 25	IrRe/ Al_2O_3-Impr1	isoeugenol (0.013)	250	100 & 48 respectively	propylcyclohexane (0.006), 1-methyl-2(3)-propylcyclohexane (0.001), dihydroeugenol (0.0002), 1,2,4-trimethylbenzene (0.0001), propylcyclopentane and cyclohexane (close to 0)	50	**"+" Total pressure=25 bar, 4 h after:** hexane, heptane and octane (0 mol/L)
mao 26	IrRe/ Al_2O_3-Impr2	isoeugenol (0.012)	250	100 & 50 respectively	propylcyclohexane (0.006), 1-methyl-2(3)-propylcyclohexane (0.001), 1,2,4-trimethylbenzene (0.0004), propylbenzene (0.0004), propylcyclopentane and cyclohexane (close to 0)	100	**"+"** for comparison with **mao41, 4 h after:** hexane and octane (0 mol/L), heptane (0.0004 mol/L)
mao 27	IrRe/ Al_2O_3-Impr1	isoeugenol (0.032)	250	100 & 44 respectively	propylcyclohexane (0.015), 1,2,4-trimethylbenzene (0.001), 1-methyl-2(3)-propylcyclohexane (0.0003), dihydroeugenol, propylbenzene, propylcyclopentane and cyclohexane (close to 0)	100	**"+"** for reproducibility test **mao32**; mass of cat.=0.17 g, mass of reactant=0.34 g; **4 h after:** hexane, heptane and octane (0 mol/L)
mao 28	PtRe/ Al_2O_3	isoeugenol (0.012)	250	100 & 45 respectively	propylcyclohexane (0.007), 1-methyl-2(3)-propylcyclohexane (close to 0)	100	**"+" 4 h after:** hexane (0.003 mol/L), heptane (0.004 mol/L) and octane (0.008 mol/L)
mao 30	PtRe/C-31	isoeugenol (0.014)	200	100 & 30 respectively	propylcyclohexane (0.005)	100	**"+" 4 h after:** hexane, heptane and octane (0 mol/L)
mao 31	IrRe/ Al_2O_3-Impr2	isoeugenol (0.015)	200	100 & 64 respectively	dihydroeugenol (0.009), propylcyclohexane (0.0001)	6	**"+" 4 h after:** hexane, heptane and octane (0 mol/L)
mao 32	regenerated IrRe/ Al_2O_3-Impr1	isoeugenol (0.027)	250	100 & 53 respectively	propylcyclohexane (0.016), 1-methyl-2(3)-propylcyclohexane (0.002), 1,2,4-	100	**"+"** mass of cat.=0.117 g, mass of reactant=0.234 g;

					trimethylbenzene, propylbenzene and cyclohexane (close to 0)		**4 h after:** hexane (0.003 mol/L), heptane (0.003 mol/L) and octane (0.003 mol/L)
mao 33	**no catalyst**	isoeugenol (0.014)	250	100 & 90 respectively	dihydroeugenol (0.013), propylcyclohexane (0.0001)	0	**"+"** glass bead blasting of reactor before use; **thermal test; 4 h after:** hexane, heptane and octane (0 mol/L)
mao 34	**no catalyst**	isoeugenol (0.014)	250	100 & 94 respectively	dihydroeugenol (0.013), propylcyclohexane (close to 0)	0	**"+"** glass bead blasting of reactor before use; **thermal test; 4 h after:** hexane, heptane and octane (0 mol/L)
mao 35	Ir/ZrO_2	**no isoeugenol**	250	-	-	-	**"+" 4 h after:** hexane (0.018 mol/L), heptane (0.017 mol/L), octane (0.024)
mao 36	Ir/C (rbb)	isoeugenol (0.013)	150 to 200	100 & 100 respectively	dihydroeugenol (0.013)	0	**"+" solventless, initial pressure=11.6 bar;** mass of cat.=0.576 g, mass of reactant=57.6 g,
mao 37	IrRe/ Al_2O_3-Impr1	isoeugenol (0.015)	250	100 & 84 respectively	propylcyclohexane (0.015), dihydroeugenol (0.001), 1,2,4-trimethylbenzene, propylbenzene, 1-methyl-2(3)-propylcyclopentane and cyclohexane (close to 0)	86	**"+" Total pressure=40 bar; 4 h after:** hexane (0.003 mol/L), heptane (0.0004 mol/L), octane (0 mol/L)
mao 38	IrRe/ Al_2O_3-DP	isoeugenol (0.013)	250	100 & 53 respectively	propylcyclohexane (0.009), 1,2,4-trimethylbenzene , 1-methyl-2(3)-propylcyclohexane and cyclohexane (close to 0)	100	**"+" 4 h after:** hexane (0.005 mol/L), heptane (0.004 mol/L), octane (0.006 mol/L)
mao 39	**no catalyst**	isoeugenol (0.014)	200	100 & 93 respectively	dihydroeugenol (0.013), propylcyclohexane (close to 0)	0	**"+" thermal test; 4 h after:** hexane, heptane and octane (0 mol/L)
mao 40	IrRe/ Al_2O_3-DP	isoeugenol (0.014)	250	100 & 44 respectively	propylcyclohexane (0.008), 1-methyl-2(3)-propylcyclohexane close to 0)	100	**"+" Total pressure=42 bar, 4 h after:** hexane and octane (0 mol/L), heptane (0.0001 mol/L)

Entry	Catalyst	Initial concentration of reactant, mol/L	Tem-pera-ture, ℃	Conversion of isoeugenol & GCLPA, % (4h)	Molar concentration of final products, mol/L	HDO, %	Remarks
mao 41	IrRe/ Al_2O_3-Impr2	isoeugenol (0.013)	250	100 & 45 respectively	propylcyclohexane (0.0057), dihydroeugenol (0.0007), propylbenzene (0.0006), 1,2,4-trimethylbenzene, 1-methyl-2(3)-propylcyclohexane, propylcyclopentane and cyclohexane (close to 0)	88	**"+" 4 h after:** hexane and octane (0 mol/L), heptane (0.0004 mol/L)
mao 42	IrRe/ Al_2O_3-DP	isoeugenol (0.076)	250	100 & 52 respectively	propylcyclohexane (0.0057), dihydroeugenol (0.036), propylbenzene (0.005), 1,2,4-trimethylbenzene (0.0003), 1-methyl-2(3)-propylcyclohexane (0.0003), propylcyclopentane and cyclohexane (close to 0)	80	**"+"** Reactant – 10x higher than cat. mass of cat.=0.1 g, mass of reactant=1 g (0.12 mol/L), **4 h after:** hexane and octane (0 mol/L), heptane (0.0003 mol/L)
mao 43	Ir/C (rbb)	isoeugenol (0.013)	200	100	dihydroeugenol (0.013)	0	**"+" solventless, initial pressure=11 bar,** mass of cat.=0.576 g, mass of reactant=57.6 g,
mao 45	**no catalyst**	vanillin (0.007)	100	63 & 91 respectively	vanillyl alcohol (0.004) vanillin (0.003)	-	**"+" thermal test;** mass of vanillin=0.1 g, volume of solvent (water)=0.1 L
mao 46	10 wt.% Ni/ZrO_2	guaiacol (0.018)	250	100 & 54 (57 including TGA) respectively	cyclohexanol (0.006), 2-methoxycyclohexanone (0.004), cyclohexane (0.0003), 1-methoxycyclohexane (close to 0)	2	**"+" 4 h after:** hexane, heptane and octane (0 mol/L)
mao 47	10 wt.% Ni/ZrO_2	vanillin (0.007)	100	94 & 92 respectively	vanillyl alcohol (0.006) vanillin (0.0004)	0	**"+"**
mao 48	Ir/ZrO_2	guaiacol (0.015)	250	100 & 43 (47 including TGA) respectively	cyclohexanol (0.004), cyclohexane (0.002), 2-methoxycyclohexanone (0.001), 1-methoxycyclohexane (0.0001)	14	**"+" 4 h after:** hexane (0.003 mol/L), heptane (0.002 mol/L), octane (0 mol/L)

Entry	Catalyst	Initial concentration of reactant, mol/L	Temperature, ℃	Conversion of isoeugenol & GCLPA, % (4h)	Molar concentration of final products, mol/L	HDO, %	Remarks
mao 49	Ir/ZrO_2	vanillin (0.008)	100	99 & 78 respectively	vanillyl alcohol (0.006) vanillin (close to zero)	0	**"+"**
mao 50	Ir/ZrO_2	isoeugenol (0.012)	250	100 & 34 respectively	propylcyclohexane (0.005), cyclohexane (0.0001)	100	**4 h after:** hexane (0.009 mol/L), heptane (0.007 mol/L), octane (0.011 mol/L)
mao 51	PtRe/C-13	isoeugenol (0.012)	250	100 & 57 respectively	propylcyclohexane (0.009), cyclohexane (close to zero)	100	**"+"** **4 h after**: hexane (0.006 mol/L), heptane (0.004 mol/L), octane (0.007 mol/L)
mao 52	IrRe/ Al_2O_3-DP	isoeugenol (0.012)	250	100 & 54 respectively	propylcyclohexane (0.008), dihydroeugenol (0.0006), 1-methyl-2(3)-propylcyclohexane and cyclohexane (close to 0)	89	**"+"** **total pressure=25 bar;** **4 h after**: hexane (0.009 mol/L), heptane (0.007 mol/L), octane (0.011 mol/L)
mao 53	IrRe/ Al_2O_3-DP	isoeugenol (0.061)	250	100 & 79 respectively	propylcyclohexane (0.060), 1-methyl-2(3)-propylcyclohexane (0.001), dihydroeugenol (0.0006), cyclohexane (0.0001)	98	**"+"** mass of cat.=0.4 g, mass of isoeugenol=0.8 g (0.098 mol/L) **4 h after**: hexane (0.02 mol/L), heptane (0.02 mol/L), octane (0.023 mol/L)
mao 54	Regenerated IrRe/ Al_2O_3-DP	isoeugenol (0.010)	250	100 & 62 respectively	propylcyclohexane (0.004), dihydroeugenol (0.003), 1-methyl-2(3)-propylcyclohexane (0.001), cyclohexane (close to 0)	45	**"+"** mass of cat.=0.05 g, mass of isoeugenol=0.1 g **4 h after**: hexane (0.014 mol/L), heptane (0.012 mol/L), octane (0.018 mol/L)

"+" – used for discussion of the results in Section 4.2